Chemical Controls on the Cycling and Reactivity of Marine Dissolved Organic Matter

by

Benjamin Nash Granzow
B.S., University of Miami, 2017

Submitted to the Department of Earth, Atmosphere, and Planetary Sciences
in partial fulfillment of the requirements for the degree of

Doctor of Philosophy

at the

MASSACHUSETTS INSTITUTE OF TECHNOLOGY

and the

WOODS HOLE OCEANOGRAPHIC INSTITUTION

February 2023

Author……
Joint Program in Oceanography/Applied Ocean Sciences & Engineering
Massachusetts Institute of Technology & Woods Hole Oceanographic Institution
December 20th, 2022

Certified by……
Dr. Daniel J. Repeta
Woods Hole Oceanographic Institution
Thesis Supervisor

Accepted by……...
Dr. Edward A. Boyle
Massachusetts Institute of Technology
Chair, Joint Committee for Chemical Oceanography

Chemical Controls on the Cycling and Reactivity of Marine Dissolved Organic Matter

by

Benjamin Nash Granzow

Submitted to the Joint Program in Oceanography/Applied Ocean Science & Engineering,
Massachusetts Institute of Technology & Woods Hole Oceanographic Institution
on December 20th, 2022 in partial fulfillment of the requirements for the degree of Doctor of Philosophy in Marine Chemistry

ABSTRACT

Marine dissolved organic matter (DOM) is an actively cycling reservoir of carbon containing thousands of unique compounds. To describe the complex dynamics that govern the biological transformation and decomposition of compounds in this molecular black box, models of DOM reactivity use chemical characteristics, as well as environmental parameters, to describe trends in the turnover time of classes of DOM. In this thesis, I describe two projects that examine hypotheses regarding the turnover of two classes of DOM. In the 1st project, I test the assumption made by the size–reactivity continuum hypothesis that high molecular weight (> 1 kDa) DOM (HMWDOM) represents a diagenetic intermediate between large labile material and small recalcitrant compounds. Size-fractions of HMWDOM were collected using size-exclusion chromatography, and the changes in MW and chemical composition of the fractions were studied using diffusion-ordered spectroscopy. The size fraction carbon isotopic values were correlated with the proportion of humic substances in the fractions. Through linear modeling, the apparent radiocarbon ages of the two major components of HMWDOM were determined to be 1-3 yrs and 2-4 kyrs, respectively. Combined with the measurements of MW distribution this work demonstrates that HMWDOM is composed of two components that have contrasting decomposition pathways in the ocean. HMWDOM cannot be treated as a single DOM pool when incorporated into models of DOM diagenesis.

The 2nd project in this dissertation examines the remineralization of phosphonates, compounds with a direct C-P bond, in the lower euphotic zone using a newly developed fluorescent assay, which measures the activity of carbon-phosphorus lyase. C-P lyase activity (CLA) profiles from the North Pacific Subtropical Gyre (NPSG) showed a sharp activity maximum near the deep-chlorophyll maximum (DCM). High-resolution nutrient measurements suggest that this subsurface CLA maximum is the result of a high nitrate flux at the top of the nitracline. The composition of particulate-P through the euphotic zone was also examined. While phosphonates were not detected in suspended particles, a significant amount of aminoethylphosphonate was measured in sinking material, suggesting eukaryotic material may be an important source of phosphonates to the ocean.

Thesis Supervisor: Dr. Daniel J. Repeta
Title: Senior Scientist, Marine Chemistry and Geochemistry, Woods Hole Oceanographic Institution

ACKNOWLEDGMENTS

Although this dissertation has my name on it, this work would not have been possible without the incredible help and support that I have received throughout my academic career. Thank you first to my advisor, Dan Repeta, for five and a half years of continuous support, mentorship, and guidance. Through your help, Dan, I was able to accomplish complex, independent research that I am extremely proud of. Through my time in the Repeta lab, I grew considerable as a scientist, and I'm so excited to take my next steps on my academic path, knowing that I have been extremely well prepared for a career in science. Thank you also to my committee members, Valier Galy, and Phil Gschwend. You both provided crucial expertise that helped me to focus my projects and ensured that I was rigorous in my analyses and conclusions. I enjoyed getting to share my work as it progressed and to bounce ideas around during committee meetings and my defense. I owe a huge thank you to Carl Johnson and Sean Sylva for all of their help and support with the NMR analyses. Carl, you especially took me under your wing and brought me from an NMR novice to someone that feels comfortable performing complex experiments on the instrument; I highly value the skills I developed with your help. Thank you also to Ben Van Mooy and Helen Fredricks for helping me to perform phosphonate uptake experiments in the Van Mooy lab. A big thank you also to the WHOI administration, particularly Mary Zawoysky and Sheila Clifford in the MC&G department, and to APO and the JP Office at MIT.

Of course, my scientific career did not start at WHOI. Thank you to Dennis Hansell and the whole Hansell lab for all of the training, mentorship, and experience you provided me as an undergraduate at the University of Miami. The Hansell lab sparked my love of DOM and I would not be in the position I am today without the opportunities you afforded me. Thank you also to Shannon Meseck and the staff and scientists at the NOAA NEFSC Milford Lab. Working with you, Shannon, I received my first chance to propose and conduct marine research, and my time at Milford affirmed my goal of pursuing a career in scientific research and education.

I am also so thankful to all of my lab mates, friends, and colleagues. Marianne, Lydia, Jay, Iulia and Luis, you were always a joy to be around, be it on long cruises, late nights in the lab, or parties in the Woods Hole Winter, and I couldn't have asked for better lab mates. Thank you to all of my friends in Woods Hole for the marathon Dungeons & Dragons sessions, board game nights, cross country skis, hikes, and Sunday brunches. Thank you to my roommates in Boston for several truly "good yards". A Ph.D. program is so much more than just an academic endeavor. It becomes your whole life for five and a half years, and I am so grateful for all of the fun and laughter I was able to share with you all during this time. Thank you also to the science party of PARAGON I, for the tremendous help while I collected thousands of liters of seawater, and for keeping me company on the long nights filtering samples.

Thank you to the SCOPE labs that provided additional sample collection, data analysis, and feedback on my projects. In particular, thank you to the Dave Karl, Karin Björkman,

Benedetto Barone, Eric Grabowski, Oscar Sosa, and Rhea Foreman for their advice, expertise and assistance on my phosphorus cycling project. Thank you also to the captain and crew of the *R/V Kilo Moana*, for several excellent expeditions into the North Pacific Subtropical Gyre.

Finally, thank you to my family for a lifetime of love and support. Mom and Dad, you both instilled in me an insatiable love of science and an awe of the natural world. You taught me the value of knowledge for knowledge's sake and always encouraged me to ask "why", and never be satisfied with the answer. You both pushed me to be my best, and supported me when I struggled, and I am so thankful to you for the upbringing you gave me. Thank you also to Alan and Karen for so warmly and immediately welcoming me into your (now our) awesome family. I have enjoyed immensely the past eight years of adventure, intellectual discussion, and appreciation for nature that we have shared together. And I owe my biggest thanks to Evan. For more than eight years you have been the biggest supporter of my triumphs and an unshakable foundation that provided the support and encouragement I needed when I felt like I was failing. Your brilliance always drives me to be the best scientist and person I can be, and your light is an eternal beacon for me though stormy nights. Thank you for your love and support, and for being a great parent to our wonderful dog, Penny. I love you.

Financial Support

The studies described in this dissertation were supported by the Simons Foundation (SCOPE award 329108 to D.M.K. and D.J.R.), the Gordon and Betty Moore Foundation (3794; D.M.K. and 6000; D.J.R.), and the National Science Foundation (NSF: OCE-1634080; D.J.R.) and I thank them for their support.

TABLE OF CONTENTS

LIST OF FIGURES

LIST OF TABLES

CHAPTER 1. THE CURRENT PARADIGM OF MARINE ORGANIC MATTER REACTIVITY

1.1 GLOBAL PATTERNS OF MARINE ORGANIC MATTER

Half of global primary production is performed by marine autotrophic organisms in the surface ocean, fixing as much as 150 Pg C per year into organic matter. While 2/3 of that carbon is respired by autotrophs, more than 50 Pg of reduced carbon is transformed into biomass that becomes available for heterotrophic metabolism and carbon export to the ocean interior. (Behrenfeld & Falkowski, 1997; Field et al., 1998; Huang et al., 2021; Westberry et al., 2008). Through several mechanisms, including grazing, leakage and exudation of organic matter across the cell membrane, and viral lysis, microbial biomass is converted into dissolved organic matter (DOM) and enters a pool of 662 Pg C, a pool similar in scale to the CO_2 in the atmosphere (Hansell et al., 2009; Zhang et al., 2018).

Operationally defined as OM that passes through a 0.2–0.7 μm filter, marine DOM is one of the largest actively cycling pools of organic carbon on the planet, and serves as an important reservoir of energy and nutrients to marine microbes. Over the past few decades, organic geochemists have endeavored to answer fundamental questions about DOM dynamics: 1) What are the major sources of marine DOM? 2) What factors impact the biological lability of DOM? 3) What are the ultimate fates of DOM and what controls the removal processes?

In this thesis, I present the results of two projects examining chemical controls that influence the degradation of DOM. The first project studied the molecular weight distribution of the components of high molecular weight DOM (HMWDOM). The work aims to critically examine the size–reactivity continuum hypothesis (SRC) and proposes a new conceptual model of HMWDOM composition and cycling (Benner & Amon, 2015). In the second project, I developed a fluorescence-based assay for measuring the activity of the C-P lyase enzyme, a

hydrolytic enzyme that degrades phosphonates—organic phosphorus compounds with a direct C-P bond—in DOM. Using this assay, I tested the hypothesis that localized phosphate limitation in the subsurface promotes dissolved organic phosphorus (DOP) degradation. Both of these projects add new knowledge and propose testable hypothesis regarding the factors that control the remineralization of DOM.

1.2 HYPOTHESES OF DOM LABILITY

The traditional framework used to describe DOM divides it into fractions based on biological reactivity. Biologically available, labile DOM ($_{l}$DOM) is the major product of photosynthetic production (Williams, 2000). $_{l}$DOM is characterized by short residence times (hours to days) and is quickly remineralized to CO_2 by microbes. This fraction of organic matter does not accumulate, and its rapid cycling supports most of the heterotrophic microbial production in the ocean (Carlson & Ducklow, 1995; Hansell et al., 2012). A portion of autochthonously produced DOM is not remineralized and accumulates as a biologically resistant, recalcitrant fraction. This accumulated DOM is divided into several subfractions based on average radiocarbon age and spatial/temporal changes in concentration. Semi-labile DOM ($_{sl}$DOM) has a residence time on the order of years to decades and contains identifiable biomolecules such as acylpolysaccharides (APS), proteins and lipids, as well as humic substances (HS) thought to be the transformation products of labile organic compounds (Aluwihare et al., 1997). Semi-refractory DOM and refractory DOM ($_{r}$DOM) have lifetimes on the order of centuries and millennia, respectively, and show increasing levels of biochemical, photochemical, and geochemical alteration (Baltar et al., 2021; Hansell, 2013; Hertkorn et al., 2006).

Several hypotheses have been proposed to explain the persistence of $_r$DOM in the ocean. The intrinsic recalcitrance hypothesis suggests that the bioavailability of a molecule is controlled by its chemical properties. This hypothesis is supported by observations of a systematic shift in molecular composition of DOM with water mass aging, preferential heterotrophic utilization of specific classes of organic matter, and the wide range in turnover times of DOM at the same location in the ocean, which indicates that remineralization of DOM is not governed purely by external environmental conditions (Flerus et al., 2012; Follett et al., 2014; Hertkorn et al., 2006; Zakem et al., 2021). In contrast, the emergent recalcitrance hypothesis states that DOM recalcitrance is a property of the DOM pool in the context of the ecosystem that arises from the continuous reworking of OM at all trophic levels of the microbial loop. DOM reactivity is based on the ability of the microbial community to utilize and rework the compounds; the model does not prescribe universal lability or recalcitrance to any specific fraction of DOM (Dittmar et al., 2021; Mentges et al., 2019).

Finally, the size-reactivity continuum hypothesis (SRC), postulates that large, reactive biomolecules are transformed through biochemical and geochemical processes into the smaller, recalcitrant organic matter that makes up the $_r$DOM pool. The diagenetic flow trends toward the production of small molecules, and the size of a compound is inversely related to its bioreactivity. Evidence for this hypothesis rests on higher rates of bacterial production and respiration of communities fed high molecular weight (> 1 kDa) DOM (HMWDOM), and on the older average radiocarbon age of low molecular weight DOM compared to HMWDOM (Amon & Benner, 1996; Benner & Amon, 2015; Broek et al., 2020; Loh et al., 2004; Walker et al., 2016). While it is likely that each of the mechanisms described in these models plays a role in

shaping the trends in DOM remineralization and the formation of $_r$DOM, each hypothesis needs additional rigorous testing.

1.3 ORGANIC NUTRIENTS

A portion of DOM contains nitrogen and phosphorus, necessary nutrients for microbial growth. In oligotrophic regions of the ocean where inorganic nutrient concentrations are low, dissolved organic nitrogen (DON), and dissolved organic phosphorus (DOP) comprises more than 80% of the dissolved N and P, suggesting the importance of those compounds as sources of nutrients for marine microorganisms. To understand the role of N and P on DOM remineralization, we need to understand the composition of the material and the microbial mechanisms for organic nutrient remineralization and incorporation.

Canonically, DOP was thought to occur only as phosphate esters. Molecules with this structural motif tend to be highly labile with residence times in the ocean of seconds to days. Recent work, however, has demonstrated the importance of organic phosphonate compounds in DOP (Acker, 2021; Clark et al., 1999; Kolowith et al., 2001; Pasek et al., 2014). Indeed, phosphonates, compounds with a direct C-P bond have been shown to make up as much as 25% of HMWDOP and their degradation can lead to the release of methane in the surface ocean, contributing the surface supersaturation of dissolved methane (Karl et al., 2008; Kolowith et al., 2001; Repeta et al., 2016).

Marine microorganisms have a suite of enzymatic systems that they use to degrade and remineralize DOP. Alkaline phosphatase (AP) is the most prevalent enzyme in this class and converts phosphate monoesters to inorganic hydrogen phosphate (HPO_4^{-2}; P_i). Studies of alkaline phosphatase activity (APA) have shown that it is ubiquitous in the ocean, both as a cell

associated mechanism, and as a free enzyme. Up to 63% of P_i in oligotrophic surface waters could be released daily from DOP due to APA, highlighting its importance in the recycling of P_i (Duhamel et al., 2011).

While phosphate ester remineralization has been well studied in the ocean, comparatively little is known about the microbial decomposition of phosphonates. Phosphonates contain a highly stable C-P bond and necessitates dedicated enzymes for P oxidation and hydrolysis. While there are several enzymes that catalyze the oxidation of specific phosphonates, the only known non-specific phosphonate degradation pathway is the C-P lyase pathway (Kononova & Nesmeyanova, 2002; Sosa et al., 2019). Due to the prevalence of phosphonates, and the connection between C-P lyase activity (CLA) and aerobic methane production, it is important to understand what factors regulate CLA in the marine environment (Karl et al., 2008; Repeta et al., 2016).

1.4 SUMMARY OF THIS DISSERTATION

This dissertation contains four chapters examining aspects of DOM and linking chemical traits to biological lability. In Chapter 2, the molecular weight distribution of HMWDOM was studied using a combination of mixed-mode, gel-permeation chromatography (MMC) and diffusion-ordered spectroscopy (DOSY). Chapter 3 examined the relationship between HS content and the carbon isotopic composition of HMWDOM. Coupled with the MW distribution measurements made in the previous chapter, this work reexamines the SRC using the framing of HMWDOM as a two-component system. Chapter 4 describes the development of a fluorescent assay for measuring the activity of CLA in natural water samples. The assay was validated under a range of conditions using both model organisms and natural heterotrophic communities. This

work presents the first vertical profiles of CLA rates in the ocean. Finally, Chapter 5 discusses the relationship between inorganic nutrient flux and phosphonate production and degradation in oligotrophic systems.

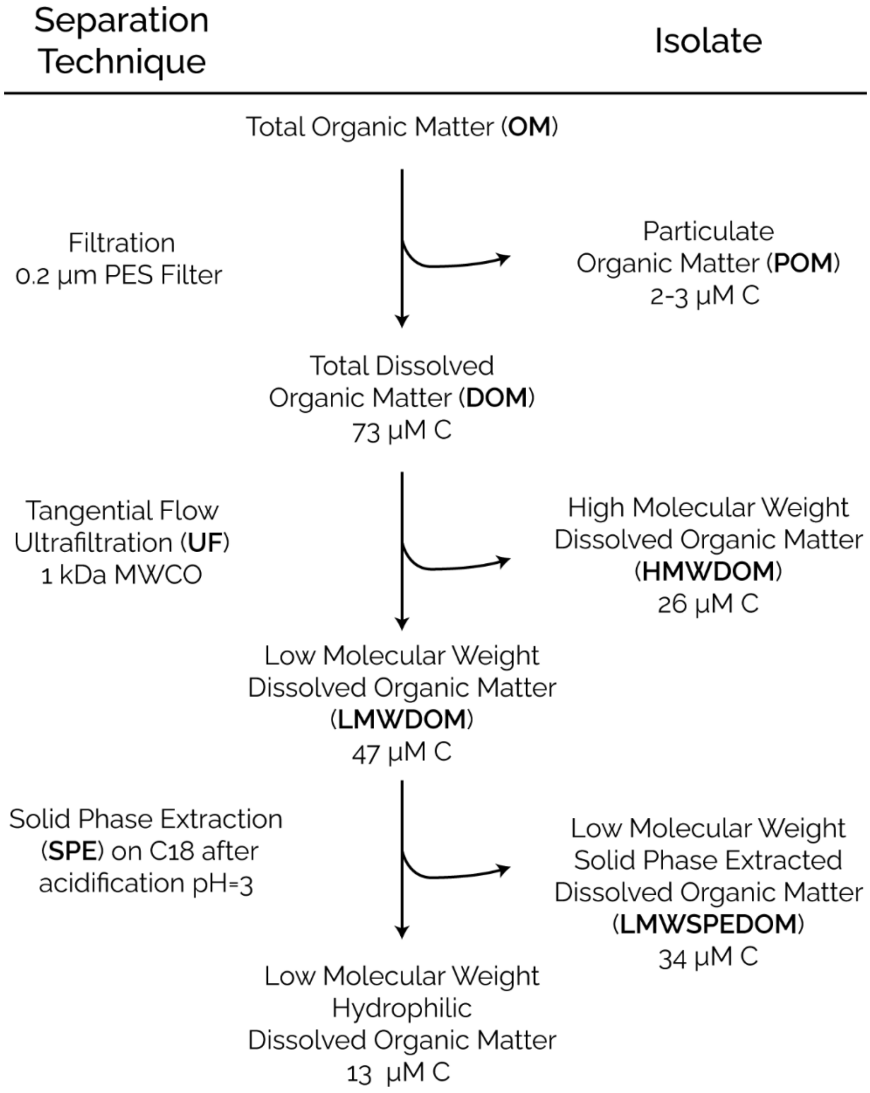

Figure 1.1: Scheme used to isolate fractions of DOM for analysis based on both size and chemical separatory techniques. Material isolated by each technique is shown in the column on the right, while material that is not retained is shown in the middle column. Also listed is the estimated amount of carbon associated with each fraction in the surface NPSG.

Chapter 2 describes the use of DOSY, coupled with mixed-mode chromatography (MMC), to assess the MW distribution of the components of HMWDOM. Fractions of DOM

were isolated using size-based separation techniques according to the scheme described in Figure 1.1. POM was separated from DOM using a 0.2 μm filter. HMWDOM was extracted from the filtered seawater via ultrafiltration (UF). Finally, LMW hydrophobic DOM (LMWSPEDOM) was extracted from the UF permeate via solid phase extraction. I found that average MW and HS content increased with depth and that HS in all samples had a lower MW than the APS. Two HMWDOM samples, one from 15 m and the other from 900 m were fractionated by MMC, yielding fractions with varying amounts of HS and APS. DOSY analysis of these fractions showed that the APS MW decreases with depth and that the distribution of MW falls into a fairly narrow range, suggesting a continuous, homogenous degradation of the material. The MW of HS in the 900 m sample was close to the MW cut-off of the filter and the MW distribution again fell within a fairly narrow range. This is in contrast with the MW distribution of HS in the surface sample, which was broad, suggesting a fraction of HS is produced in the surface but is degraded and replaced by smaller compounds or transformed into small HS, which persist in the mesopelagic.

In Chapter 3, the relationship between HS content and the carbon isotopic composition of HMWDOM was examined. The APS and HS components of HMWDOM were partially separated by MMC, and the relative HS content in different MMC fractions was determined via ^{1}H-NMR spectral subtraction. The proportion of HS in MMC fractions spanned 4%–80%, while the Δ^{14}C values of the fractions spanned a broad range from 2‰ to -309‰, representing a wide range of apparent radiocarbon ages. Δ^{14}C values correlated well with the proportion of HS in each fraction. The results from this analysis suggest that HMWDOM is a two-component mixture of APS, which has a modern radiocarbon age and a short residence time in the surface ocean, and HS, which has a radiocarbon age intermediate between LMWSPEDOM and APS.

The HS endmember in the deep HMWDOM sample also had a predicted $\delta^{13}C$ endmember that is isotopically depleted compared to total DOM, suggesting HS is the degradation product of material with a light $\delta^{13}C$ signature, such as lipids. Together, this work demonstrates that APS is autochthonously produced while HS decomposition results in a reduction in MW without a change in age. This work demonstrates that HMWDOM is not a diagenetic intermediate between POM and $_r$DOM and highlights the intricate and diverse mechanisms that control the cycling of HMWDOM.

Chapter 4 describes the development of a new chemical assay to measure CLA in natural waters. This assay uses a synthetic, fluorescent phosphonate compound, which is added to environmental or culture samples and incubated, allowing C-P lyase to cleave the phosphonate from the probe. Both the artificial substrate and the cleavage product are recovered from the sample by solid phase extraction, and the rate of phosphonate degradation is determined by measuring the amount of cleavage product produced. This assay was tested with several strains of heterotrophic bacteria known to degrade phosphonates. Only the bacteria containing the C-P lyase pathway showed any activity with this assay. This work also presents the first profiles of CLA in the seawater, from samples collected at Station ALOHA. The profiles displayed a maximum in CLA concurrent with the DCM and the top of the nitracline, suggesting that an imbalance in the flux of nutrients from depth may promote the degradation of organic phosphorus compounds.

Finally, two of the hypotheses explaining the subsurface CLA maximum are tested in Chapter 5. A high-resolution sampling scheme centered on DCM was employed to study the localized nutrient fluxes and DOP degradation rates. The relative N:P flux at the DCM during these experiments was low, and no CLA maxima were observed. These results serve as a

negative test of the hypothesis and continue to support the idea that CLA is enhanced when the N:P flux leads to P limitation; however, the lack of a strong CLA signal precludes making generalized conclusions. Rates of P uptake and reduction were also measured to determine if phosphonate production is enhanced at the DCM. No signal of enhanced P reduction was measured. Additionally, the P composition of suspended POM was examined for phosphonate concentrations. Few phosphonates were detected, a result that does not support the hypothesis of greater phosphonate concentrations in the subsurface promoting CLA. Further observations of nutrient fluxes and CLA are needed to understand the localized controls on DOP remineralization in the NPSG.

Together, these research projects add further insight into the multifaceted mechanisms that control organic matter remineralization and chemical recalcitrance in the ocean. Chapters 2 and 3 demonstrate that HMWDOM should not be considered one, uniform pool of carbon with a uniform reactivity, but rather as two distinct components that happen to have similar size distributions. Thus, operationally defined factions of DOM must be rigorously defined if models of DOM remineralization are to be based on bulk characterization of these fractions. Chapters 4 and 5 provide new a method for measuring the degradation of an important fraction of DOP in the ocean. The results of this project add to our understanding of an important mechanism for P uptake in oligotrophic systems, and highlight novel aspects of phosphonate cycling in the subsurface. Future studies of DOM dynamics should continue the practice of using chemical characteristics to define the fraction of interest and should thoroughly define the chemical space of the DOM being studied. This will improve the field's ability to peer into the black box of DOM.

1.5 REFERENCES

Acker, M. (2021). *Phosphonate biogeochemical cycling in the marine environment: From an ocean scale to a molecular scale* [Doctor of Philosophy]. Massachusetts Institute of Technology.

Aluwihare, L. I., Repeta, D. J., & Chen, R. F. (1997). A major biopolymeric component to dissolved organic carbon in surface sea water. *Nature*, *387*(6629), 166–169. https://doi.org/10.1038/387166a0

Amon, R. M. W., & Benner, R. (1996). Bacterial utilization of different size classes of dissolved organic matter. *Limnology and Oceanography*, *41*(1), 41–51.

Baltar, F., Alvarez-Salgado, X. A., Arístegui, J., Benner, R., Hansell, D. A., Herndl, G. J., & Lønborg, C. (2021). What is refractory organic matter in the ocean? *Frontiers in Marine Science*, *8*(April), 1–7. https://doi.org/10.3389/fmars.2021.642637

Behrenfeld, M. J., & Falkowski, P. G. (1997). Photosynthetic rates derived from satellite-based chlorophyll concentration. *Limnology and Oceanography*, *42*(1), 1–20. https://doi.org/10.4319/LO.1997.42.1.0001

Benner, R., & Amon, R. M. W. (2015). The size-reactivity continuum of major bioelements in the ocean. *Annual Review of Marine Science*, *7*(1), 185–205. https://doi.org/10.1146/annurev-marine-010213-135126

Broek, T. A. B., Walker, B. D., Guilderson, T. P., Vaughn, J. S., Mason, H. E., & McCarthy, M. D. (2020). Low molecular weight dissolved organic carbon: Aging, compositional changes, and selective utilization during global ocean circulation. *Global Biogeochemical Cycles*, *34*(6). https://doi.org/10.1029/2020GB006547

Carlson, C. A., & Ducklow, H. W. (1995). Dissolved organic carbon in the upper ocean of the central equatorial Pacific Ocean, 1992: Daily and finescale vertical variations. *Deep-Sea Research Part II: Topical Studies in Oceanography*, *42*(2–3), 639–656. https://doi.org/10.1016/0967-0645(95)00023-J

Clark, L. L., Ingall, E. D., & Benner, R. (1999). Marine organic phosphorus cycling: Novel insights from nuclear magnetic resonance. *American Journal of Science*, *299*, 724–737. https://doi.org/10.2475/ajs.299.7-9.724

Dittmar, T., Lennartz, S. T., Buck-Wiese, H., Hansell, D. A., Santinelli, C., Vanni, C., Blasius, B., & Hehemann, J. H. (2021). Enigmatic persistence of dissolved organic matter in the ocean. *Nature Reviews Earth and Environment*, *2*(8), 570–583. https://doi.org/10.1038/s43017-021-00183-7

Duhamel, S., Björkman, K. M., Van Wambeke, F., Moutin, T., & Karl, D. M. (2011). Characterization of alkaline phosphatase activity in the North and South Pacific Subtropical Gyres: Implications for phosphorus cycling. *Limnology and Oceanography*, *56*(4), 1244–1254. https://doi.org/10.4319/lo.2011.56.4.1244

Field, C. B., Behrenfeld, M. J., Randerson, J. T., & Falkowski, P. G. (1998). Primary production of the biosphere: Integrating terrestrial and oceanic components. *Science*, *281*(5374), 237–240.

Flerus, R., Lechtenfeld, O. J., Koch, B. P., McCallister, S. L., Schmitt-Kopplin, P., Benner, R., Kaiser, K., & Kattner, G. (2012). A molecular perspective on the ageing of marine dissolved organic matter. *Biogeosciences*, *9*(6), 1935–1955. https://doi.org/10.5194/bg-9-1935-2012

Follett, C. L., Repeta, D. J., Rothman, D. H., Xu, L., & Santinelli, C. (2014). Hidden cycle of dissolved organic carbon in the deep ocean. *Proceedings of the National Academy of Sciences of the United States of America*, *111*(47), 16706–16711. https://doi.org/10.1073/pnas.1407445111

Hansell, D. A. (2013). Recalcitrant dissolved organic carbon fractions. *Annual Review of Marine Science*, *5*, 421–425. https://doi.org/10.1146/annurev-marine-120710-100757

Hansell, D. A., Carlson, C. A., Repeta, D. J., & Schlitzer, R. (2009). Dissolved organic matter in the ocean: A controversy stimulates new insights. *Oceanography*, *22*(4), 202–211. https://doi.org/10.1038/ncomms8422

Hansell, D. A., Carlson, C. A., & Schlitzer, R. (2012). Net removal of major marine dissolved organic carbon fractions in the subsurface ocean. *Global Biogeochemical Cycles*, *26*(1), 1–9. https://doi.org/10.1029/2011GB004069

Hertkorn, N., Benner, R., Frommberger, M., Schmitt-Kopplin, P., Witt, M., Kaiser, K., Kettrup, A., & Hedges, J. I. (2006). Characterization of a major refractory component of marine dissolved organic matter. *Geochimica et Cosmochimica Acta*, *70*(12), 2990–3010. https://doi.org/10.1016/j.gca.2006.03.021

Huang, Y., Nicholson, D., Huang, B., & Cassar, N. (2021). Global estimates of marine gross primary production based on machine learning upscaling of field observations. *Global Biogeochemical Cycles*, *35*(3). https://doi.org/10.1029/2020GB006718

Karl, D. M., Beversdorf, L. J., Björkman, K. M., Church, M. J., Martínez, A., & Delong, E. F. (2008). Aerobic production of methane in the sea. *Nature Geoscience*, *1*(7), 473–478. https://doi.org/10.1038/ngeo234

Kolowith, L. C., Ingall, E. D., & Benner, R. (2001). Composition and cycling of marine organic phosphorus. *Limnology and Oceanography*, *46*(2), 309–320. https://doi.org/10.4319/lo.2001.46.2.0309

Kononova, S. V., & Nesmeyanova, M. A. (2002). Phosphonates and their degradation by microorganisms. *Biochemistry. Biokhimiia*, *67*(2), 184–195. https://doi.org/10.1023/A:1014409929875

Loh, A. N., Bauer, J. E., & Druffel, E. R. M. (2004). Variable ageing and storage of dissolved organic components in the open ocean. *Nature*, *430*, 877–880.

Mentges, A., Feenders, C., Deutsch, C., Blasius, B., & Dittmar, T. (2019). Long-term stability of marine dissolved organic carbon emerges from a neutral network of compounds and microbes. *Scientific Reports*, *9*(17780), 1–13. https://doi.org/10.1038/s41598-019-54290-z

Pasek, M. A., Sampson, J. M., & Atlas, Z. (2014). Redox chemistry in the phosphorus biogeochemical cycle. *Proceedings of the National Academy of Sciences of the United States of America*, *111*(43), 15468–15473. https://doi.org/10.1073/PNAS.1408134111

Repeta, D. J., Ferrón, S., Sosa, O. A., Johnson, C. G., Repeta, L. D., Acker, M., Delong, E. F., & Karl, D. M. (2016). Marine methane paradox explained by bacterial degradation of dissolved organic matter. *Nature Geoscience*, *9*(12), 884–887. https://doi.org/10.1038/ngeo2837

Sosa, O. A., Casey, J. R., & Karl, D. M. (2019). Methylphosphonate oxidation in *Prochlorococcus* strain MIT9301 supports phosphate acquisition, formate excretion, and carbon assimilation into purines. *Applied and Environmental Microbiology*, *85*(13), e00289-19. https://doi.org/10.1128/AEM.00289-19

Walker, B. D., Beaupré, S. R., Guilderson, T. P., McCarthy, M. D., & Druffel, E. R. M. (2016). Pacific carbon cycling constrained by organic matter size, age and composition relationships. *Nature Geoscience*, *9*(12), 888–891. https://doi.org/10.1038/ngeo2830

Westberry, T., Behrenfeld, M. J., Siegel, D. A., & Boss, E. (2008). Carbon-based primary productivity modeling with vertically resolved photoacclimation. *Global Biogeochem. Cycles*, *22*. https://doi.org/10.1029/2007GB003078

Williams, P. J. (2000). Heterotrophic bacteria and the dynamics of dissolved organic material. In D. L. Kirchman (Ed.), *Microbial Ecology of the Oceans* (pp. 153–200).

Zakem, E. J., Cael, B. B., & Levine, N. M. (2021). A unified theory for organic matter accumulation. *Proceedings of the National Academy of Sciences*, *118*(6), e2016896118. https://doi.org/10.1073/pnas.2016896118

Zhang, C., Dang, H., Azam, F., Benner, R., Legendre, L., Passow, U., Polimene, L., Robinson, C., Suttle, C. A., & Jiao, N. (2018). Evolving paradigms in biological carbon cycling in the ocean. *National Science Review*, *5*(4), 481–499. https://doi.org/10.1093/nsr/nwy074

CHAPTER 2. COMPOSITIONAL DIVERSITY OF HIGH MOLECULAR WEIGHT DISSOLVED ORGANIC MATTER

2.1 ABSTRACT

The use of ultrafiltration to isolate high molecular weight dissolved organic matter (HMWDOM) from seawater is a fundamental tool in the marine organic chemist's tool box. Yet, many of the characteristics of HMWDOM remain poorly defined, such as the origins of its components and the size distribution of the isolated material. In this chapter, I use diffusion-ordered spectroscopy coupled with mixed-mode chromatography, to partially separate and examine the two major components of HMWDOM, acylpolysaccharides (APS) and humic substances (HS). The molecular weights (MW) of both APS and HS fall into a narrow size envelope with most of the material ranging from 1 to 6 kDa. The average size of both components also decreases with depth. In HMWDOM collected from both the surface and 900 m, APS has a narrow a size range that is normally distributed about the mean, suggesting a constant, monotonic degradation mechanism. In contrast, HS in the surface has a broad size distribution compared to APS, which shrinks at depth to a narrow size range just above the filter cut-off. Despite the decrease in MW distribution, the concentration of HS does not decrease with depth, suggesting that large HS in the surface is decomposed into smaller compounds without significant remineralization, or an additional source of small material supplies HS to the deep ocean. Based on these results, I propose a conceptual model of HMWDOM as a two-component mixture with APS and HS having different diagenetic fates.

2.2 INTRODUCTION

Marine dissolved organic matter (DOM) is comprised of a pool of hundreds of thousands of unique compounds in extremely low concentrations (Hansell et al., 2009). These low concentrations, in tandem with the high salt content of seawater, limit the number of analytical

techniques suitable for direct study of DOM composition. Therefore, techniques have been developed to isolate and concentrate DOM and reduce potential interferences from salt so that a broader array of analytical techniques can be deployed. The two most prevalent techniques used to concentrate and isolate DOM are solid phase extraction (SPE) and tangential flow ultrafiltration (UF). SPE is a chemical separatory technique in which seawater is passed over a hydrophobic resin, which adsorb a fraction of DOM for later elution with an organic solvent such as methanol (Dittmar et al., 2008). The extraction efficiency is highest for hydrophobic aliphatic and aromatic constituents of DOM, while highly polar, charged, and oxidized compounds pass through the SPE column more easily, resulting lower extraction efficiencies (Johnson et al., 2017). UF, the other DOM concentration technique, is performed by passing seawater through a filtration membrane at high pressure, with the direction of flow usually tangential to the membrane's pores. Water, most salts and dissolved organic species smaller than the nominal molecule weight cut-off (MWCO) of the filter pass through the pores and are discarded, while organic species larger than the MWCO retained in a reservoir and recirculated (Roland et al., 2009). This material is known as high molecular weight dissolved organic matter (HMWDOM; Benner et al., 1992). In an ideal UF system, all dissolved species larger than the MWCO would be retained while anything smaller is discarded. The MWCO of a membrane is established using model compounds, however, and studies of ultrafiltration systems have shown that the chemical characteristics of the DOM alter the retention efficiency (Guo & Santschi, 2007). Thus, HMWDOM collected by ultrafiltration can have a spectrum of sizes and chemical characteristics.

HMWDOM comprises up to 35% of marine DOM and has an average residence time in the surface ocean on the order of decades, making up a large pool of semi-labile organic carbon

(Hansell, 2013; Loh et al., 2004; Walker et al., 2016). Compositional analyses of HMWDOM have shown it to be a mixture of two distinct molecular classes; 50-70% of the carbon is in biopolymers (BP) such as acylpolysaccharides (APS), proteins, nucleic acids, and lipids, while up to 40% of the carbon is uncharacterized humic substances, which are a diverse class of molecules characterized as being carboxylic rich and alicyclic (HS; Repeta & Aluwihare, 2006).

While HMWDOM is functionally defined as organic matter (OM) larger than the MWCO of the filter, little is known about the MW distribution of the components that comprise it. Two studies conducted in the coastal Atlantic Ocean in the Mid-Atlantic Bight and the Gulf of Maine, and two studies in the Gulf of Mexico found that HMWDOC isolated by a 1 kDa MWCO filter comprised 20-35% of the total DOC, while HMWDOC with isolated by a 10 kDa MWCO filter comprised just 3-6% of DOC (Carlson et al., 1985; Guo et al., 1994, 1996; Maurer, 1976). This indicates that the majority of HMWDOM is comprised of compounds within a narrow molecular weight (MW) envelope between 1 and 10 kDa, and that the BP component is not comprised of very large, complex macromolecules. These studies, however, did not constrain the MW distribution of HMWDOM within that 10 kDa envelope, and did not differentiate between the BP and HS fractions. Additionally, three of these studies were conducted along the coast and one in a marginal sea, and the collected material may not have been representative of pelagic HMWDOM composition (Carlson et al., 1985; Guo et al., 1994, 1996). Further elucidation of the MW distribution of HMWDOM could help answer outstanding questions about the composition and cycling of this globally important pool of organic carbon.

APS is the most abundant component of BP, comprising up to 90% of the identifiable biomolecules. Its spectral characteristics are highly conserved through the ocean interior and across ocean basins. Monosaccharide analysis reveals APS is composed in part of seven major

neutral sugars in approximately equimolar concentrations and the relative abundance of these monosaccharides is spatially and temporally uniform (Aluwihare et al., 1997; McCarthy et al., 1996; Repeta et al., 2002; Repeta & Aluwihare, 2006; Sakugawa & Handa, 1985). The exact biological source of APS is unknown but its ubiquity in the ocean suggests either production by a globally abundant microbe, or that APS production is highly conserved (McCarthy et al., 1993). Radiocarbon analysis of neutral monosaccharides hydrolyzed from APS yields a turnover time of 1-3 or 20-25 years, longer than common energy storage polysaccharides such as laminarin, suggesting the presence of a structural motif that resists biological degradation (Panagiotopoulos et al., 2019; Piontek et al., 2011; Repeta & Aluwihare, 2006). APS is also rich in macronutrients such as nitrogen and phosphorus, making its biological recalcitrance surprising (Aluwihare et al., 2005; Karl et al., 2001; Repeta et al., 2016). A more accurate assessment of the MW of APS could elucidate reasons for its recalcitrance by examining changes in the spectral characteristics and MW distribution between freshly synthesized APS in the surface and degraded APS in the subsurface. If APS MW decreases continuously during degradation while the MW remains normally distributed around the mean MW, that could suggest a slow diagenesis of the material, potentially due to exoenzyme activity continuously removing sugars (Arnosti, 2011). Conversely, if the decrease in average MW is accompanied by a shift in the MW distribution, that would suggest the preferential remineralization of some component of APS. This may reflect a biological strategy for metabolizing APS—such as hydrolysis of the polysaccharide backbone to halve the MW or rapid extracellular binding of HMW APS followed by partial hydrolysis on the cell membrane—which allows for its rapid uptake and removal (Arnosti, 2011; Cuskin et al., 2015; Nagata et al., 2003; Reintjes et al., 2017).

HS, the other major component of HMWDOM, is a broad class of compounds. ^{13}C nuclear magnetic resonance (NMR) spectroscopy shows HS is carboxylic acid and alkyl rich, containing both alicyclic and aliphatic moieties. The processes of HS production in the ocean are unknown, but proposed mechanisms include the abiotic condensation of small molecules, photopolymerization of large biomolecules, and the aggregation of refractory compounds into supramolecular conformations (Arakawa et al., 2017; Gagosian & Stuermer, 1977; Piccolo, 2001; Stuermer & Harvey, 1974). Analysis of HS in HMWDOM by high-resolution mass spectrometry (HR-MS) showed that the average MW of HS was much lower than the 1 kDa MWCO of UF membranes and similar in MW distribution to the material extracted via SPE (Hertkorn et al., 2006; Zark & Dittmar, 2018). This could be due to a bias in HR-MS for the detection of low molecular weight compounds or due to the retention of these compounds by the UF membrane. It is possible that much of the HS fraction is smaller than the MWCO of the filter and is retained by fouling of the filter membrane, exaggerating its contribution to the >1 kDa size class. In fact, membrane fouling and the retention of low molecular weight compounds is frequently observed in UF systems (Guo et al., 2000; Ly & Hur, 2018). Analysis of the MW distribution of HS is needed to determine how much of the material in this fraction is below the MWCO of the filter and to investigate the relationship between HS in HMWDOM and low molecular weight HS retained by SPE (LMWSPEDOM).

In this study, I examined the size distribution of APS and HS in HMWDOM. Using mixed-mode chromatography (MMC), I separated HMWDOM into fractions with different amounts of APS and HS. While MCC is a size dependent separation technique, it also performs some selective separation based on chemical characteristics (De Nobili & Chen, 1999). To overcome this obstacle, I used diffusion-order spectroscopy (DOSY) to independently estimate

the MWs of the APS and HS components of HMWDOM in the different fractions separated by MMC. DOSY is a pseudo-2D NMR technique that applies pulsed-field gradients to the NMR sample, causing different spin states to evolve along the length of the NMR tube. The sample is then allowed to diffuse before an inverse gradient is applied to reset the spin states. When signals are collected under varying gradient strengths, the change in peak intensity with increased gradient strength can be used to determine the diffusivity of the compounds in the sample. The diffusivity of a molecule is related to its hydrodynamic radius by the Stokes-Einstein equation (Johnson Jr., 1999). Through the use of MW standards, an approximate relationship between diffusivity and molecular weight can be developed (Šmejkalová & Piccolo, 2008). With this tool, I examined the MW distribution of the components of HMWDOM in order to determine the potential retention of low molecular weight compounds by UF and refine MW estimates of HMWDOM, providing new insight into longstanding questions about the cycling of organic matter in the ocean.

2.3 MATERIALS AND METHODS

2.3.1 Isolation and Concentration of DOM

Large volume seawater samples were collected from 15 m, 615 m, and 900 m at the Natural Energy Laboratory in Kona, Hawaii (NELHA) during March, 2019. Whole seawater was prefiltered through a 0.2 μm PES cartridge filter to remove particulate matter. HMWDOM samples were extracted via UF using a custom continuous UF system. For a complete description see Roland et al. (2009), but in brief, prefiltered seawater is pumped through spiral wound tangential flow filtration membranes with a nominal MWCO ≥1 kDa, retaining DOM larger than 1 kDa. Filtration was performed in 24-hour batches during which time, approximately 2,000 L of seawater were concentrated to between 20-40 L. After 7 filtration cycles, the concentrates

(retentates) were combined and the sample volume was reduced again to 20 L. This final volume contains the HMWDOM from approximately 12,000 L of seawater. In the lab at Woods Hole Oceanographic Institution, the samples were further concentrated and desalted by diafiltration with deionized water, and lyophilized, yielding a fluffy, white powder. Freeze-drying has been demonstrated as an efficient method for isolating HMWDOM without changing DOM size (Minor et al., 2002). Approximately 15% of the total DOM was recovered, giving similar yields as reported by others (Broek et al., 2017; McCarthy et al., 2010).

LMWSPEDOM was extracted from the UF permeate. SPE cartridges (Supelclean™ ENVI™-18; Supelco) with a 10 g bed weight were rinsed and activated before use with 50 mL of methanol followed by 100 mL of high purity water (18.2 MΩ cm [MQ-H2O]). The permeate (< 1 kDa) from the UF system was pumped into PTFE lined barrels and acidified to pH = 2 with HCl. 200 L of permeate was pumped through the SPE cartridge at a flow rate of 75 mL/min and the cartridges were frozen until they could be analyzed. To recover LMWSPEDOM, the cartridges were thawed and rinsed with 100 mL of MQ-H_2O to remove salts. LMWSPEDOM was then eluted with 100 mL of methanol pumped through the bed at 5 mL/min. The samples were dried under vacuum at room temperature. Previous studies show that ~45% of DOC is captured in the LMWSPEDOC fraction (Dittmar et al., 2008; Zigah et al., 2017).

2.3.2 Size Separation of HMWDOM

Mixed-mode chromatography (MMC) was used to separate the components of HMWDOM. Chromatography was performed with a column (7.8 x 300 mm, 9 μm; Supelcogel) packed with sulfonated (8% crosslinked) polystyrene/divinylbenzene gel with calcium as the counter ion. This column separates components based on size, with higher MW components being less retained and eluting early in the analysis, while lower MW components are more

strongly retained and elute later in the analyses. The column also has some chemical specificity, whereby the Ca^{+2} interacts with specific vicinal -OH groups of carbohydrates, and with carboxyl groups in HS, improving the separation of the sample (Honda et al., 1984). MMC was performed on an Agilent HPLC (Agilent 1260 Series) consisting of a degasser, quaternary pump, autosampler, heated column compartment, diode array and refractive index detectors (DAD and RID respectively), and a fraction collector. The column compartment was used to maintain a consistent column temperature of 45ºC. MQ-H_2O was used as the mobile phase at a flowrate of 0.25 mL min-1 and each chromatographic run lasted for 40 minutes. In total 296 chromatographic injections were performed for the surface sample and 236 injections were performed for the 900 m sample. It is expected that the Ca^{+2} counterion was continuously being stripped from the column through ionic interactions with the HMWDOM. To ensure that this stripping was not affecting the separation, all chromatograms were compared after each batch of 35 injections and the size fractions were only pooled if no deviation in the chromatography was detected. There was no detectable difference between the first and last chromatographic runs (injection #1 and #296), suggesting a decline in the separation did not occur.

Freeze-dried HMWDOM samples were dissolved in MQ-H_2O to a concentration of 20 mg mL^{-1} and 25 µL (0.5 mg) of sample were injected in each run. One-minute fractions were collected between 17 and 28 minutes, coinciding with sample elution. Corresponding fractions from multiple collections were pooled and dried under vacuum at ambient temperature for analysis.

Molecular weight (MW) standards were used to calibrate the MMC and to measure the size-based separation capabilities of the column. Polystyrene sulfonate, globular protein, and pullulan standards (all from PSS Polymer Standard Services, Germany) with a MW range of 0.3

to 22 kDa were used to represent the continuum of expected molecular weights and conformations in HMWDOM.

2.3.3 NMR Analysis of HMWDOM

NMR spectra were acquired on a Bruker Avance Neo NMR spectrometer operating at 400.13 MHz (B_0 = 9.4 Tesla) using TopSpin™ 4.1.3 software. Freeze-dried samples were dissolved in 1 mL D_2O (99.8%), frozen, and dried three times to fully deuterate exchangeable protons on the organic matter and to reduce interference from a (water) solvent peak. Before analysis, samples were dissolved a fourth time in 0.7 mL to a final concentration of 1 mg mL^{-1} D_2O (≥99.96 atom % D), transferred to 5 mm Wilmad® NMR tubes, and immediately analyzed. All spectra were acquired on a Bruker Prodigy inverse geometry 5 mm z-gradient broad band probe. All spectra were acquired at 302 K.

1D ^{1}H-NMR experiments were carried out using the Noesy-presaturation water suppression pulse program (NOESYGPPR1D; Bruker). The 90^o hard pulse length was set to 12 µs and a 10 ms mixing time was used. Acquisition time was 1.7 s and the relaxation delay (D1) was 2 s. For each spectrum, 128 scans and were collected.

DOSY experiments were performed using the STEBPGP1S19 pulse program (Bruker) which uses bipolar gradient pulses for diffusion, contains a z-axis spoiler gradient and uses a 3-9-19 water suppression sequence to reduce noise from the solvent peak. The maximum gradient strength was 53.5 G cm^{-1} and 32 linear gradient steps were used with power increments from 2 to 95% of the maximum gradient strength. For each gradient increment, 256 scans were collected. Gradient recovery delay was 200 µs, relaxation delay (D1) was 2 s, and the diffusion time (Δ) was 0.2 s. The magnetic field gradient pulse length (δ /2) was 1150 µs. DOSY spectra were processed with Bruker Dynamic Center 2.7.1. All peaks above baseline were analyzed. To

compare the size distribution of samples, the tenth, fiftieth, and ninetieth percentiles (D_{v10}, D_{v50}, and D_{v90} respectively) of the diffusivity distribution measured by DOSY were calculated. The span, expressed as $(D_{v90}-D_{v10})/D_{v50}$, provides a unitless metric for the broadness of the diffusivity distribution. Samples with a broader range of diffusivities, and presumably a broader range of MWs, will have higher span values. The full parameter set for each experiment can be found in the supplemental information.

The same MW standards were used to calibrate DOSY experiments and to create a MW-diffusivity standard curve. Additionally, Suwannee River Humic Acid (SRHA; International Humic Substances Society) was analyzed using the same parameter set. The molecular weight distribution of SRHA has been extensively studied and is well agreed upon, making it an excellent natural organic matter standard for intercomparison (Beckett, 1987; Reid et al., 1990; Song et al., 2010).

2.4 RESULTS AND DISCUSSION

2.4.1 NMR Spectroscopy of HMWDOM

2.4.1.1 Proton NMR of HMWDOM

^{1}H-NMR spectra of HMWDOM (Figure 2.1) are similar to those previously reported for marine samples (Aluwihare et al., 1997, 2002; Repeta et al., 2002). There is a broad peak centered at 3.5 ppm from protons associated with carbohydrates and a peak at 1.8 and 1.2 ppm from N-acetyl functional groups and alkyl moieties, respectively. The peaks at 3.5 and 1.8 are associated primarily with APS, while the peak at 1.2 is the combination of signals from APS and HS. Beneath these features, is a broad background signal from 4 to 1 ppm associated with alicyclic and aliphatic materials that make up HS (Hertkorn et al., 2006; Repeta et al., 2002). The

broad peaks, which are characteristic of DOM NMR spectra, arise because DOM is a complex mixture of chemically similar compounds. The peaks in the spectra represent the averages of all the compounds in the sample. The relative peak areas of the APS and HS signals can provide a semi-qualitative estimate of the amount of each class of HMWDOM. The HS regions show increased resonance in the deeper samples (Figure 2.1), suggesting that the proportion of HS in HMWDOM increases with depth.

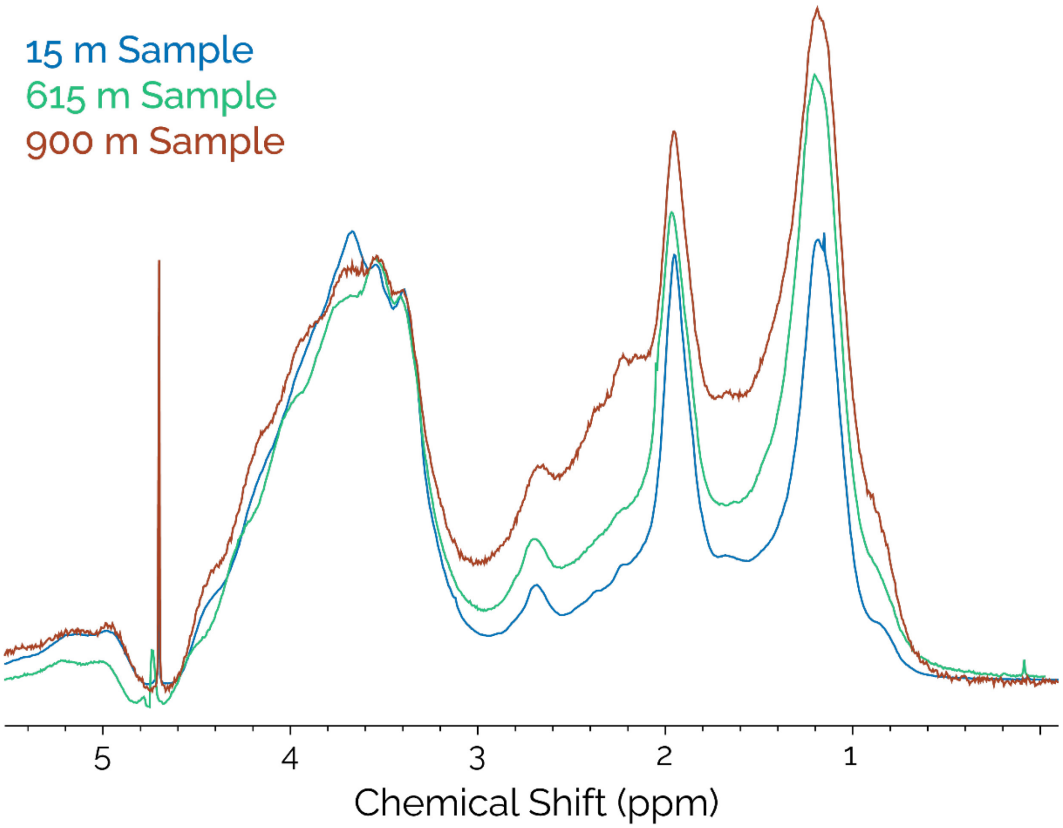

Figure 2.1: ^{1}H-NMR spectra of 15 m (blue), 615 m (green), and 900 m (red) HMWDOM. All spectra were normalized at 3.3 ppm.

2.4.1.2 Diffusivity analysis of HMWDOM

MW standards were used to correlate diffusivity with MW for the different components of HMWDOM. Double-logarithmic plots of diffusivity against MW were highly linear (r^2 >

0.99) across the MW range of HMWDOM (Figure 2.2). Due to the complex nature of DOM, DOSY can only be used to provide an estimate of MW based on assumptions made about the conformation of the molecules. It is believed that molecular shape exists in a spectrum between molecules that have a primary axis (rods) and molecules that are more spherical in shape (balls). Using MW standards that represent the extrema of this continuum, the MW range of components of DOM can be constrained (Lam & Simpson, 2009). From the ^{1}H-NMR spectra and from previous work, the components of HMWDOM were related to one of the MW standards. Polystyrene sulfonate displays rod-like characteristics and is commonly used as a MW standard for natural humic acid samples (Daoud & Tremblay, 2019; Guéguen & Cuss, 2011; Pelekani et al., 1999; Perminova et al., 2003; Reemtsma & These, 2003; Šmejkalová & Piccolo, 2008; Song et al., 2010). Studies of HS macromolecular structure suggest that, at low concentrations and pH greater than 3.5, HS takes on a flexible rod-like conformation, and thus is well represented by polystyrene sulfonate (Ghosh & Schnitzer, 1980; Kawahigashi et al., 2005). The APS component is modeled by pullulan, a long chain linear polysaccharide comprised of repeating maltotriose subunits that has an intermediate shape between rods and balls (Politi et al., 2006; Viel et al., 2003). The diffusivities of globular protein (GP) standards were also measured as representative of the ball-like extreme of the shape continuum model. As APS is a branched polysaccharide, its shape may fall between pullulan and GP, although I expect it to more closely resemble pullulan due to similarities in functional groups and conformation (Vink, 1990). For the rest of this discussion, the MW of APS and HS will be calculated using DOSY standard curves of pullulan and polystyrene respectively as they are a good representation of the hydrodynamic shape of the HMWDOM components.

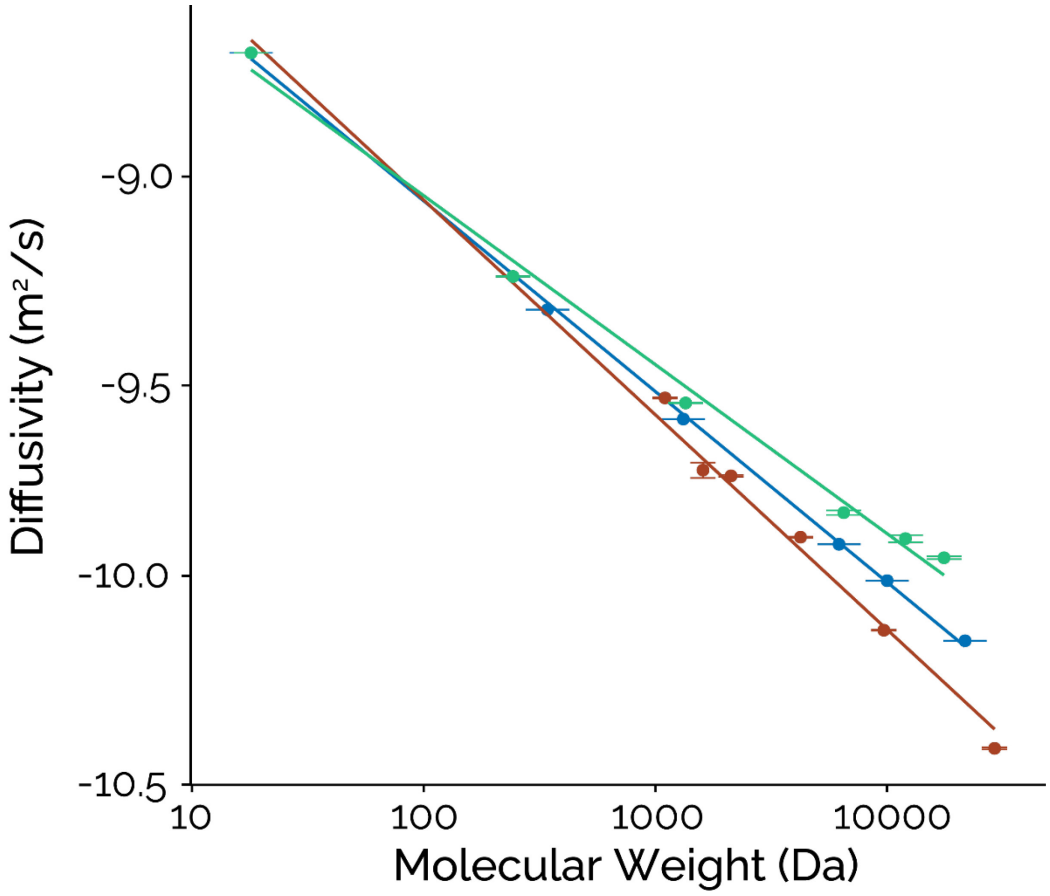

Figure 2.2: MW standard curves generated using polystyrene sulfonate (red), pullulan (blue), and globular protein (green) standards. The coefficient of determination (r^2) for each curve is greater than 0.99. The slopes for each curve are -0.54, -0.48, and -0.42 for the polystyrene sulfonate (red), pullulan (blue), and globular protein (green) standards, respectively.

In the DOSY spectra of HMWDOM, the peaks in the ^{1}H-NMR spectra assigned to APS and HS separate along the diffusion dimension (Figure 2.3). The peaks assigned to APS (3.5 ppm, 1.8 ppm) have a lower diffusivity and so a higher average MW as compared to peaks assigned to HS (2.2 ppm, 1.5 ppm) in all samples. Using the standard curves for pullulan, the MW of the APS component of the 15, 615, and 900 m HMWDOM were 6.1 ± 0.3, 4.4 ± 0.1, and 3.1 ± 0.1 kDa while the HS MWs calculated using the polystyrene sulfonate standard curves were 2.7 ± 0.2, 1.6 ± 0.1, and 1.3 ± 0.1 kDa respectively. The reported uncertainties represent the error in diffusivity curve fitting based on covariance analysis. They are not a measure of the MW

distribution of each component but instead indicate how closely the observed changes in signal intensity under varied gradient field strengths match with the predicted weakening of the signal. A small error indicates that the sample behaves as expected in the DOSY experiment (Johnson Jr., 1999). The span of both the APS and HS components decreased with depth in all three HMWDOM samples. The HS span in the 15 m, 615 m, and 900 m samples was 0.54, 0.45, and 0.28, respectively while the APS span in those samples was 0.18, 0.15, and 0.15, respectively. The width of the HS MW distribution showed a large decrease, suggesting that the 900 m sample became more homogenous with regards to MW as compared to the 15 m sample. The APS span has only a slight decrease, suggesting that the MW distribution is fairly constant with depth.

The diffusivity values measured for each component in the HMWDOM samples are a weighted average of the MWs of HS and APS constituents. Notice that the diffusivity at 1.2 ppm is higher than the diffusivity at 3.3 ppm in both the 15 m and 900 m samples. The 1.2 ppm signal sees contributions from both HS and APS, and thus reflects a diffusivity value between the two constituents. To most accurately determine the MW of the individual components, diffusivity was analyzed at regions of the spectra where the signal can be attributed largely to one component (3.38 and 2.20 ppm for APS and HS, respectively).

The DOSY analyses also showed that the surface sample had a lower diffusivity and therefore a higher MW than the 900 m sample. The measured average MW of total HMWDOM decreases with depth from 3.5 kDa to 2.5 kDa. Two distinct mechanisms can explain this pattern. A decrease in MW of both APS (3.38 ppm) and HS (2.20 ppm) was observed between the 15 and 900 m samples, which contributed to the lower overall MW, as the measured diffusivity reflects the distribution of MWs of each component. Many mechanisms such as exoenzyme catabolism and UV degradation have been proposed for the breakdown of HMWDOM resulting in the

production of smaller molecules (Lechtenfeld et al., 2014). It is unclear whether all the material decreases in size, or if the larger material is remineralized, leaving only the smaller fractions behind.

A second contributor to the observed decrease in total MW is a change in the relative abundances of APS and HS in HMWDOM with depth, resulting in a shift in the net MW of sample. As the HS has a lower MW than the APS, an increase in HS contribution to HMWDOM with depth as indicated by the 1H NMR spectra, would result in a lower MW. Based on the ^{1}H-NMR spectra, the proportion of HS does appear to increase with depth, lending credence to the conclusion that the shift in MW also reflects a shift in the composition of HMWDOM. Both explanations contributed to the observed MW trends.

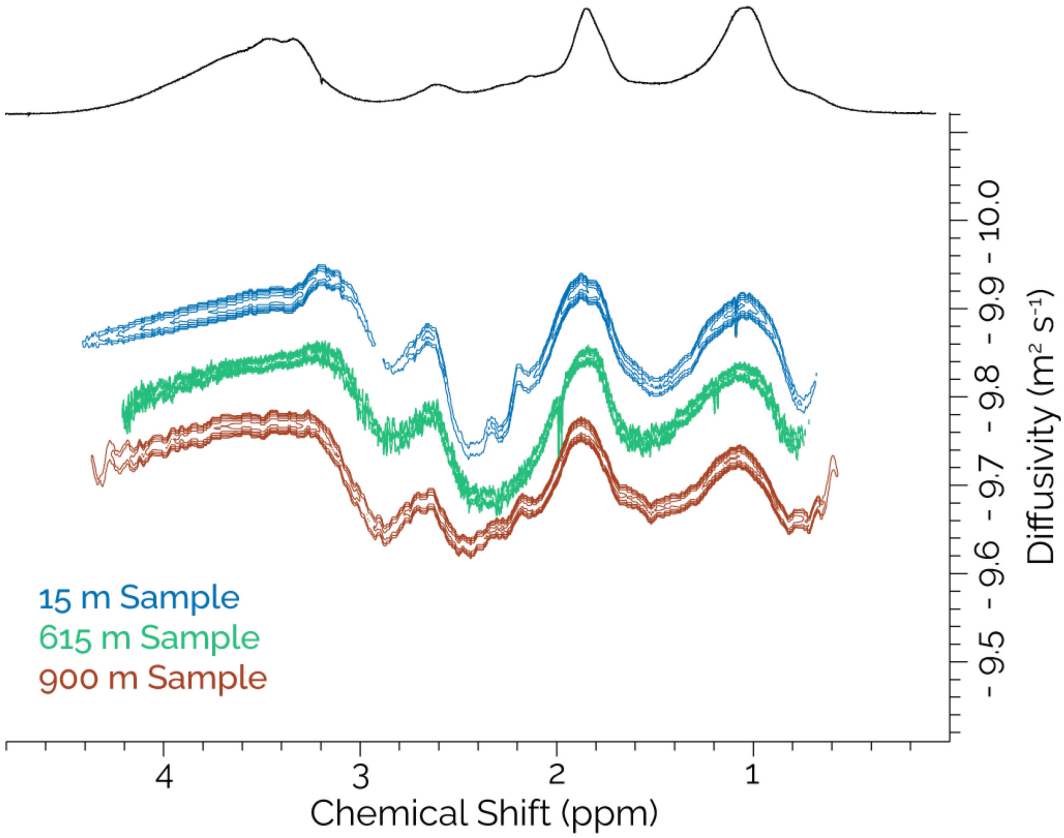

Figure 2.3: DOSY spectra of HMWDOM samples. Diffusivity is plotted on the vertical axis. A lower (more negative) diffusivity corresponds to a higher molecular weight.

2.4.2 MMC of HMWDOM

As the two components of HMWDOM have different MWs, MMC was used to further separate them. HMWDOM size-separated samples were collected in one-minute intervals between 17 and 28 min during the MMC chromatographic runs, yielding 11 discrete fractions. The mass of HMWDOM recovered in each fraction of the MMC is shown in Figure 2.4. As MMC is time and labor-intensive, only HMWDOM from 15 m and 900 m were size-fractioned. Samples from those two depths will be discussed in detail for the rest of this chapter. For both samples, most of the sample mass eluted in the middle of the chromatographic run, although a greater amount of material eluted in the later fractions (7-11) of the 900 m sample, indicating a greater proportion of this HMWDOM is lower MW, consistent with a greater relative

contribution from HS. The use of MMC results in separation based both on size and chemical composition, thus it is not expected that all the material in one fraction will have the same MW. MMC relies primarily on size exclusion to separate compounds by size, but has enhanced retention of hydroxylated compounds; as the ratio of Ca^{+2}-interacting to total hydroxyl groups on a compound increases, the compound will be more strongly retained, thereby improving the chromatography. The enhanced retention of vicinal-OH containing compounds caused APS to be better retained on the column than HS causing an offset between the MWs of APS and HS in earlier eluting fractions.

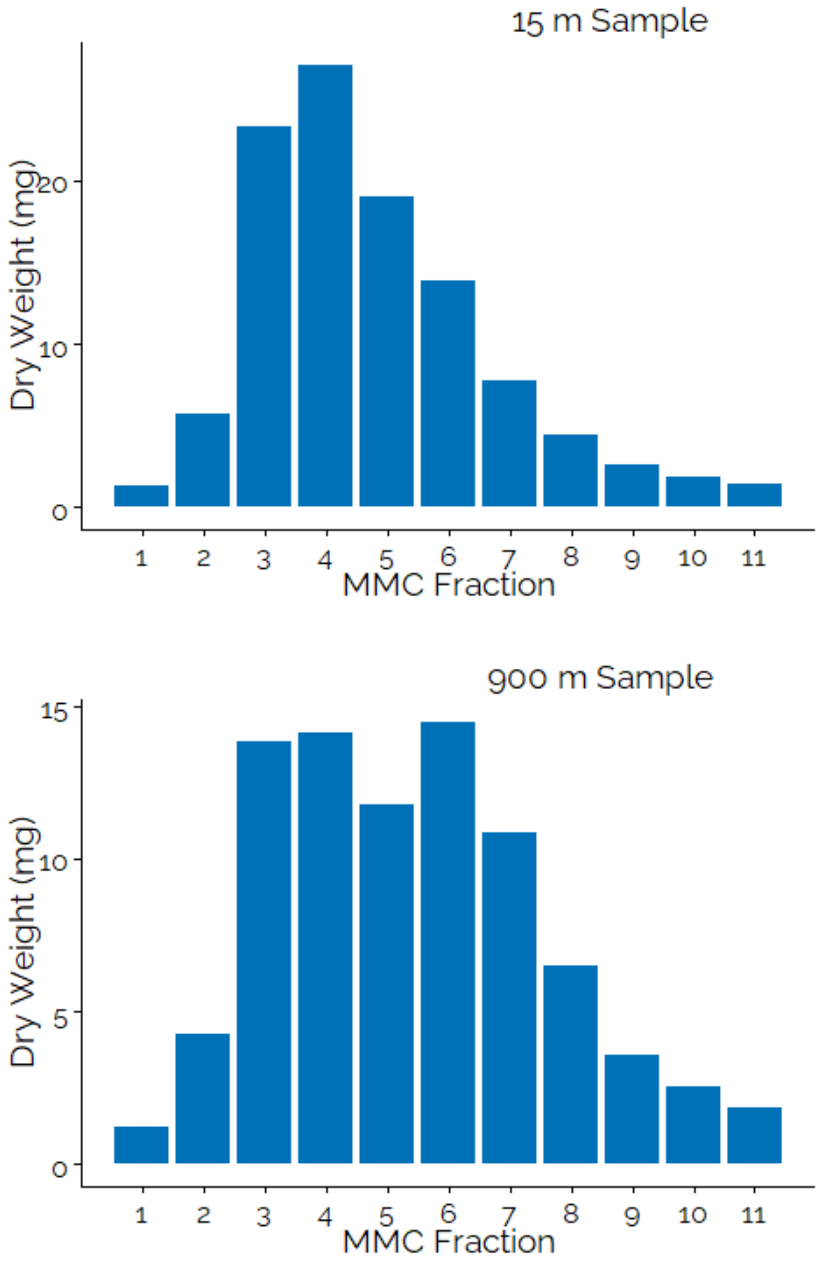

Figure 2.4: Dry weights of MMC fractions.

2.4.3 Spectral Analysis of HMWDOM MMC Fractions

^{1}H-NMR spectra from select MMC fractions (Figure 2.5) show the change in sample composition across the MMC separation. Fractions that elute later in the chromatography have greater resonance in the spectral regions associated with HS, indicating that the sample

composition shifts to a higher proportion of HS in the small size fractions. The peak centered at 1.2 ppm sees contributions from both HS and APS. In later-eluting fractions that peak increases in intensity and peak width (measured at half height) as the HS contribution to that region increases. The relative intensity of the other two APS peaks decreases throughout the chromatography.

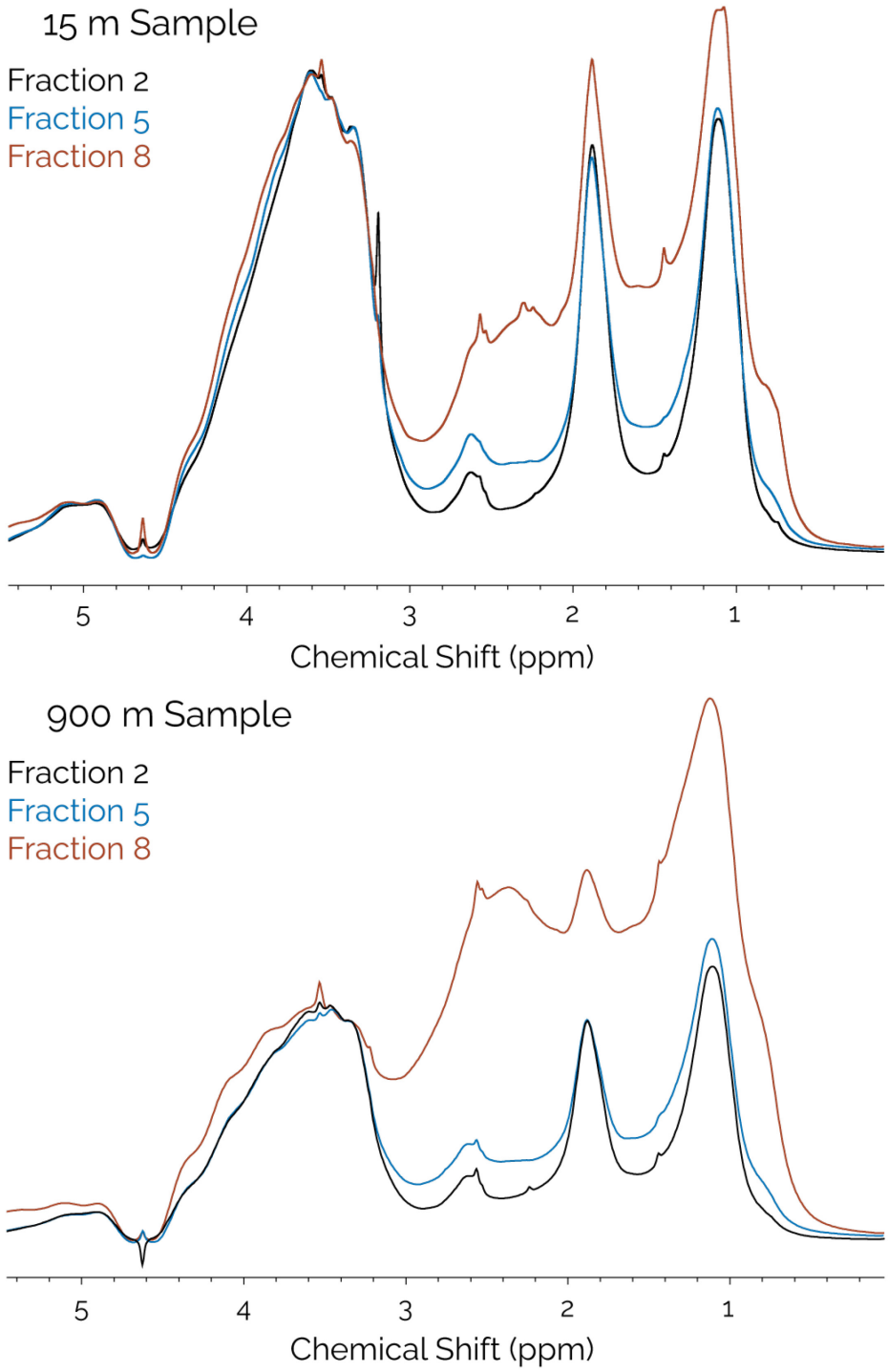

Figure 2.5: ^{1}H-NMR spectra of select MMC fractions, which are representative of the compositional changes that occur throughout the chromatography. Spectral intensities are normalized at 3.4 ppm. Peaks at 3.5 (**H**COH), 1.8(**H**$_3$CC=OND), and 1.2 (deoxy-C**H**$_3$) are attributed to APS while the large background signal between 4 and 1 ppm is attributed to HS.

The results of DOSY analysis of the MMC fractions were as expected, with earlier-eluting fractions having a higher MW than later-eluting fractions in both the 15 m and 900 m samples (Figure 2.6). MW of the two components in each fraction are plotted in Figure 2.7. The APS component is significantly larger than the HS component in all fractions, a result consistent with the chemical selectivity of the MMC. The molecular weights of both components level off in the later-eluting fractions, with the APS reaching a minimum MW of 3.5 and 2.0 kDa in the 15 m and 900 m samples respectively, and the HS reaching a minimum MW of 0.9 kDa in both samples. Most of the collected material is above the 1 kDa MWCO of the filter, suggesting that minimal membrane fouling and that insignificant retention of LMW HS is occurring. The DOSY results confirm that both size and composition shift continuously during the chromatography. There is, therefore, an intrinsic relationship between size and composition, demonstrating that the size distribution of HMWDOM cannot be considered separately from its chemical characteristics.

It is interesting that the MW of APS plateaus well above the MWCO, suggesting that APS of a MW lower than 3.5 kDa is not present in surface seawater. This result could be due to loss of material during the concentration and diafiltration steps. Previous work has shown that the MW of material retained by UF during concentration increases with the concentration factor (Carlson et al., 1985). Additionally, as the MWCO of the membranes is based on the rejection of marker compounds such as polyethylene glycol and dextran, marine APS may interact differently with the membranes than either marker, resulting in a higher MWCO than is reported by membrane manufacturers. If this result is correct, it raises important questions about the diagenesis of APS. Is a MW of 3.5 kDa a cut-off for remineralization, such that larger material is slowly degraded to that size, at which point the polysaccharides are quickly metabolized,

resulting in an undetectable standing stock of APS lower than 3.5 kDa? To answer this question, two-dimensional MMC could be used to further size fractionate HMWDOM to look for evidence of smaller APS in surface seawater.

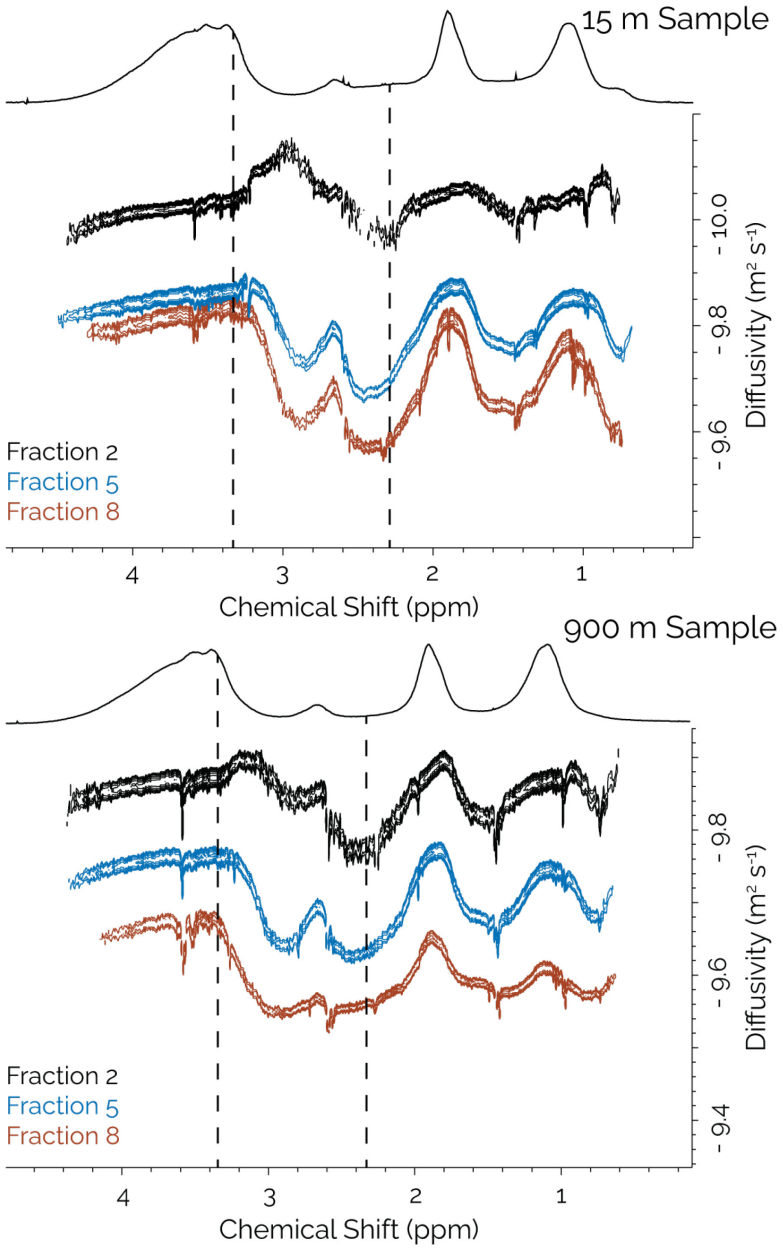

Figure 2.6: DOSY spectra of 15 m and 900 m DOM fractions collected during MMC. Diffusivity is plotted on the vertical axis. A lower diffusivity corresponds to a higher molecular weight. The vertical dashed lines at 3.4 and 2.2 ppm represent the diffusivity values used to calculate the molecular weight of the APS and HS components, respectively.

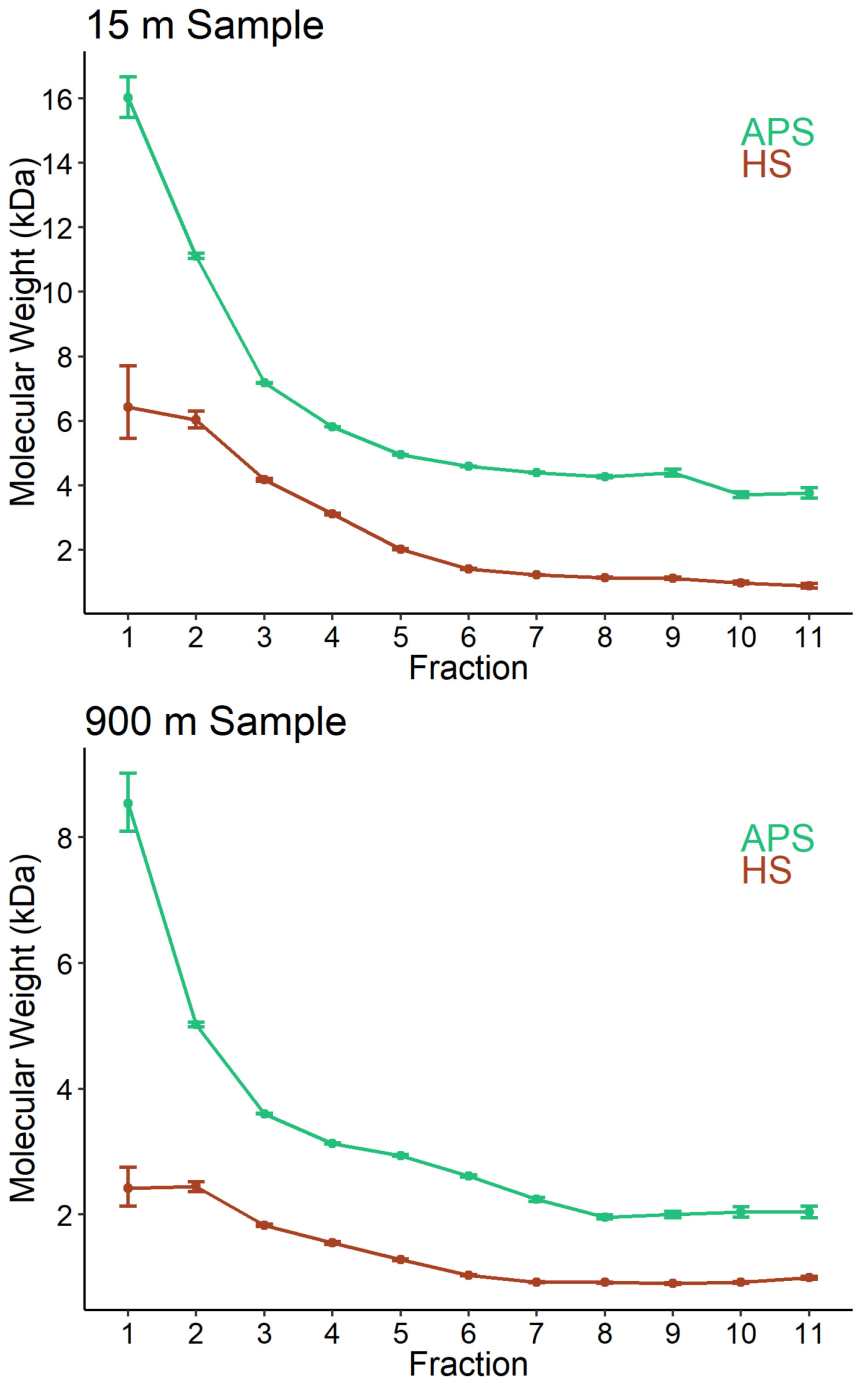

Figure 2.7: Average MW of HMWDOM APS (green) and HS (red) MMC fractions for the 15 m and 900 m samples. Error bars represent the deviation from an idealized diffusion decay curve and do not represent the molecular weight distribution of each component. APS MW was calculated using a pullulan standard curve and HS MW was calculated using a polystyrene sulfonate standard curve.

2.4.4 Validation of the DOSY technique

MWs of HMWDOM components were determined by measuring their diffusivity in D_2O and converting to MW using calibrations of pullulan and sulfonated polystyrene of known MWs. In addition to molecular conformation, several factors influence the measured diffusivity of a molecule, including the viscosity of the solution and molecular association/aggregation. D_2O was used as the solvent for all samples and variations in solution viscosity were minimized by using the same sample concentration of 1 mg mL^{-1} for all samples throughout the analysis. The effects of molecular aggregation were explored by measuring diffusivity of HMWDOM and LMWSPEDOM in different solvents. Diffusivity was also measured under three pH conditions (4, 7, and 10) and three salinities representing 50%, 100% and 125% of the average seawater salinity of 35 (Figure 2.10). Finally, diffusivities were measured in methanol (MeOH) and in a 10 mM EDTA solution to promote disaggregation (Orellana & Leck, 2015). No difference in the calculated MW or in the hydrodynamic radii of the components were detected in any treatment, suggesting that neither molecular aggregation nor viscosity had a significant impact on the apparent MW of the samples in aqueous solution. The determination of hydrodynamic radii requires extrapolation of the diffusivity to infinite dilution, however, at concentrations less than 2.5 mg mL^{-1}, the effect of concentration on the density of the solution becomes negligible (Nishinari et al., 1991). Therefore, my diffusion measurements provide a good approximation of hydrodynamic radii at the concentrations used in these experiments. These results are supported by previous studies, which observed minimal aggregation of HS at concentrations below 4 mg mL^{-1} (Lam & Simpson, 2009; Šmejkalová & Piccolo, 2008).

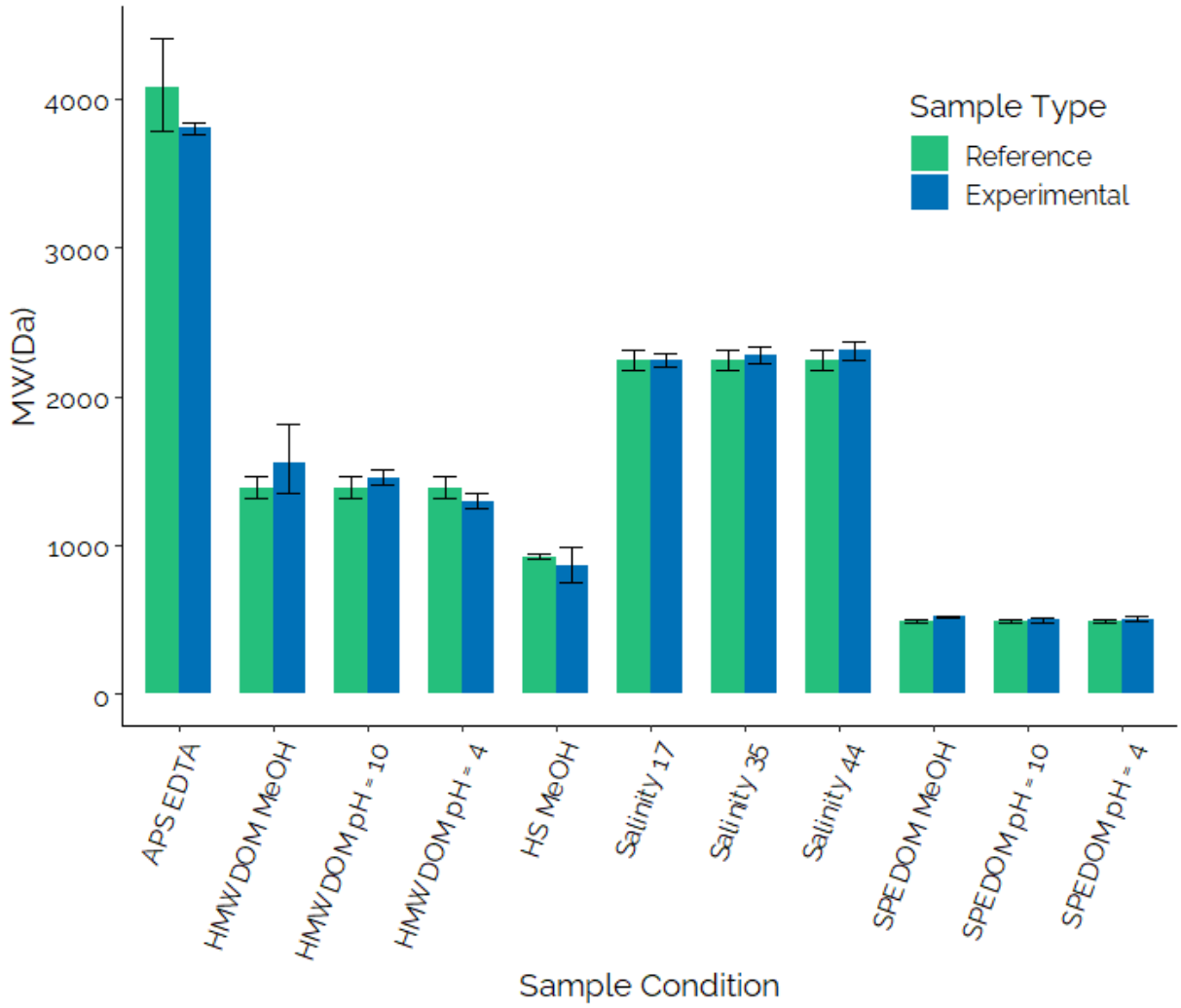

Figure 2.8: DOSY molecular weight validation. The measured MW (blue) of samples of HMWDOM and LMWSPEDOM under various pH conditions and in organic solvents as compared to their reference MW (green) measured at pH = 7 in D_2O. Not significant deviation was detected for any of the sample conditions ($\alpha = 0.05$). Error bars represent the uncertainty in diffusivity calculations ($p = 0.05$).

2.4.5 Two Components of HMWDOM

The results of this study support the conclusion that HMWDOM is a two-component mixture consisting primarily of a polysaccharide (APS) component and a humic substances (HS) component. Each component has a different molecular weight distribution. The sum of the mass-weighted average of molecular weights of the MMC fractions for APS (5.9 and 2.9 kDa for the

15 m and 900 m samples) and HS (2.8 and 1.3 kDa for the 15 m and 900 m samples) matched the average MW measured for these components in the whole HMWDOM samples (6.1 and 3.1 for the 15 m and 900 m APS samples; 2.7 and 1.3 kDa for the 15 m and 900 m HS samples), indicating the chromatography did not alter the MW and that the fractions are representative of the whole HMWDOM sample. Figure 2.8 shows a histogram of component molecular weight for each sample. These results suggest a new conceptual model should be used to describe the diagenesis of HMWDOM, one that treats each component separately (Figure 2.9).

The APS of the surface sample has an average molecular weight of 6.1 ± 1.1 kDa, indicating it has a degree of polymerization (DP) of approximately ~30 monosaccharides (DP-30). At 900 m, the MW decreased to 3.1 ± 0.6 kDa, equivalent to ~DP-17. Based on NMR analysis the material does not appear to change in composition with depth or MW. These results corroborate previous studies of HMW APS, which found that the relative abundance of major neutral sugars did not shift substantially with depth (Repeta & Aluwihare, 2006). The MW of APS decreases with depth and showed no evidence of non-normality (Shapiro-Wilk: $W = 0.85$, $p > 0.05$ for the 15 m sample and $W = 0.86$, $p > 0.05$ for the 900 m sample) suggesting a slow, continuous diagenesis of material during advection from the surface, likely due to enzymatic hydrolysis. It is also possible that a portion of APS in the mesopelagic is produced autochthonously through chemoautotrophy, and that the average MW of the deep material is less than the average MW of APS produced in the surface.

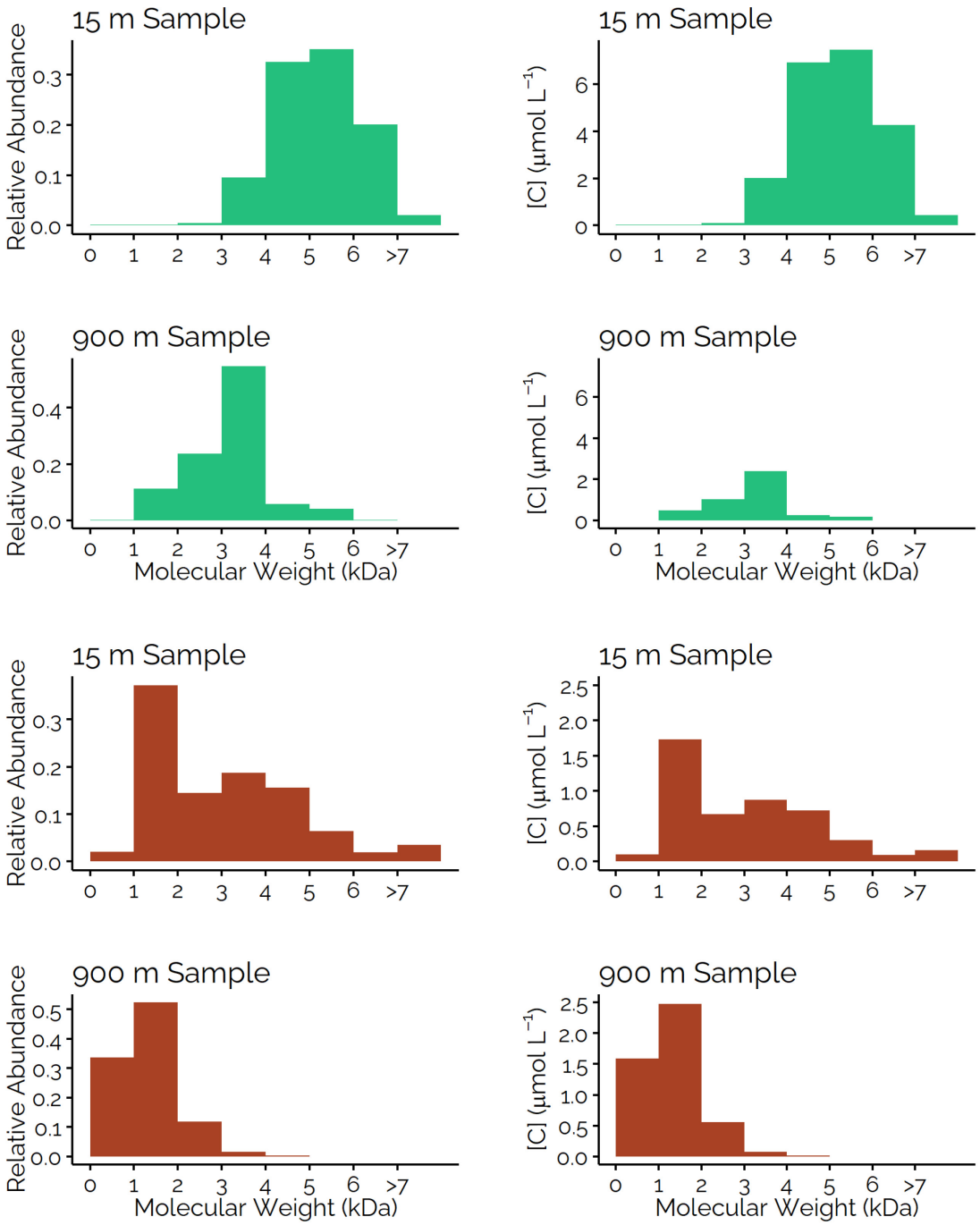

Figure 2.9: Distribution of MW in HMWDOM APS (Green) and HS (Orange) for the 15 m and 900 m samples. APS MW was calculated using a pullulan standard curve and HS MW was calculated using a polystyrene sulfonate standard curve. The histograms on the left show the relative abundance of each MW bin in each sample while the histograms on the right show the seawater carbon concentration of the component of HMWDOM in represented by each bin.

The HS in the 15 m sample has a broad MW range (0.9–6.4 kDa) and is not normally distributed (Shapiro-Wilk: $W = 0.81$, $p < 0.05$). The MW range observed here agrees well with DOSY-based MW estimates of terrestrial humic and fulvic acids, suggesting multi-kDa HS is present across the aquatic continuum (Šmejkalová & Piccolo, 2008). One explanation for the broad MW distribution in the 15 m sample is that HS in the surface is a mixture of material from multiple sources. In this conceptual model, aged organic matter that is advected to the surface makes up the lower MW material in surface HS while newly formed HS has a higher MW. As this material is advected, its MW decreases to reflect the MW of 900 m HS. The HS in both the 15 and 900 m samples plateau at MW of 928±38 and 924±10 Da respectively, reflecting the old, persistent HS. The uncertainties in these values describe the standard error of the mean. The absolute abundance of HS (7 μM C) does not change significantly between the two depths, suggesting that either a significant portion of the newly produced material is not remineralized, or that there are additional sources of HS to the deep ocean. If most of the newly produced HS is advected to depth, the decrease in the MW distribution suggests that it is decomposed into smaller compounds. Conversely, if the HS produced in the surface is remineralized, it is replaced with HS with a lower average MW, resulting in the observed decrease in the MW distribution at 900 m.

HMWDOM with a MW greater than 10 kDa made up only 6% of the material, supporting the conclusion that the majority of HMWDOM has a narrow size distribution near the MWCO of the ultrafiltration system (Guo et al., 1996). Little evidence of LMWDOM fouling was found in these HMWDOM samples. Had fouling of LMW material occurred, a continued MW decrease in later-eluting MMC fractions would have been expected, as the MW of LMWSPEDOM is ~500 Da. As the MW of HS plateaued just below the MWCO of the filter membranes, it is likely that

most of the retained material should be classified as HMW. It is interesting that the concentration of HS does not decrease between the 15 m and 900 m samples. Carbon isotope analysis of the HS fraction could provide additional information about the sources of HS to the deep ocean.

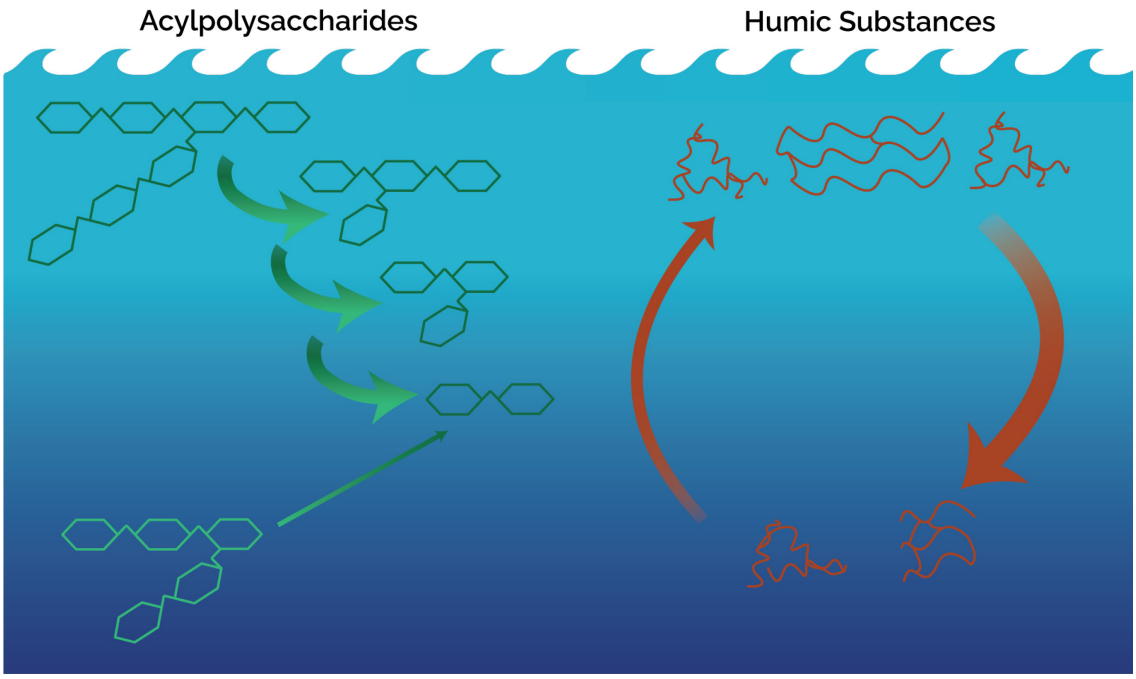

Figure 2.10: A generalized one dimensional schematic of the cycling of the components of HMWDOM. The width of the arrows indicates the relative magnitude of that transformation process. APS is formed autochthonously and is quickly and continuously remineralized. HS in the surface is a mixture of newly formed compounds and old material that is advected from depth and persists for several ocean mixing cycles. HS in the deep ocean is comprised of smaller compounds from several sources.

2.5 CONCLUSIONS

HMWDOM is a mixture of two components with different mechanism of degradation. Autochthonously produced APS is homogenously and continuously degraded, resulting in a normal MW distribution around the mean and a smaller average MW in the subsurface. HS is also produced in the surface and has a broad MW range that is bimodally distributed, suggesting that HS in the surface may be comprised of two components. As the HS concentration does not

decrease between the surface and deep, it is unclear if the newly produced HS is remineralized and replaced, or if it survives advection, but is decomposed into smaller compounds at depth. Further testing is required to distinguish between these two models.

This work provides a new framework for assessing HMWDOM dynamics which relies on grouping DOM based on chemical characteristics instead of size fractions. It also proposes testable hypothesis for the primary degradation pathways for HMW HS and APS. If APS is continually and uniformly degraded during advection, the size of APS should continue to decrease without a corresponding shift in MW distribution. HMWDOM diffusion measurements could be made from deeper depths, along paths of deep-water formation. In contrast, HS MW should remain constant below the surface, and a decrease in MW distribution would be expected along advection pathways due to the removal of newly produced HS.

2.6 REFERENCES

Aluwihare, L. I., Repeta, D. J., & Chen, R. F. (1997). A major biopolymeric component to dissolved organic carbon in surface sea water. *Nature*, *387*(6629), 166–169. https://doi.org/10.1038/387166a0

Aluwihare, L. I., Repeta, D. J., & Chen, R. F. (2002). Chemical composition and cycling of dissolved organic matter in the Mid-Atlantic Bight. *Deep-Sea Research Part II: Topical Studies in Oceanography*, *49*(20), 4421–4437. https://doi.org/10.1016/S0967-0645(02)00124-8

Aluwihare, L. I., Repeta, D. J., Pantoja, S., & Johnson, C. G. (2005). Two chemically distinct pools of organic nitrogen accumulate in the ocean. *Science*, *308*(5724), 1007–1010. https://doi.org/10.1126/science.1108925

Arakawa, N., Aluwihare, L. I., Simpson, A. J., Soong, R., Stephens, B. M., & Lane-Coplen, D. (2017). Carotenoids are the likely precursor of a significant fraction of marine dissolved organic matter. *Science Advances*, *3*(9), 1–12. https://doi.org/10.1126/sciadv.1602976

Arnosti, C. (2011). Microbial extracellular enzymes and the marine carbon cycle. *Annual Review of Marine Science*, *3*(1), 401–425. https://doi.org/10.1146/annurev-marine-120709-142731

Beckett, R. (1987). *Field-Flow Fractionation*. 289–295.

Benner, R., Pakulski, J. D., McCarthy, M. D., Hedges, J. I., & Hatcher, P. G. (1992). Bulk chemical characteristics of dissolved organic matter in the ocean. *Science*, *789*(March), 1561–1564.

Broek, T. A. B., Walker, B. D., Guilderson, T. P., & McCarthy, M. D. (2017). Coupled ultrafiltration and solid phase extraction approach for the targeted study of semi-labile high molecular weight and refractory low molecular weight dissolved organic matter. *Marine Chemistry*, *194*(January), 146–157. https://doi.org/10.1016/j.marchem.2017.06.007

Carlson, D. J., Brann, M. L., Mague, T. H., & Mayer, L. M. (1985). Molecular weight distribution of dissolved organic materials in seawater determined by ultrafiltration: A re-examination. *Marine Chemistry*, *16*(2), 155–171. https://doi.org/10.1016/0304-4203(85)90020-9

Cuskin, F., Lowe, E. C., Temple, M. J., Zhu, Y., Cameron, E. A., Pudlo, N. A., Porter, N. T., Urs, K., Thompson, A. J., Cartmell, A., Rogowski, A., Hamilton, B. S., Chen, R., Tolbert, T. J., Piens, K., Bracke, D., Vervecken, W., Hakki, Z., Speciale, G., … Gilbert, H. J. (2015). Human gut *Bacteroidetes* can utilize yeast mannan through a selfish mechanism. *Nature*, *517*(7533), 165–169. https://doi.org/10.1038/nature13995

Daoud, A. B. A., & Tremblay, L. (2019). HPLC-SEC-FTIR characterization of the dissolved organic matter produced by the microbial carbon pump. *Marine Chemistry*, *215*(June), 103668. https://doi.org/10.1016/j.marchem.2019.103668

De Nobili, M., & Chen, Y. (1999). Size exclusion chromatography of humic substances: Limits, perspectives and prospectives. *Soil Science*, *164*(11), 825–833. https://doi.org/10.1097/00010694-199911000-00007

Dittmar, T., Koch, B. P., Hertkorn, N., & Kattner, G. (2008). A simple and efficient method for the solid-phase extraction of dissolved organic matter (SPE-DOM) from seawater. *Limnology and Oceanography: Methods*, *6*, 230–235.

Gagosian, R. B., & Stuermer, D. H. (1977). The cycling of biogenic compounds and their diagenetically transformed products in seawater. *Marine Chemistry*, *5*(4–6), 605–632. https://doi.org/10.1016/0304-4203(77)90045-7

Ghosh, K., & Schnitzer, M. (1980). Macromolecular structures of humic substances. *Soil Science*, *129*(5), 266–276. https://doi.org/10.1097/00010694-198005000-00002

Guéguen, C., & Cuss, C. W. (2011). Characterization of aquatic dissolved organic matter by asymmetrical flow field-flow fractionation coupled to UV-Visible diode array and excitation emission matrix fluorescence. *Journal of Chromatography A*, *1218*(27), 4188–4198. https://doi.org/10.1016/j.chroma.2010.12.038

Guo, L., Coleman, C. H., & Santschi, P. H. (1994). The distribution of colloidal and dissolved organic carbon in the Gulf of Mexico. *Marine Chemistry*, *45*(1), 105–119. https://doi.org/10.1016/0304-4203(94)90095-7

Guo, L., & Santschi, P. H. (2007). Ultrafiltration and its applications to sampling and characterisation of aquatic colloids. In *Environmental Colloids and Particles: Behaviour, Separation and Characterisation*. https://doi.org/10.1002/9780470024539.ch4

Guo, L., Santschi, P. H., Cifuentes, L. A., Trumbore, S. E., & Southon, J. (1996). Cycling of high-molecular-weight dissolved organic matter in the Middle Atlantic Bight as revealed by carbon isotopic (^{13}C and ^{14}C) signatures. *Limnology and Oceanography*, *41*(6), 1242–1252. https://doi.org/10.4319/lo.1996.41.6.1242

Guo, L., Wen, L. S., Tang, D., & Santschi, P. H. (2000). Re-examination of cross-flow ultrafiltration for sampling aquatic colloids: Evidence from molecular probes. *Marine Chemistry*, *69*(1–2), 75–90. https://doi.org/10.1016/S0304-4203(99)00097-3

Hansell, D. A. (2013). Recalcitrant dissolved organic carbon fractions. *Annual Review of Marine Science*, *5*, 421–425. https://doi.org/10.1146/annurev-marine-120710-100757

Hansell, D. A., Carlson, C. A., Repeta, D. J., & Schlitzer, R. (2009). Dissolved organic matter in the ocean: A controversy stimulates new insights. *Oceanography*, *22*(4), 202–211. https://doi.org/10.1038/ncomms8422

Hertkorn, N., Benner, R., Frommberger, M., Schmitt-Kopplin, P., Witt, M., Kaiser, K., Kettrup, A., & Hedges, J. I. (2006). Characterization of a major refractory component of marine dissolved organic matter. *Geochimica et Cosmochimica Acta*, *70*(12), 2990–3010. https://doi.org/10.1016/j.gca.2006.03.021

Honda, S., Suzuki, S., & Kakehi, K. (1984). Improved analysis of aldose anomers by high-performance liquid chromatography on cation-exchange columns. *Journal of Chromatography A*, *291*, 317–325. https://doi.org/10.1016/S0021-9673(00)95034-9

Johnson Jr., C. S. (1999). Diffusion ordered nuclear magnetic resonance spectroscopy: Principles and applications. *Progress in Nuclear Magnetic Resonance Spectroscopy*, *34*, 203–256.

Johnson, W. M., Kido Soule, M. C., & Kujawinski, E. B. (2017). Extraction efficiency and quantification of dissolved metabolites in targeted marine metabolomics. *Limnology and Oceanography: Methods*, *15*(4), 417–428. https://doi.org/10.1002/lom3.10181

Karl, D. M., Björkman, K. M., Dore, J. E., Fujieki, L., Hebel, D. V., Houlihan, T., Letelier, R. M., & Tupas, L. M. (2001). Ecological nitrogen-to-phosphorus stoichiometry at station ALOHA. *Deep-Sea Research Part II: Topical Studies in Oceanography*, *48*(8–9), 1529–1566. https://doi.org/10.1016/S0967-0645(00)00152-1

Kawahigashi, M., Sumida, H., & Yamamoto, K. (2005). Size and shape of soil humic acids estimated by viscosity and molecular weight. *Journal of Colloid and Interface Science*, *284*(2), 463–469. https://doi.org/10.1016/j.jcis.2004.10.023

Lam, B., & Simpson, A. J. (2009). Investigating aggregation in Suwannee River, USA, dissolved organic matter using diffusion-ordered nuclear magnetic resonance spectroscopy. *Environmental Toxicology and Chemistry*, *28*(5), 931–939. https://doi.org/10.1897/08-441.1

Lechtenfeld, O. J., Kattner, G., Flerus, R., Mccallister, S. L., Schmitt-kopplin, P., & Koch, B. P. (2014). Molecular transformation and degradation of refractory dissolved organic matter in the Atlantic and Southern Ocean. *Geochimica et Cosmochimica Acta*, *126*, 321–337.

Loh, A. N., Bauer, J. E., & Druffel, E. R. M. (2004). Variable ageing and storage of dissolved organic components in the open ocean. *Nature*, *430*, 877–880.

Ly, Q. V., & Hur, J. (2018). Further insight into the roles of the chemical composition of dissolved organic matter (DOM) on ultrafiltration membranes as revealed by multiple advanced DOM characterization tools. *Chemosphere*, *201*, 168–177. https://doi.org/10.1016/j.chemosphere.2018.02.181

Maurer, L. G. (1976). Organic polymers in seawater: Changes with depth in the Gulf of Mexico. *Deep Sea Research and Oceanographic Abstracts*, *23*(11), 1059–1064. https://doi.org/10.1016/0011-7471(76)90881-0

McCarthy, M. D., Beaupré, S. R., Walker, B. D., Voparil, I., Guilderson, T. P., & Druffel, E. R. M. (2010). Chemosynthetic origin of ^{14}C-depleted dissolved organic matter in a ridge-flank hydrothermal system. *Nature Geoscience*, *4*(1), 32–36. https://doi.org/10.1038/ngeo1015

McCarthy, M. D., Hedges, J. I., & Benner, R. (1993). The chemical composition of dissolved organic matter in seawater. *Chemical Geology*, *107*(3–4), 503–507. https://doi.org/10.1016/0009-2541(93)90240-J

McCarthy, M. D., Hedges, J. I., & Benner, R. (1996). Major biochemical composition of dissolved high molecular weight organic matter in seawater. *Marine Chemistry*, *55*(3–4), 281–297. https://doi.org/10.1016/S0304-4203(96)00041-2

Minor, E. C., Simjouw, J. P., Boon, J. J., Kerkhoff, A. E., & Van der Horst, J. (2002). Estuarine/marine UDOM as characterized by size-exclusion chromatography and organic mass spectrometry. *Marine Chemistry*, *78*(2–3), 75–102. https://doi.org/10.1016/S0304-4203(02)00011-7

Nagata, T., Meon, B., & L. Kirchman, D. (2003). Microbial degradation of peptidoglycan in seawater. *Limnology and Oceanography*, *48*(2), 745–754. https://doi.org/10.4319/lo.2003.48.2.0745

Nishinari, K., Kohyama, K., Williams, P. A., Phillips, G. O., Burchard, W., & Ogino, K. (1991). Solution properties of pullulan. *Macromolecules*, *24*(20), 5590–5593. https://doi.org/10.1021/ma00020a017

Orellana, M. V., & Leck, C. (2015). Marine Microgels. In *Biogeochemistry of Marine Dissolved Organic Matter* (pp. 451–480). Elsevier. https://doi.org/10.1016/B978-0-12-405940-5.00009-1

Panagiotopoulos, C., Pujo-Pay, M., Benavides, M., Van Wambeke, F., & Sempéré, R. (2019). The composition and distribution of semi-labile dissolved organic matter across the southwest Pacific. *Biogeosciences*, *16*(1), 105–116. https://doi.org/10.5194/bg-16-105-2019

Pelekani, C., Newcombe, G., Snoeyink, V. L., Hepplewhite, C., Assemi, S., & Beckett, R. (1999). Characterization of natural organic matter using high performance size exclusion chromatography. *Environmental Science and Technology*, *33*(16), 2807–2813. https://doi.org/10.1021/es9901314

Perminova, I. V., Frimmel, F. H., Kudryavtsev, A. V., Kulikova, N. A., Abbt-Braun, G., Hesse, S., & Petrosyan, V. S. (2003). Molecular weight characteristics of humic substances from different environments as determined by size exclusion chromatography and their

statistical evaluation. *Environmental Science and Technology*, *37*(11), 2477–2485. https://doi.org/10.1021/es0258069

Piccolo, A. (2001). The supramolecular structure of humic substances. *Soil Science*, *166*(11), 810–832. https://doi.org/10.1097/00010694-200111000-00007

Piontek, J., Handel, N., De Bodt, C., Harlay, J., Chou, L., & Engel, A. (2011). The utilization of polysaccharides by heterotrophic bacterioplankton in the Bay of Biscay (North Atlantic Ocean). *Journal of Plankton Research*, *33*(11), 1719–1735. https://doi.org/10.1093/plankt/fbr069

Politi, M., Groves, P., Chávez, M. I., Cañada, F. J., & Jiménez-Barbero, J. (2006). Useful applications of DOSY experiments for the study of mushroom polysaccharides. *Carbohydrate Research*, *341*(1), 84–89. https://doi.org/10.1016/j.carres.2005.11.008

Reemtsma, T., & These, A. (2003). On-line coupling of size exclusion chromatography with electrospray ionization-tandem mass spectrometry for the analysis of aquatic fulvic and humic acids. *Analytical Chemistry*, *75*(6), 1500–1507. https://doi.org/10.1021/ac0261294

Reid, P. M., Wilkinson, A. E., Tipping, E., & Jones, M. N. (1990). Determination of molecular weights of humic substances by analytical (UV scanning) ultracentrifugation. *Geochimica et Cosmochimica Acta*, *54*(1), 131–138. https://doi.org/10.1016/0016-7037(90)90201-U

Reintjes, G., Arnosti, C., Fuchs, B. M., & Amann, R. (2017). An alternative polysaccharide uptake mechanism of marine bacteria. *The ISME Journal*, *11*(7), Article 7. https://doi.org/10.1038/ismej.2017.26

Repeta, D. J., & Aluwihare, L. I. (2006). Radiocarbon analysis of neutral sugars in high-molecular-weight dissolved organic carbon: Implications for organic carbon cycling. *Limnology and Oceanography*, *51*(2), 1045–1053. https://doi.org/10.4319/lo.2006.51.2.1045

Repeta, D. J., Ferrón, S., Sosa, O. A., Johnson, C. G., Repeta, L. D., Acker, M., Delong, E. F., & Karl, D. M. (2016). Marine methane paradox explained by bacterial degradation of dissolved organic matter. *Nature Geoscience*, *9*(12), 884–887. https://doi.org/10.1038/ngeo2837

Repeta, D. J., Quan, T. M., Aluwihare, L. I., & Accardi, A. (2002). Chemical characterization of high molecular weight dissolved organic matter in fresh and marine waters. *Geochimica et Cosmochimica Acta*, *66*(6), 955–962. https://doi.org/10.1016/S0016-7037(01)00830-4

Roland, L. A., McCarthy, M. D., Peterson, T. D., & Walker, B. D. (2009). A large-volume microfiltration system for isolating suspended particulate organic matter: Fabrication and assessment versus GFF filters in central North Pacific. *Limnology and Oceanography: Methods*, *7*(1), 64–80. https://doi.org/10.4319/lom.2009.7.64

Sakugawa, H., & Handa, N. (1985). Chemical studies on dissolved carbohydrates in the water samples collected from the North Pacific and Bering Sea. *Oceanologica Acta*, *8*(2), 185–196.

Šmejkalová, D., & Piccolo, A. (2008). Aggregation and disaggregation of humic supramolecular assemblies by NMR diffusion ordered spectroscopy (DOSY-NMR). *Environmental Science and Technology*, *42*(3), 699–706. https://doi.org/10.1021/es071828p

Song, J., Huang, W., Peng, P., Xiao, B., & Ma, Y. (2010). Humic acid molecular weight estimation by high-performance size-exclusion chromatography with ultraviolet absorbance detection and refractive index detection. *Soil Science Society of America Journal*, *74*(6), 2013–2020. https://doi.org/10.2136/sssaj2010.0011

Stuermer, D. H., & Harvey, G. R. (1974). Humic substances from seawater. *Nature*, *250*(5466), 480–481. https://doi.org/10.1038/250480a0

Viel, S., Capitani, D., Mannina, L., & Segre, A. (2003). Diffusion-ordered NMR spectroscopy: A versatile tool for the molecular weight determination of uncharged polysaccharides. *Biomacromolecules*, *4*(6), 1843–1847. https://doi.org/10.1021/bm0342638

Vink, H. (1990). Ionic charge effects on the transport processes in polyelectrolyte solutions. *Journal of Colloid and Interface Science*, *135*(1), 218–226. https://doi.org/10.1016/0021-9797(90)90302-5

Walker, B. D., Beaupré, S. R., Guilderson, T. P., McCarthy, M. D., & Druffel, E. R. M. (2016). Pacific carbon cycling constrained by organic matter size, age and composition relationships. *Nature Geoscience*, *9*(12), 888–891. https://doi.org/10.1038/ngeo2830

Zark, M., & Dittmar, T. (2018). Universal molecular structures in natural dissolved organic matter. *Nature Communications*, *9*(1), 1–8. https://doi.org/10.1038/s41467-018-05665-9

Zigah, P. K., McNichol, A. P., Xu, L., Johnson, C. G., Santinelli, C., Karl, D. M., & Repeta, D. J. (2017). Allochthonous sources and dynamic cycling of ocean dissolved organic carbon revealed by carbon isotopes. *Geophysical Research Letters*, *44*(5), 2407–2415. https://doi.org/10.1002/2016GL071348

CHAPTER 3. THE DIAGENETIC FATE OF HIGH MOLECULAR WEIGHT DISSOLVED ORGANIC MATTER

3.1 ABSTRACT

The size–reactivity continuum hypothesis (SRC) proposes a conceptual framework for the biodegradation of dissolved organic matter (DOM), in which large, labile biomolecules are transformed into small, refractory compounds as a biproduct of biological decomposition. Evidence for this hypothesis includes bacterial growth experiments using amendments of different size fractions of DOM, and radiocarbon analysis of high and low molecular weight size-fractions of DOM. These studies suggest that high molecular weight DOM (DOM with a MW nominally greater than 1 kDa; HMWDOM) represents an intermediate in the continuum between labile cellular material (POM) and low molecular weight, refractory ($_r$DOM) that persists for several millennia in the ocean. However, the SRC does not incorporate information about the diversity of compounds and their degradation pathways in HMWDOM. In this chapter, I examine the reactivity of the acylpolysaccharides (APS) and humic substances (HS) components of HMWDOM characterized in Chapter 2. By examining the carbon isotopic composition of fractions of HMWDOM with different relative abundances of HS and APS, a relationship between HS content and $\Delta^{14}C$ can be modeled. Extrapolation of this model reveals that APS has a turnover time of 1–3 yrs. The HS endmember radiocarbon value does not change significantly between the surface and deep samples, despite a shift in MW and stable isotope composition, suggesting multiple mechanisms control the removal and supply of HS to the ocean interior. The difference in the diagenetic fate of these two components demonstrates that HMWDOM is not an intermediate between POC and $_r$DOM, but rather a mixture of modern APS and HS. I find no evidence to support the framework of the SRC and therefore propose a new conceptual model for HMWDOM based on two chemically distinct components.

3.2 INTRODUCTION

The radiocarbon age of DOM in the deep ocean (>1000 m) is between 4,000 and 6,000 yrs, but studies have shown that different classes of DOM have residence times ranging from hours to more than ten thousand years (Follett et al., 2014; Hansell, 2013). Radiocarbon age can be used as a measure of the relative lability of a fraction of DOM and can provide insight into the mechanisms and rates of remineralization of that material. To target a specific class of DOM for radiocarbon analysis, the class of interest must be physically isolated. Several chemical separation methods (solid phase extraction, ramped pyrolysis) and size-based techniques (ultrafiltration, size exclusion chromatography) have been used to isolate fractions of DOM (Arakawa et al., 2017; Hemingway et al., 2019; Walker, Primeau, et al., 2016). Ultrafiltration (UF) isolates high molecular weight dissolved organic matter (HMWDOM), an operationally defined size fraction of DOM greater than the nominal molecular weight cutoff (MWCO) of 1 nm pore–size membrane. Analysis of HMWDOM ^{1}H-NMR (Figure 2.1) spectra shows that the material is composed primarily of two distinct chemical components, acylpolysaccharides (APS) and humic substances (HS) (Repeta & Aluwihare, 2006). Radiocarbon analysis of total HMWDOM isolated from the surface waters of the North Pacific Ocean in 2014 yielded a radiocarbon age of 135 yrs, suggesting that HMWDOM is remineralized more quickly than total DOC and that HMWDOM represents a large pool of semi-labile DOM ($_{sl}$DOM) (Zigah et al., 2017). The observation that HMWDOM has a younger radiocarbon age than total DOM forms the basis of the size–reactivity continuum hypothesis (SRC).

The SRC, first proposed by Amon and Benner (1994, 1996), posits that organic matter is continuously altered to become less bioreactive and physically smaller during decomposition, resulting in a continuum between large, labile compounds and small, refractory organic matter

($_r$DOM). Importantly, the SRC suggests that OM predominantly flows from a "highly structured cellular state to a seemingly random and complex molecular state" through diagenetic processes (Benner & Amon, 2015). The SRC was initially proposed to explain higher rates of bacterial production and respiration from heterotrophic bacterial assemblages incubated with HMWDOM as compared to incubations with low molecular weight DOM (LMWDOM). Recently, radiocarbon measurements of the size classes of DOM have shown that material isolated using filters with a larger MWCO have a younger radiocarbon age and shorter residence time, lending support to the SRC (Walker, Beaupré, et al., 2016; Walker, Primeau, et al., 2016). While models of DOM dynamics utilizing the SRC framework allow for estimation of DOM diagenesis and the formation of $_r$DOM, the SRC is agnostic as to the chemical diversity within size classes of DOM, instead ascribing bulk properties to each fraction of DOM and assuming a monotonic decrease in reactivity with a decrease in size.

This chapter examines the assumption that the material within a size class of DOM behaves uniformly with respect to degradation. In this study, the radiocarbon ages of the APS and HS components of HMWDOM are determined. In Chapter 2, it was found that APS has a larger average MW than HS. This suggested that the two components could be separated by mixed-mode chromatography (MMC). By creating a suite of samples of HMWDOM with different proportions of APS and HS, the relationship between APS and HS content to radiocarbon age can be determined. From these results, the relationship between HMWDOM size, composition, and age are examined and a new model of HMWDOM diagenesis is proposed.

3.3 MATERIALS AND METHODS

3.3.1 DOM Sample Collection

Dissolved organic matter samples were collected at the National Energy Laboratory Hawai'i Authority (NELHA) on the island of Hawai'i in the North Pacific Subtropical Gyre (NPSG) in March, 2019. At NELHA, seawater is piped from two depths, 15 m and 900 m, to on-shore pumping stations at high flow rates (36,000 to 50,000 L min^{-1}). Previous studies have found that organic carbon concentration and carbon isotope values at NELHA are similar to those found at Station ALOHA, a nearby hydrographic study site with biogeochemical properties characteristic of the greater North Pacific Subtropical Gyre (P. M. Williams & Druffel, 1987). The NELHA pumping site is, therefore, an excellent location for collecting large quantities of environmentally representative DOM for characterization and ^{14}C analysis.

Dissolved inorganic carbon (DIC) samples were collected in acid-cleaned, combusted, 500 mL borosilicate bottles directly from the pump outlet. Samples were spiked with $HgCl_2$ to inhibit biological activity, and sealed with no headspace. A 1 L sample for total DOC radiocarbon analysis was collected from 900 m into an acid-cleaned, combusted borosilicate bottle. The sample was spiked with UV treated o-phosphoric acid and sealed. HMWDOM was collected via ultrafiltration. A full description of this method can be found in Chapter 2. Briefly, DOM was concentrated from seawater using a tangential flow filtration system with a nominal 1 kDa MWCO. The concentrate was desalted via diafiltration and freeze-dried, resulting in a white, fluffy powder. HMWDOM from approximately 12,000 L of seawater was isolated from both depths during the field campaign.

LMWDOM isolated by solid phase extraction (LMWSPEDOM) was collected by passing the ultrafiltration permeate (nominally < 1 kDa MW) through SPE columns packed with C18 modified polystyrene/divinylbenzene beads. DOM from 200 L of acidified (~pH 2) permeate was collected on SPE cartridges. The columns were washed by passing 100 mL (15 column volumes) of high purity water (18.2 MΩ cm [MQ-H_2O]) to remove salts and LMWSPEDOM was recovered with 50 mL of methanol and dried under vacuum (see Chapter 2 for additional details).

3.3.2 Mixed-Mode Chromatographic Separation and NMR analysis of HMWDOM

High performance liquid chromatography (HPLC) was used to separate the components of HMWDOM using a column (7.8 x 300 mm, 9 μm; Supelcogel) packed with sulfonated polystyrene/divinylbenzene (8% crosslinked) with Ca^{+2} as a counter ion. Separation was primarily size based but the calcium counterions interact with vicinal, axial-equatorial -OH groups, improving separation (Honda et al., 1984). Thus, mixed-mode chromatography (MMC) is the best designation for the technique. Samples were analyzed on an Agilent HPLC (Agilent 1200 Series). MQ-H_2O was used as the mobile phase at a flow rate of 0.25 mL min^{-1} and the column was kept at 45ºC to improve separation. Lyophilized HMWDOM was redissolved in MQ-H_2O to a concentration of 20 mg mL^{-1} and repeat 25 μL (0.5 mg) injections were performed to collect enough material for further analysis. Each chromatographic run lasted 35 minutes with a 5-minute post-run time. Fractions were collected every minute from 17 to 29 minutes during the chromatographic run. Fractions from each run were pooled under vacuum at room temperature. A total of 148 g of 15 m HMWDOM and 118 g of 900 m HMWDOM were processed by MMC. 73% of the HMWDOM was recovered after the MMC, although this likely represents a lower estimate of recovery as salt content of the whole HMWDOM sample was

higher than the salt content of the MW fractions, and the fractions were more thoroughly dried before gravimetry than whole HMWDOM sample. Polystyrene sulfonate and pullulan MW standard (PSS Polymer Standard Services, Germany) were used to relate retention time and MW.

NMR spectra were collected on a Bruker Avance Neo NMR 400 MHz. Samples were dissolved in D_2O at a concentration of 1 mg mL^{-1} and all spectra were acquired at 302 K. 1D ^1H-NMR spectra are recorded using a Noesy-presaturation solvent suppression. ^1H spectra were analyzed using the TopSpin™ 4.1.3 software. Spectral subtraction was used to determine the proportion of APS and HS in each fraction (Figure 3.1). A ^1H spectrum of nearly pure APS was subtracted from the ^1H spectra of the MMC fractions to determine the HS component (Hertkorn et al., 2006). Spectra were normalized at 3.3 ppm, assuming all signals at that chemical shift are due to the APS component. To convert from proton to carbon content, the ^1H signal was multiplied by the C:H ratio for the functional groups attributed to each resonance. For APS, a 1:1 ratio was used for signals between 4.5 and 3.2 ppm (**H**COD), a 2:3 ratio was used for signals between 2.1 and 1.6 ppm (**H**$_3$CC=OND), and a 1:3 ratio is used for signals between 1.4 and 0.9 ppm (C**H**$_3$) (Aluwihare et al., 1997). For HS, all signal between 4.5 and 0.5 ppm were converted using 1:1.6 ratio of carbon to protons, which is based on the stoichiometry of HS chemical formula determined by high-resolution mass spectrometry performed in negative mode. The identified formulas have a number averaged MW of 372 Da, much lower than the average MW of HS calculated from DOSY but have similar spectroscopic properties to HS (Hertkorn et al., 2013).

Diffusion-ordered spectroscopy (DOSY) spectra were recorded using the STEBPGP1S19 pulse program with bipolar gradient pulses and a 3-9-19 water suppression sequence. A maximum gradient strength of 53.5 G cm^{-1} was varied between 2 and 95%. Diffusion parameters

were optimized using an aprotinin and polystyrene sulfonate. DOSY spectra were analyzed using Bruker Dynamic Center 2.7.1. Pullulan and polystyrene sulfonate MW standards were used to create a MW–diffusivity standard curve, allowing for the conversion of sample diffusivity to MW.

3.3.3 Isotopic Analysis of HMWDOM

Stable carbon and radiocarbon isotope analyses were performed at the National Ocean Sciences Accelerator Mass Spectrometry (NOSAMS) Facility in Woods Hole, MA. DIC samples and the total DOC sample were processed following the standard seawater protocols (Beaupré et al., 2007; McNichol et al., 1994). Dried HMWDOM samples were transferred to quartz combustion tube along with precombusted silver and copper oxide. Tubes were sealed and heated at 850ºC for 5 hr to convert the organic carbon to CO_2, which was then cryogenically trapped. A subsample of CO_2 was taken for stable carbon isotope analysis (reported as $\delta^{13}C$), while the remaining gas was reduced to graphite with H_2 and an Fe catalyst. Graphite samples were analyzed for radiocarbon content via accelerator mass spectrometry. Process blanks and radiocarbon standards were measured, and all radiocarbon values presented here are reported in $\Delta^{14}C$ notation following standard conventions (Stuiver & Polach, 1977). Analytical precision of the radiocarbon analysis is 1‰–5‰ and all uncertainties presented in this work describe the standard error of the mean. Stable carbon isotope samples were measured on a dual-inlet Optima or Prism IRMS system. Instrument precision was ±0.15‰. Further information on the carbon isotope analysis procedures can be found on the NOSAMS website (https://www2.whoi.edu/site/nosams/client-services/submitting_guidelines/sample_processes/).

Pullulan and polystyrene sulfonate standards were run in parallel with the HMWDOM samples through the MMC and DOSY analyses to detect and evaluate isotopic contamination.

Pullulan has a measured modern $\Delta^{14}C$ value (41‰) and polystyrene sulfonate was measured to be isotopically depleted ($\Delta^{14}C$ = -1000‰). 20 mg of the pullulan and 12 mg of the polystyrene sulfonate standard were prepared, fraction collected, and analyzed via DOSY in the same fashion as the HMWDOM samples to ensure that any contamination introduced by MMC and sample processing was detected. The $\Delta^{14}C$ values of the pullulan and polystyrene after MMC and DOSY procedures were 12‰ and -973‰, respectively.

3.4 RESULTS AND DISCUSSION

3.4.1 HMWDOM Component Analysis

Eleven MMC fractions of HMWDOM were collected from the 15 m and 900 m HMWDOM samples during each chromatographic run. Each fraction was analyzed by ^{1}H-NMR and DOSY spectroscopy to track composition and MW distribution. The fractions decreased in average MW with increasing fraction number (retention time), with the MW plateauing in the late-eluting fractions (Figure 2.7). Spectral subtraction yielded the proportion of HS and APS in each fraction (Figure 3.1). The fractions from both HMWDOM samples taken together span a broad range of HS content from 4% to 80%. This estimation gives a lower bound for HS content as the spectrum representing the APS endmember likely contains trace HS, resulting in a small underestimation of HS signal during processing.

The dry weight of each fraction and the relative amounts of HS and APS are shown in Table 1. In both the 15 m and 900 m samples, the amount of HS increased in later eluting fractions, indicating that HS is smaller than APS, agreeing with the DOSY analysis of the total HMWDOM, which found that HS had a greater diffusivity, and therefore a lower MW than APS. The 900 m sample fractions also contained the same concentration of HS as the 15 m sample,

suggesting that APS is preferentially removed, and that HS has a longer residence time and is more recalcitrant than APS.0

Table 3.1: HMWDOM fraction abundance, carbon content, and HS content. The abundance is based on dry weight and normalized for carbon content. The HS content of each fraction was determined via ^{1}H-NMR spectral subtraction and is given as a percentage of total carbon.

Depth (m)	Sample	Dry Weight (mg)	Percent Carbon (%)	Fraction Abundance (%)	HS-Carbon (%)
	Total HMWDOM	5.0	34	100	16
	F1	1.3	35	1.2	16
	F2	5.7	39	5.2	7
	F3	23.4	40	21	4
	F4	27.1	36	25	5
	F5	19.0	31	17	11
	F6	13.9	33	13	26
	F7	7.8	37	7.1	35
	F8	4.5	39	4.1	39
	F9	2.6	36	2.4	43
	F10	1.9	35	1.7	44
	F11	1.4	34	1.3	45
900	Total HMWDOM	5.0	28	100	45
	F1	1.2	36	1.4	33
	F2	4.3	39	4.9	19
	F3	13.9	39	16	18
	F4	14.1	33	16	23
	F5	11.8	27	14	30
	F6	14.5	28	17	52
	F7	10.9	28	13	64
	F8	6.5	35	7.6	74
	F9	3.6	40	4.2	76
	F10	2.9	40	3.0	76
	F11	1.9	40	2.2	80

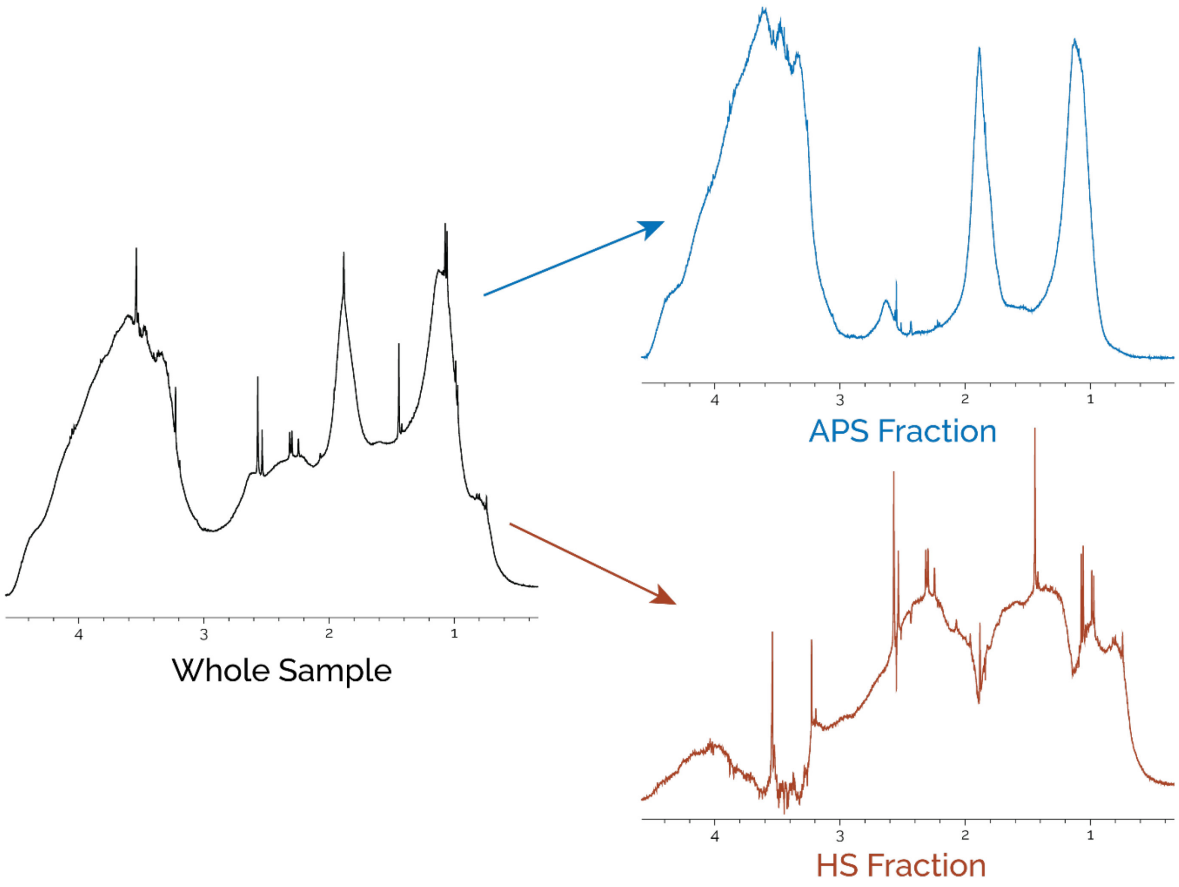

Figure 3.1: Example of ^{1}H-NMR spectral subtraction results yielding APS and HS components from spectrum from the 900 m sample.

3.4.2 Radiocarbon Content of MMC Fractions

The carbon isotope results for the MMC fractions of each HMWDOM sample are shown in Table 3.2. Radiocarbon values for the total HMWDOM were -30 ± 2‰ and -238 ± 2‰ for the 15 m and 900 m samples, respectively, agreeing well with previously reported measurements (Repeta & Aluwihare, 2006; Walker et al., 2011; Walker, Beaupré, et al., 2016; Zigah et al., 2017). The 15 m HMWDOM radiocarbon value is more depleted than surface seawater DIC by 43‰ and HMWDOM continues the observed trend of a temporal decrease in radiocarbon coinciding with the decline of the bomb spike over the past 35 years. The fact that our samples

continue this trend is good indication that the samples used in this experiment are comparable to material analyzed in other studies, and represent HMWDOM in the environment.

Table 3.2: Carbon isotope values for DIC, total HMWDOM, MMC fractions of HMWDOM and LMWSPEDOM from 900 m. Standard error is shown for the ^{14}C isotopic values.

Depth (m)	Sample	δ13C (‰)	Δ14C (‰)	±SE (‰)
15	DIC	0.60	13.1	2.8
	Total HMWDOM	-22.78	-29.9	2.3
	F1	-23.99	-25.6	3.4
	F2	-23.56	-0.5	2.2
	F3	-22.62	1.6	2.4
	F4	-22.29	-7.2	2.4
	F5	-21.91	-37.9	2.3
	F6	-22.14	-75.1	1.9
	F7	-22.12	-88.0	1.9
	F8	-22.26	-87.0	1.9
	F9	-22.15	-80.2	2.3
	F10	-23.89	-123.0	2.6
	F11	-23.82	-178.7	2.7
900	DIC	-0.18	-193.5	1.8
	Total DOC	-23.62	-499.2	4.7
	Total HMWDOM	-21.66	-238.7	1.8
	F1	-22.8	-174.9	3.0
	F2	-20.54	-212.9	1.9
	F3	-20.85	-227.3	1.9
	F4	-20.76	-230.9	2.8
	F5	-22.12	-230.2	2.0
	F6	-22.94	-251.1	2.5
	F7	-23.48	-297.7	1.9
	F8	-23.83	-271.1	2.6
	F9	-25.62	-239.5	3.3
	F10	-25.3	-308.7	3.2
	F11	n.d.	n.d.	
	LMWSPEDOM	-23.41	-507.3	2.3

n.d.: Sample contaminated and unable to be analyzed

The radiocarbon content of the MMC fractions had a broad range of values with later-eluting fractions tending toward more depleted $\Delta^{14}C$ values. In the 15 m sample fractions, $\Delta^{14}C$ values ranged from 2 ± 2‰ to -179 ± 3‰. The most enriched fraction had a radiocarbon content near DIC (13‰) while the most depleted fraction (-179‰) resembled total surface DOC radiocarbon (-179 ± 2‰ (Zigah et al., 2017)), indicating that the carbon in HMWDOM is not turning over homogenously. A portion of the 15 m sample is not freshly synthesized indicating that a fraction of HMWDOM is capable of resisting microbial degradation and surviving over the timescales of ocean mixing. In the 900 m sample, radiocarbon content ranged from -175 ± 3‰ to -309 ± 3‰, with the most enriched value only slightly more enriched than $\Delta^{14}C$-DIC from 900 m (-193‰). Total DOC radiocarbon at that depth is more depleted (-499 ± 5‰) than any of the 900 m HMWDOM fractions, suggesting that a significant fraction of younger material remains in deep HMWDOM.

3.4.3 A Relationship Between Radiocarbon and Humic Content

Neutral sugar radiocarbon analysis has shown previously that APS has a short residence time of 1–3 or 20–25 yrs in the surface ocean (Repeta & Aluwihare, 2006). It follows then, that the degree of depletion of the radiocarbon value of HMWDOM, relative to $\Delta^{14}C$-DIC, is likely the result of the HS content of the material. To examine this further, the relative HS content of each fraction of the 15 m and 900 m samples was plotted against its $\Delta^{14}C$ value (Figure 3.2). A Model II linear regression (geometric mean linear regression) was used to examine the relationship between HS and $\Delta^{14}C$ (Legendre & Legendre, 2012; Sokal & Rohlf, 1995). Linear regression analysis of the 15 m sample suggests a good correlation between HS and $\Delta^{14}C$ (r^2 = 0.84, $p < 0.0001$). Extrapolation to the theoretical surface APS endmember (zero HS content) predicts that APS should have a radiocarbon value of 13 ± 27‰, equal to $\Delta^{14}C$-DIC (13‰). The

uncertainty represents the 95% confidence interval around the extrapolated value. This result constrains the APS turnover time to 1-3 yrs based on a simple box model for APS in the surface ocean (Repeta & Aluwihare, 2006; P. M. Williams & Druffel, 1987). The model uses Δ^{14}C-DIC from several previous studies and assumes that the Δ^{14}C-DIC value and the Δ^{14}C of APS in the prebomb ocean to be -80‰ (Mahadevan, 2001; Pearson, 1999; Repeta & Aluwihare, 2006; Walker et al., 2011; Zigah et al., 2017). APS Δ^{14}C values are calculated by equation 1:

$$\Delta^{14}C_{APS}(t) = \Delta^{14}C_{DIC}(t_0)(k) + \Delta^{14}C_{APS}(t_{-1})(1-k) \quad (1)$$

Where *t* is the year and *k* is the fractional annual replacement of APS (reciprocal of the turnover time in years). The model assumes that the concentration of APS in the surface ocean is in steady state, the annual removal rate remains constant, and that there is no isotopic fractionation in APS removal (Figure 3.5, in Supplemental). Δ^{14}C values were determined using this model for 4 different turnover times (1.5 yrs, 3 yrs, 10 yrs, & 20 yrs). Previous work constrained the turnover of APS to 1-3 yrs or 20-25 yrs based on radiocarbon modeling. If the turnover time of APS was 20-25 yrs, APS sampled in 2019 would have a Δ^{14}C of approximately 66‰, which is more enriched than the surface HMWDOM linear regression predicts. This result confirms that APS has a short lifetime in the surface ocean.

Linear regression of the 900 m sample ($r^2 = 0.52$, $p < 0.05$) showed a weaker, but statistically significant correlation between HS content and radiocarbon. The APS endmember was predicted to have a Δ^{14}C of -190 ± 43‰, similar to the Δ^{14}C-DIC from 900 m (-193‰). There are two possible sources for this aged APS in the deep sea. 1) APS is produced in the surface and is slowly removed as the water parcel is advected to depth. While the radiocarbon age of surface APS suggests a short turnover time, microbial respiration decreases rapidly below the mixed layer (~50 m in the NPSG) resulting in a decrease in remineralization rates for

advected material, allowing APS to survive to depth (Martínez-García, 2017; P. J. le B. Williams et al., 2004). In this model, the APS in HMWDOM should continue to age with water mass age and the concentration of APS would be controlled by the balance between the remineralization rate and water mass ventilation time. 2) APS carbon is fixed *in situ* at 900 m, by chemoautotrophic organisms. Recent work examining nitrite oxidizing autotrophs in the mesopelagic estimated that *Nitrospinae* fixed roughly 1 Pg C yr^{-1} between 500 m and 1000 m, nearly 10% of the particulate carbon flux from the euphotic zone (Dunne et al., 2007; Pachiadaki et al., 2017). A Previous study of lipid biomarker radiocarbon analysis also found as much as 86% of glycerol dialkyl glycerol tetraether could be produced *in situ* at 670 m by the archaeal community (Ingalls et al., 2006). It is plausible, then, that a major fraction of APS could be synthesized at depth, and that the true turnover time of the material is much shorter than the radiocarbon value reflects (Middelburg, 2011).

Extrapolating the linear regression to 100% HS content provides a theoretical radiocarbon value for the HS endmember. As this extrapolation extends far beyond the HS values of measured samples, a large uncertainty is associated with the predicted value, and so it is more difficult to draw concise conclusions about the age of this material. It is also likely that this endmember is itself a mixture of compounds with a spectrum of radiocarbon ages, resulting in a theoretical endmember with a decay rate that represents the average of parallel first-order day rates for each of the component compounds individually (Follett et al., 2014). The HS endmembers of both the 15 m and 900 m samples had similar radiocarbon values of -295 ± 74‰ and $\Delta^{14}C$ of -306 ± 49‰, respectively. These values are more enriched, within the uncertainty, compared to the fraction of $\Delta^{14}C$ of HMWDOM isolated by anion exchange chromatography (-416‰; Repeta & Aluwihare, 2006; Zigah et al., 2017) potentially suggesting this analysis is

capturing a compositionally different fraction of HS than can be chemically extracted using SPE or anion exchange resins. The radiocarbon value of the surface HS endmember suggests that it is a mixture of modern HS ($_{m}$HS), which likely has a radiocarbon value similar to the autochthonously produced APS (+13‰), and refractory HS ($_{r}$HS) which has an old but undetermined radiocarbon age. By assuming that the radiocarbon value of $_{r}$HS falls between the value of the material extracted from HMWDOM by SPE (-416‰) and deep DOC (-540‰; P. M. Williams & Druffel, 1987), the portion of HS that is comprised of $_{r}$HS likely ranges from 55% to 71%, indicating that a majority of HS in the surface ocean is old, advected material.

The difference in age between the surface and 900 m endmembers ranges from ~200 to ~1500 yrs, with the uncertainty from extrapolation preventing a more precise determination of the differences in age. If the $\Delta^{14}C$ values of the surface and deep HS endmembers are similar, that would suggest there is a source of radiocarbon replete HS that shifts the average HS age in the deep to be more modern, balancing the aging that occurred during advection. Source of $_{m}$HS to the deep ocean could come from *in situ* production as described for chemoautotrophy-derived APS, or from dissolution of sinking particles (Follett et al., 2014; Orellana & Hansell, 2012). Alternatively, if the difference in age between the surface and 900 m HS components is ~1500 yrs, this would suggest that APS and mHS age at a similar rate below the surface. In Chapter 2, it was demonstrated that the size distribution of HS decreases between the 15 m and 900 m samples. If the highest MW component of HS is degraded into smaller material without significant remineralization, the radiocarbon ages of the two samples, would be offset only by the average age of the material at the surface. The APS and HS endmembers would appear to age at the same rate between the two samples. While it is not possible to determine which of these models of HS cycling is dominant based on these radiocarbon measurements alone, both models

suggest a unique cycling of HS in the ocean and lead to further questions about the sources of HS to the ocean interior.

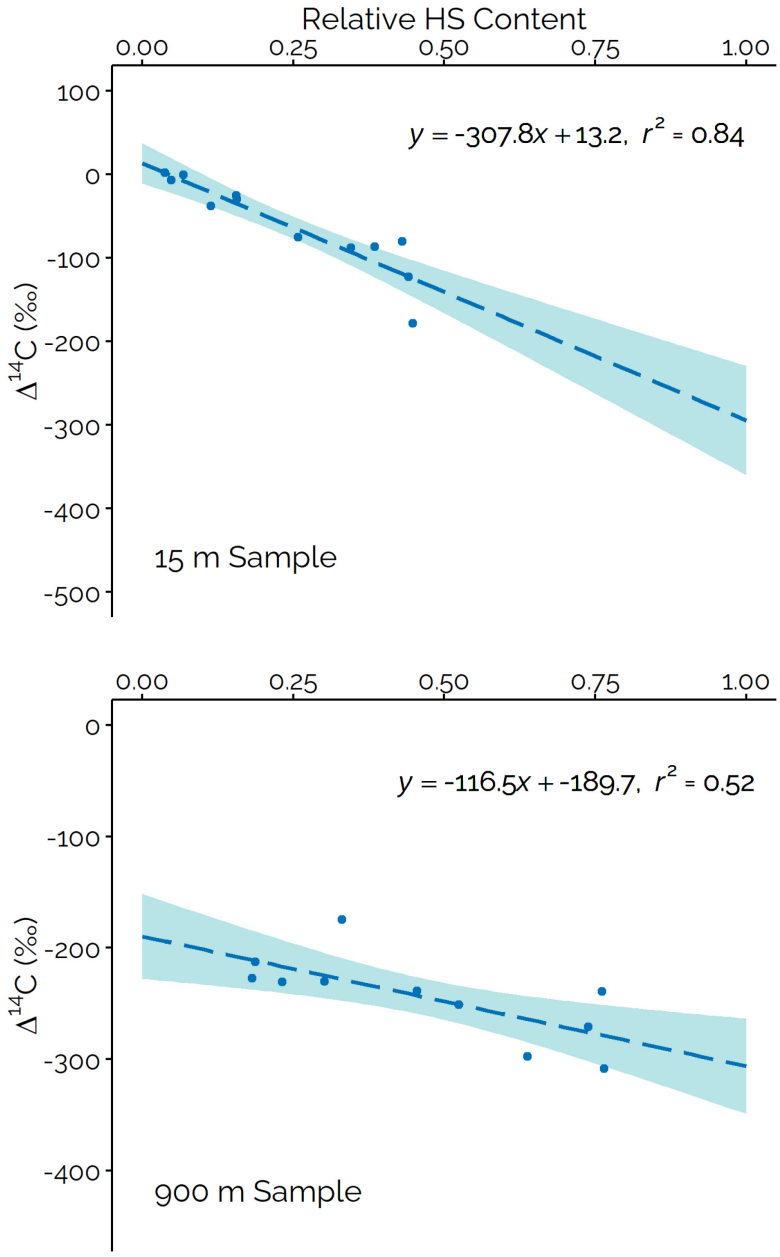

Figure 3.2: Geometric mean linear regression modeling suggests a strong relationship between HS content and $\Delta^{14}C$ value in both the 15 m (top) and 900 m (bottom) samples. Shaded blue regions are the 95% confidence limits for the regression lines. Slopes are statistically significant ($\alpha = 0.05$, $p < 0.05$).

3.4.4 A Relationship Between Stable Carbon Isotope Values and Humic Content

Stable carbon isotope analysis added a second dimension by which to examine the changes in HS composition between the two samples. Linear regression revealed a strong correlation ($r^2 = 0.88$, $p < 0.0001$) between $\delta^{13}C$ and HS content in the 900 m sample (Figure 3.3). The APS endmember has a predicted $\delta^{13}C$ value of -19.7 ± 1.0‰, which is similar, within the uncertainties of the extrapolation, to typical $\delta^{13}C$ values of autochthonously produced DOM (-21.0 ± 2‰) in the ocean (Druffel et al., 1992; Walker et al., 2014; P. M. Williams & Druffel, 1987). This supports the conclusion that APS is autochthonously produced, without significant input from littoral (-17 ± 2‰) DOM (Foley & Koch, 2010).

The HS endmember is predicted to have a $\delta^{13}C$ value of -26.6 ± 1.1‰, significantly lighter than the average $\delta^{13}C$-DOM signature. It has been shown that DOM extracted by SPE (SPEDOM) has a lighter $\delta^{13}C$ value compared to total DOM, however the $\delta^{13}C$ values for SPEDOM are typically -22‰ to -24‰, more enriched than the predicted HS endmember. This result provides further support for the conclusion that the methods used in this chapter are capturing a compositionally distinct fraction of HS from SPE. The deleted isotope signature also supports the hypothesis that HS is derived from the degradation and oxidation of lipids. Phytoplankton lipids can be as much as 8‰ depleted in ^{13}C compared to TPOM due to metabolic fractionation, which may explain the light $\delta^{13}C$ value predicted for HS (Lamb et al., 2006; Park & Epstein, 1961). It is interesting that this light isotope signature is not observed in the 15 m sample. No correlation between HS and $\delta^{13}C$ was observed in that sample (not shown). This suggests that a portion of HS with a heavy $\delta^{13}C$ value is removed from the surface ocean during advection, resulting in a light isotopic value for the remaining material. Chapter 2 demonstrated that the total amount of HS in seawater does not decrease significantly between the 15 m and 900

m samples, despite a decrease in the concentrations of TDOM and HMWDOM. If HS with an enriched $\delta^{13}C$ signature is removed from the surface HS during advection, the material must be replaced to keep the concentration of HS constant. This result lends evidence to the hypothesis that a source of $_{m}HS$ with a light $\delta^{13}C$ signature supplies DOM to the deep ocean.

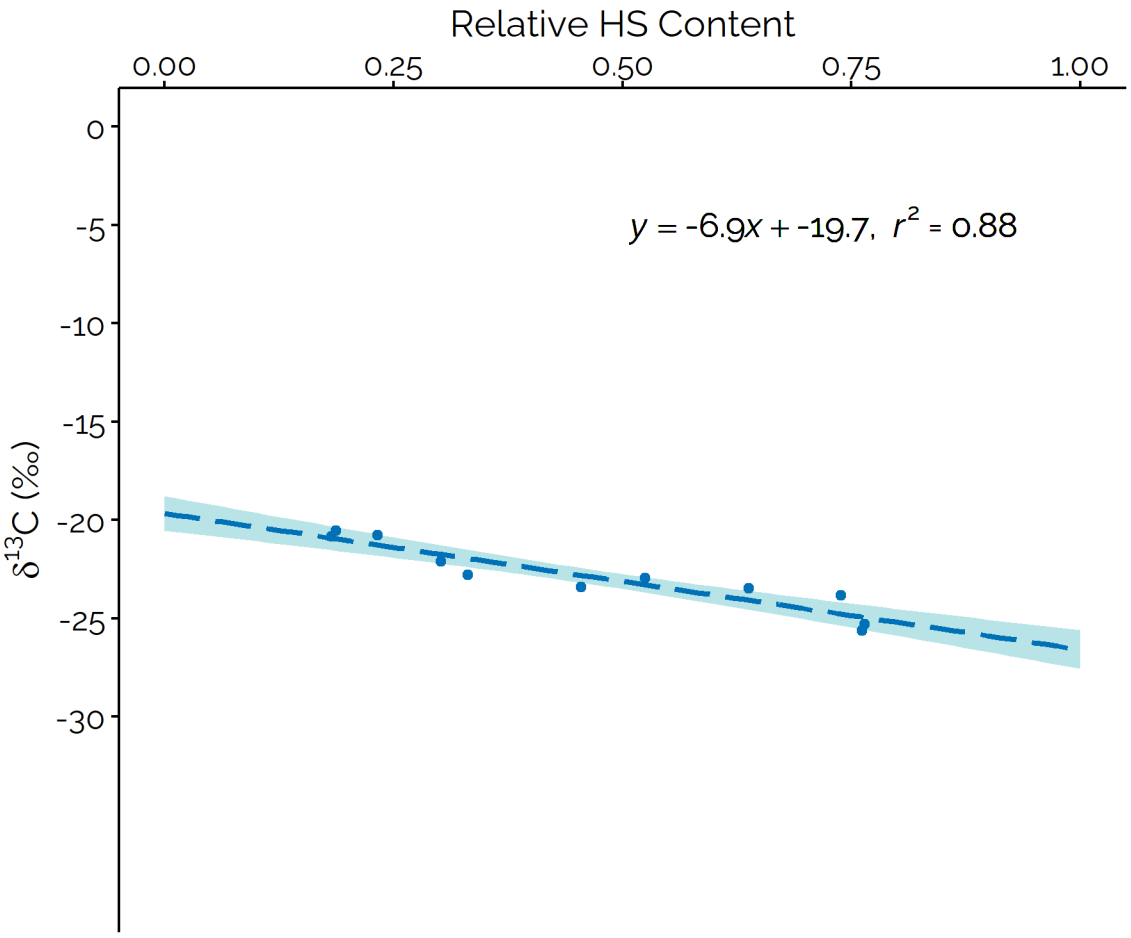

Figure 3.3: Geometric mean linear regression modeling suggests a strong relationship between HS content and $\delta^{13}C$ value in and 900 m HMWDOM sample. Shaded blue regions are the 95% confidence limits for the regression lines. Slopes are statistically significant ($\alpha = 0.05$, $p < 0.001$).

3.4.5 Implications for the Size–Reactivity Continuum Hypothesis

In Chapter 2, HMWDOM was described as containing two distinct chemical components and it was proposed that each component has a different diagenetic fate. APS is produced autochthonously and is rapidly and monotonically remineralized, likely through ectoenzyme activity. Radiocarbon analysis of the APS endmember suggests a turnover time in the ocean of 1–3 yrs. HS diagenesis follows a different path where, in surface waters, $_{m}$HS is produced alongside a pool of $_{r}$HS, which has a radiocarbon age of 2–6 kyr. There is a shift in the MW distribution of HS between the surface and 900 m towards smaller material, however the concentration of HS does not decrease significantly with depth (Chapter 2), suggesting that either $_{m}$HS is decomposed into compounds with a lower MW, or $_{m}$HS is removed and replaced with material that has a lower average MW. Stable carbon isotope analysis suggests that the replacement model is more likely as there is a large shift in $\delta^{13}C$ of HS between the surface and deep samples. The process of $_{r}$HS formation is still not well characterized, but models of humification include the polymerization of refractory biomolecules, secondary synthesis of small molecules, and the formation of supramolecular aggregates from $_{r}$DOM.

Based on the size-distribution and radiocarbon analysis data, HMWDOM is not an intermediate between POC and $_{r}$DOM and radiocarbon measurements of whole HMWDOM do not represent the complex composition of HMWDOM and do not support the SRC. When the $\Delta^{14}C$ of the two end-members are plotted alongside radiocarbon measurements of other organic matter size fractions, the size-age relationship disappears. Instead, in the surface APS has a similar $\Delta^{14}C$ value to the largest OM fractions, containing fresh biomass and cellular material, while HS has a similar $\Delta^{14}C$ value LMWDOM. In the deep ocean, APS continues to resemble $\Delta^{14}C$-DIC while HS has a similar or slightly older radiocarbon value than in the surface, despite

a shift in average MW that appears decoupled from aging. With this new framework, several questions emerge about the sources of the deep HMWDOM components. Is APS preserved by advection into the ocean interior, or does chemoautotrophic production account for a significant fraction of APS in the deep ocean? Is there a source of modern HS to the ocean interior? These questions should be the focus of future research on DOM cycling.

3.4.6 Future Implementations of This Work

While the importance of HS in the marine carbon cycle has been demonstrated repeatedly, the dominant mechanism of HS formation and the relationship between HS and LMWSPEDOM remain unknown (Arakawa et al., 2017; Cao et al., 2018; He et al., 2022; Hertkorn et al., 2006). Based on studies of soil organic matter degradation, three mechanisms for HS formation have been proposed. 1) The spontaneous secondary synthesis (SSS) model suggests that small molecules can abiotically react to form large geopolymers through radical or enzyme mediated reactions (De Nobili et al., 2020). 2) The biopolymer degradation and polymerization model (BDP) suggests that large, refractory biopolymers are preferentially conserved and then partially degraded to form HS (Sollins et al., 1996). 3) The supramolecular structure hypothesis (SMS) states that HS is a collection of small recalcitrant molecules that are non-covalently bonded together forming a supramolecular aggregate in equilibrium with the surrounding medium (Piccolo, 2001). While evidence for each of these theories has been presented, it remains unclear which process is most important for marine HS production.

The techniques described in this study could be applied to glean new information about $_{r}$DOM formation. By isolating DOM via UF and SPE and then creating size fractions that span the division between LMW and HMW through the use of MMC, it would be possible to determine which HS production mechanism is dominant. If BDP is the dominant process of

humification, then it would be expected that larger MW compounds become smaller with time as the large biopolymers are degraded. If SSS is the dominant process, then the larger MW $_r$DOM should have the oldest radiocarbon age, as this process involves the formation of larger molecules through the abiotic condensation of small molecules. This mechanism would be counter to the prevailing diagenetic flow described by the SRC. If the SMS model is the dominant process, then there would be no relationship between size and radiocarbon age, as SPEDOM would represent an equilibrium between individual small molecules and the condensed aggregates. Size fractionation, DOSY spectroscopy, and radiocarbon analysis in tandem could provide a powerful tool to probe these mechanisms.

3.5 CONCLUSIONS

This work provides a new conceptual framework for describing the diagenetic fate of HMWDOM. Instead of treating HMWDOM as a single class of DOM representing the diagenetic intermediate between particulate organic matter and $_r$DOM, this model treats HMWDOM as a composite of newly derived algal compounds such as APS, and HS. These two components are degraded at different rates through the water column and the mechanisms of degradation may be different. This work also shows that HS isolated by UF is compositionally distinct from SPEDOM and suggests that several different mechanisms impact the age, size, and concentration of HS in the ocean interior. The source of HS to the deep ocean and the decomposition mechanisms of HS are not well defined and are important areas of future study to understand the processes of OM formation and preservation in the ocean.

3.6 REFERENCES

Aluwihare, L. I., Repeta, D. J., & Chen, R. F. (1997). A major biopolymeric component to dissolved organic carbon in surface sea water. *Nature*, *387*(6629), 166–169. https://doi.org/10.1038/387166a0

Amon, R. M. W., & Benner, R. (1994). Rapid cycling of high-molecular weight dissolved organic matter in the ocean. *Nature*, *369*, 549–552.

Amon, R. M. W., & Benner, R. (1996). Bacterial utilization of different size classes of dissolved organic matter. *Limnology and Oceanography*, *41*(1), 41–51.

Arakawa, N., Aluwihare, L. I., Simpson, A. J., Soong, R., Stephens, B. M., & Lane-Coplen, D. (2017). Carotenoids are the likely precursor of a significant fraction of marine dissolved organic matter. *Science Advances*, *3*(9), 1–12. https://doi.org/10.1126/sciadv.1602976

Beaupré, S. R., Druffel, E. R. M., & Griffin, S. (2007). A low-blank photochemical extraction system for concentration and isotopic analyses of marine dissolved organic carbon. *Limnology and Oceanography: Methods*, *5*(6), 174–184. https://doi.org/10.4319/lom.2007.5.174

Benner, R., & Amon, R. M. W. (2015). The size-reactivity continuum of major bioelements in the ocean. *Annual Review of Marine Science*, *7*(1), 185–205. https://doi.org/10.1146/annurev-marine-010213-135126

Cao, X., Aiken, G. R., Butler, K. D., Huntington, T. G., Balch, W. M., Mao, J., & Schmidt-Rohr, K. (2018). Evidence for major input of riverine organic matter into the ocean. *Organic Geochemistry*, *116*, 62–76. https://doi.org/10.1016/j.orggeochem.2017.11.001

De Nobili, M., Bravo, C., & Chen, Y. (2020). The spontaneous secondary synthesis of soil organic matter components: A critical examination of the soil continuum model theory. *Applied Soil Ecology*, *154*. https://doi.org/10.1016/j.apsoil.2020.103655

Druffel, E. R. M., Williams, P. M., Bauer, J. E., & Ertel, J. R. (1992). Cycling of dissolved and particulate organic matter in the open ocean. *Journal of Geophysical Research: Oceans*, *97*(C10), 15639–15659.

Dunne, J. P., Sarmiento, J. L., & Gnanadesikan, A. (2007). A synthesis of global particle export from the surface ocean and cycling through the ocean interior and on the seafloor. *Global Biogeochemical Cycles*, *21*(4). https://doi.org/10.1029/2006GB002907

Foley, M. M., & Koch, P. L. (2010). Correlation between allochthonous subsidy input and isotopic variability in the giant kelp *Macrocystis pyrifera* in central California, USA. *Marine Ecology Progress Series*, *409*, 41–50. https://doi.org/10.3354/meps08600

Follett, C. L., Repeta, D. J., Rothman, D. H., Xu, L., & Santinelli, C. (2014). Hidden cycle of dissolved organic carbon in the deep ocean. *Proceedings of the National Academy of Sciences of the United States of America*, *111*(47), 16706–16711. https://doi.org/10.1073/pnas.1407445111

Hansell, D. A. (2013). Recalcitrant dissolved organic carbon fractions. *Annual Review of Marine Science*, *5*, 421–425. https://doi.org/10.1146/annurev-marine-120710-100757

He, C., Liu, J., Wang, R., Li, Y., Zheng, Q., Jiao, F., He, C., Shi, Q., Xu, Y., Zhang, R., Thomas, H., Batt, J., Hill, P., Lewis, M., Maclntyre, H., Lu, L., Zhang, Q., Tu, Q., Shi, T., … Jiao, N. (2022). Metagenomic evidence for the microbial transformation of carboxyl-rich alicyclic molecules: A long-term macrocosm experiment. *Water Research*, *216*, 118281. https://doi.org/10.1016/J.WATRES.2022.118281

Hemingway, J. D., Rothman, D. H., Grant, K. E., Rosengard, S. Z., Eglinton, T. I., Derry, L. A., & Galy, V. V. (2019). Mineral protection regulates long-term global preservation of natural organic carbon. *Nature*, *570*(7760), 228–231. https://doi.org/10.1038/s41586-019-1280-6

Hertkorn, N., Benner, R., Frommberger, M., Schmitt-Kopplin, P., Witt, M., Kaiser, K., Kettrup, A., & Hedges, J. I. (2006). Characterization of a major refractory component of marine dissolved organic matter. *Geochimica et Cosmochimica Acta*, *70*(12), 2990–3010. https://doi.org/10.1016/j.gca.2006.03.021

Hertkorn, N., Harir, M., Koch, B. P., & Michalke, B. (2013). High-field NMR spectroscopy and FTICR mass spectrometry: Powerful discovery tools for the molecular level characterization of marine dissolved organic matter. *Biogeosciences*, *10*, 1583–1624. https://doi.org/10.5194/bg-10-1583-2013

Honda, S., Suzuki, S., & Kakehi, K. (1984). Improved analysis of aldose anomers by high-performance liquid chromatography on cation-exchange columns. *Journal of Chromatography A*, *291*, 317–325. https://doi.org/10.1016/S0021-9673(00)95034-9

Ingalls, A. E., Shah, S. R., Hansman, R. L., Aluwihare, L. I., Santos, G. M., Druffel, E. R. M., & Pearson, A. (2006). Quantifying archaeal community autotrophy in the mesopelagic ocean using natural radiocarbon. *Proceedings of the National Academy of Sciences of the United States of America*, *103*(17), 6442–6447. https://doi.org/10.1073/pnas.0510157103

Lamb, A. L., Wilson, G. P., & Leng, M. J. (2006). A review of coastal palaeoclimate and relative sea-level reconstructions using δ13C and C/N ratios in organic material. *Earth-Science Reviews*, *75*(1), 29–57. https://doi.org/10.1016/j.earscirev.2005.10.003

Legendre, P., & Legendre, L. (2012). Interpretation of ecological structures. In *Developments in Environmental Modelling* (Vol. 24, pp. 521–624). Elsevier. https://doi.org/10.1016/B978-0-444-53868-0.50010-1

Mahadevan, A. (2001). An analysis of bomb radiocarbon trends in the Pacific. *Marine Chemistry*, *73*(3), 273–290. https://doi.org/10.1016/S0304-4203(00)00113-4

Martínez-García, S. (2017). Microbial respiration in the mesopelagic zone at Station ALOHA. *Limnology and Oceanography*, *62*(1), 320–333. https://doi.org/10.1002/lno.10397

McNichol, A. P., Jones, G. A., Hutton, D. L., Gagnon, A. R., & Key, R. M. (1994). The rapid preparation of seawater ΣCO_2 for radiocarbon analysis at the national ocean sciences ams facility. *Radiocarbon*, *36*(2), 237–246. https://doi.org/10.1017/S0033822200040522

Middelburg, J. J. (2011). Chemoautotrophy in the ocean. *Geophysical Research Letters*, *38*(24), n/a-n/a. https://doi.org/10.1029/2011GL049725

Orellana, M. V., & Hansell, D. A. (2012). Ribulose-1,5-bisphosphate carboxylase/oxygenase (RuBisCO): A long-lived protein in the deep ocean. *Limnology and Oceanography*, *57*(3), 826–834. https://doi.org/10.4319/lo.2012.57.3.0826

Pachiadaki, M. G., Sintes, E., Bergauer, K., Brown, J. M., Record, N. R., Swan, B. K., Mathyer, M. E., Hallam, S. J., Lopez-Garcia, P., Takaki, Y., Nunoura, T., Woyke, T., Herndl, G. J., & Stepanauskas, R. (2017). Major role of nitrite-oxidizing bacteria in dark ocean carbon fixation. In *Science* (Vol. 358, pp. 1046–1051). https://www.science.org

Park, R., & Epstein, S. (1961). Metabolic fractionation of C13 & C12 in plants 12. *Plant Physiology*, *36*(2), 133–138.

Pearson, A. (1999). *Biogeochemical applications of compound-specific radiocarbon analysis* [Thesis, Massachusetts Institute of Technology]. https://dspace.mit.edu/handle/1721.1/44599

Piccolo, A. (2001). The supramolecular structure of humic substances. *Soil Science*, *166*(11), 810–832. https://doi.org/10.1097/00010694-200111000-00007

Repeta, D. J., & Aluwihare, L. I. (2006). Radiocarbon analysis of neutral sugars in high-molecular-weight dissolved organic carbon: Implications for organic carbon cycling. *Limnology and Oceanography*, *51*(2), 1045–1053. https://doi.org/10.4319/lo.2006.51.2.1045

Sokal, R. R., & Rohlf, F. J. (1995). Linear Regression. In *Biometry: The principles and practice of statistics in biological research* (3rd ed, pp. 451–556). W.H. Freeman.

Sollins, P., Homann, P., & Caldwell, B. A. (1996). Stabilization and destabilization of soil organic matter: Mechanisms and controls. *Geoderma*, *74*(1–2), 65–105. https://doi.org/10.1016/S0016-7061(96)00036-5

Stuiver, M., & Polach, H. A. (1977). Discussion reporting of ^{14} C data. *Radiocarbon*, *19*(3), 355–363. https://doi.org/10.1017/S0033822200003672

Walker, B. D., Beaupré, S. R., Guilderson, T. P., Druffel, E. R. M., & McCarthy, M. D. (2011). Large-volume ultrafiltration for the study of radiocarbon signatures and size vs. Age relationships in marine dissolved organic matter. *Geochimica et Cosmochimica Acta*, *75*(18), 5187–5202. https://doi.org/10.1016/j.gca.2011.06.015

Walker, B. D., Beaupré, S. R., Guilderson, T. P., McCarthy, M. D., & Druffel, E. R. M. (2016). Pacific carbon cycling constrained by organic matter size, age and composition relationships. *Nature Geoscience*, *9*(12), 888–891. https://doi.org/10.1038/ngeo2830

Walker, B. D., Guilderson, T. P., Okimura, K. M., Peacock, M. B., & McCarthy, M. D. (2014). Radiocarbon signatures and size–age–composition relationships of major organic matter pools within a unique California upwelling system. *Geochimica et Cosmochimica Acta*, *126*, 1–17. https://doi.org/10.1016/j.gca.2013.10.039

Walker, B. D., Primeau, F. W., Beaupré, S. R., Guilderson, T. P., Druffel, E. R. M., & McCarthy, M. D. (2016). Linked changes in marine dissolved organic carbon molecular size and radiocarbon age. *Geophysical Research Letters*, 1–8. https://doi.org/10.1002/2013GL058740.Received

Williams, P. J. le B., Morris, P. J., & Karl, D. M. (2004). Net community production and metabolic balance at the oligotrophic ocean site, station ALOHA. *Deep Sea Research Part I: Oceanographic Research Papers*, *51*(11), 1563–1578. https://doi.org/10.1016/J.DSR.2004.07.001

Williams, P. M., & Druffel, E. R. M. (1987). Radiocarbon in dissolved organic matter in the central North Pacific Ocean. *Nature*, *330*(6145), 246–248. https://doi.org/10.1038/330246a0

Zigah, P. K., McNichol, A. P., Xu, L., Johnson, C. G., Santinelli, C., Karl, D. M., & Repeta, D. J. (2017). Allochthonous sources and dynamic cycling of ocean dissolved organic carbon revealed by carbon isotopes. *Geophysical Research Letters*, *44*(5), 2407–2415. https://doi.org/10.1002/2016GL071348

3.7 SUPPLEMENTAL INFORMATION

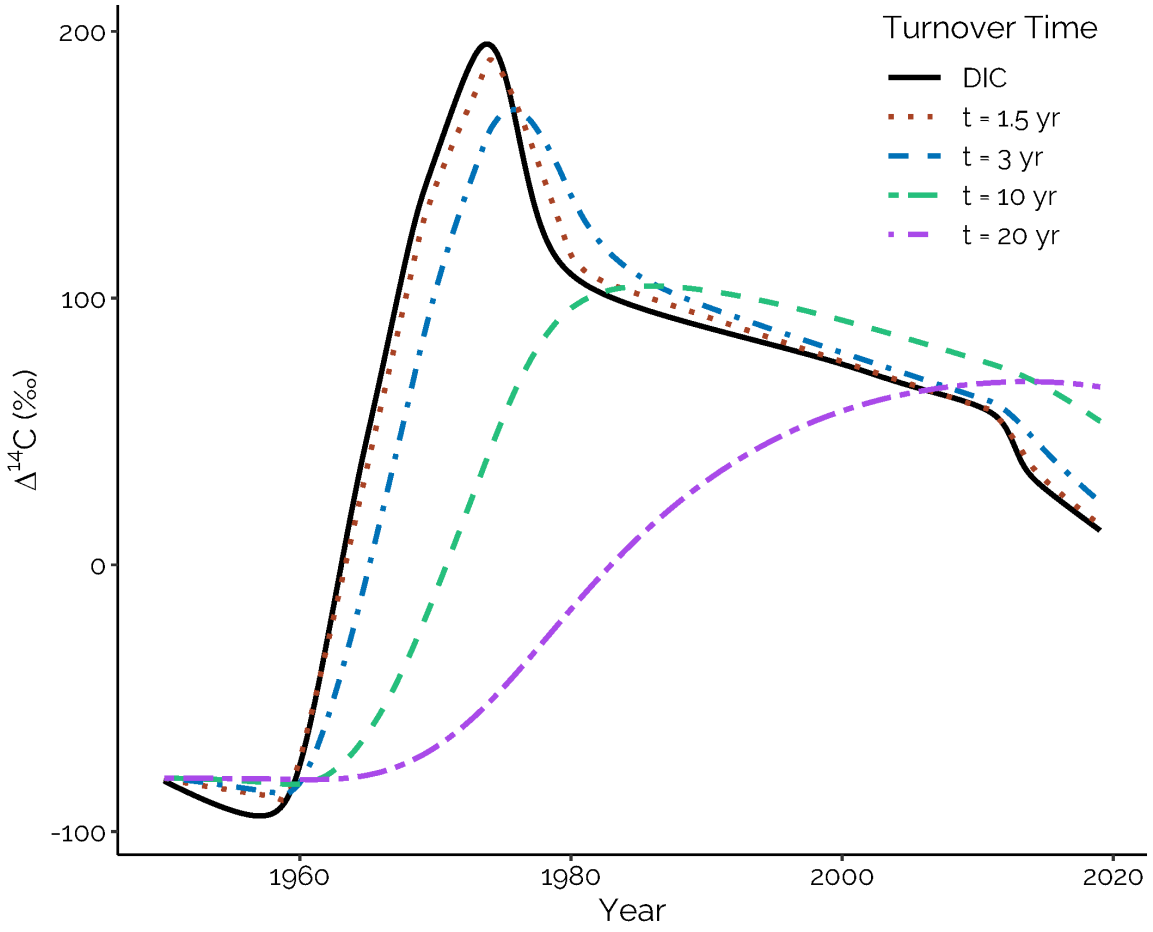

Figure 3.4: Model outputs for $\Delta^{14}C$ of surface APS with different turnover times in the NPSG from 1950 to 2019. The black line shows $\Delta^{14}C$-DIC in the NPSG taken from several data sets (see text). The colored lines show the predicted $\Delta^{14}C$ APS for four different turnover times. In ~2005, the models with turnover times of 3 yrs and 20 yrs yield the same $\Delta^{14}C$ value, preventing the determination of a single residence time for APS at that time. Measurements of APS $\Delta^{14}C$ today are similar to $\Delta^{14}C$-DIC, indicating that a 1–3 yr turnover time best models APS remineralization I the surface ocean.

CHAPTER 4. A SENSITIVE FLUORESCENT ASSAY FOR MEASURING CARBON-PHOSPHORUS LYASE ACTIVITY IN AQUATIC SYSTEMS

Reprinted with permission from Granzow, B. N., Sosa, O. A., Gonnelli, M., Santinelli, C., Karl, D. M., & Repeta, D. J. (2021). A sensitive fluorescent assay for measuring carbon-phosphorus lyase activity in aquatic systems. Limnology and Oceanography: Methods, 19(4), 235–244. https://doi.org/10.1002/lom3.10418

4.1 ABSTRACT

In the oligotrophic ocean where inorganic phosphate (P_i) concentrations are low, microorganisms supplement their nutrient requirements with phosphorus (P) extracted from dissolved organic matter (DOM). Most P in DOM is bound as phosphate esters, which are hydrolyzed by phosphoesterases to P_i. However, a large fraction of DOM-P occurs as phosphonates, organophosphorus compounds with a C-P bond that do not yield Pi after simple ester hydrolysis alone. Phosphonates require an additional step that cleaves the C-P bond to yield Pi. Most phosphonates are metabolized by the C-P lyase pathway, which cleaves C-P bonds and hydrolyzes phosphonate to P_i, enabling microbial assimilation. While the activity of common phosphoesterases such as alkaline phosphatase and phosphodiesterase can be measured by a fluorescent assay, a comparable method to assess C-P lyase activity (CLA) in natural water samples does not exist. To address this, we synthesized a dansyl-labeled phosphonate compound, and measured its hydrolysis by C-P lyase using high performance liquid chromatography. We found that laboratory cultures of marine bacteria expressing the C-P lyase pathway are able to hydrolyze the dansyl phosphonate, while bacteria expressing other phosphonate degradation pathways do not. Finally, we performed several field tests of the assay to measure water column profiles of CLA at Station ALOHA in the North Pacific Subtropical Gyre. Activity was elevated near the deep chlorophyll maximum suggesting high levels of phosphonate degradation in that region.

4.2 INTRODUCTION

Phosphorus (P) is an essential macronutrient needed by all forms of life on Earth. In marine microorganisms, P most commonly occurs as inorganic orthophosphate (HPO_4^{-3} [P_i]) and

as phosphate esters in biomolecules such as nucleic acids, phospholipids, and phosphoglycans. Due to its stability and abundance in seawater, as well as its ease of transport into and within the cell, the most bioavailable form of P is P_i (Johansson & Wedborg, 1979; Karl & Yanagi, 1997). Across large areas of the ocean however, the concentration of P_i is extremely low (< 100 nM), and in these regions, microbes supplement their P requirement by metabolizing dissolved organic phosphorus (DOP), a complex mixture of compounds derived from the synthesis and recycling of microbial biomass (Björkman & Karl, 2003; Dyhrman & Ruttenberg, 2006; Karl & Yanagi, 1997; Monaghan & Ruttenberg, 1999).

Approximately one third to one half of DOP in surface seawater is bound to a novel family of acylated polysaccharides that can be isolated by ultrafiltration as part of the high molecular weight fraction of DOP (HMWDOP). Most HMWDOP (75%) occurs as phosphate monoesters, which are readily hydrolyzed by the alkaline phosphatase (AP) family of enzymes, and pyrophosphate diesters, which are hydrolyzed by phosphodiesterase (Karl, 2014). Alkaline phosphatase activity (APA) is often high in low P_i regions of the ocean and microbial catabolism of phosphate esters via AP can account for more than half of their P_i requirement in the North Pacific Subtropical Gyre (NPSG). The remaining ~25% of polysaccharide-P in HMWDOP occur as phosphonates, organophosphorus compounds wherein P is bound directly to carbon (Clark et al., 1999; Kolowith et al., 2001; Repeta et al., 2016).

Several distinct metabolic pathways have evolved to degrade the large diversity of phosphonates found in nature. Each pathway cleaves the phosphonate C-P bond, however the mechanism of C-P cleavage and, therefore, the degradation products of the pathways are unique (Kamat & Raushel, 2013). Most pathways are substrate specific and are not expected to hydrolyze the phosphonates in HMWDOP (Quinn et al., 2007; White & Metcalf, 2007). The C-P

lyase pathway, however, employs a multi-protein complex that is capable of hydrolyzing a broad suite of phosphonates (Wackett et al., 1987); bacteria with the C-P lyase phosphonate degradation pathway are able to degrade the phosphonates in HMWDOP (Karl et al., 2008; Repeta et al., 2016; Sosa et al., 2017).

The C-P lyase enzyme complex is encoded by a multi-cistron *phn* operon (*phnCDEFGHIJKLMNOP)* that controls phosphonate uptake, transport, and degradation (Jochimsen et al., 2011; Kamat & Raushel, 2013; Manav et al., 2018; Metcalf & Wanner, 1993; Seweryn et al., 2015). Metagenomic analyses of the *phnJ* gene in surface-dwelling microbes have shown that several distantly related marine bacterial taxa including *Proteobacteria*, *Bacteroidetes*, *Firmicutes,* and *Cyanobacteria* are capable of expressing the C-P lyase pathway (Dyhrman et al., 2006; Karl et al., 2008; Kononova & Nesmeyanova, 2002; Sosa, Repeta, et al., 2019; Villarreal-Chiu et al., 2012). The relative abundance of *phn* gene copies is inversely correlated with P_i concentration, but positively correlated with genes encoding high affinity P_i transport systems and AP (Duhamel et al., 2011; Hoppe & Ullrich, 1999; Sosa, Repeta, et al., 2019). In oligotrophic regions where P_i concentrations are low or become limiting, such as the Western Tropical Atlantic Ocean and Mediterranean Sea, a large proportion of microbes (10 – 30%) carry C-P lyase genes, suggesting that in these regions, phosphonates in HMWDOP are a valuable source of P (Sosa, Repeta, et al., 2019). At Station ALOHA, a long-term ecological study site off the coast north of Oahu, Hawaii, the percentage of genomes containing C-P lyase catalytic pathway genes is relatively low (0.1 – 0.5% of genomes), but the presence of this pathway extends from surface waters to at least 1000 m (Sosa et al., 2017). This suggests that C-P lyase enzyme activity (CLA) should be detectable across these depths in the water column at Station ALOHA, despite the relatively high P_i concentrations (2-3 μM) found in the

mesopelagic. The persistence of CLA despite high P_i concentration would parallel enigmatic observations of high APA in the mesopelagic ocean in the NPSG (Duhamel et al., 2011; Karl, 2014; Thomson et al., 2019).

Metagenomic analyses of C-P lyase encoding genes provide a sense of where P acquisition from phosphonates may be most significant, but quantifying the contribution of phosphonates to P cycling requires direct measurements of CLA. To date all estimates of phosphonate degradation rates have relied on methane production from methylphosphonate as a proxy for CLA. del Valle and Karl (2014) measured the rate of methane production in ALOHA surface waters from ^{14}C labeled methylphosphonic acid (MPn), providing an estimate of CLA of MPn of 8 – 47 pM d^{-1}, while Repeta et al. (2016) inferred similar rates of CLA at Station ALOHA (5 – 8 pM d^{-1}) by assuming loss of methane to the atmosphere is in steady state with C-P lyase catalyzed methane production from methylphosphonates in DOM. In freshwater lakes, CLA has been measured from 0.22 –73.8 nM d^{-1} from ^{13}C labeled MPn degradation suggesting CLA can vary widely under different environmental conditions (Li et al., 2020; Wang et al., 2017).

In this paper, we describe an alternative method for assessing CLA in seawater by measuring the hydrolysis of a fluorescently labeled phosphonate, 3-(5-(dimethylamino)naphthalene-1-sulfonamido)propylphosphonic acid (**n-DPPh**). Microbes with the C-P lyase pathway degrade n-DPPh to 3-(5-(dimethylamino)naphthalene-1-sulfonamido)propane (**n-DP**) which can be recovered and quantified (Figure 1). This assay provides a rapid, sensitive measurement of CLA that can be performed in the field with minimal water requirements and a high-throughput post-processing procedure. To provide an assessment of CLA in an oligotrophic setting, we amended a suite of water samples collected from Station

ALOHA with n-DPPh and measured the production of n-DP to generate depth profiles of CLA at this site.

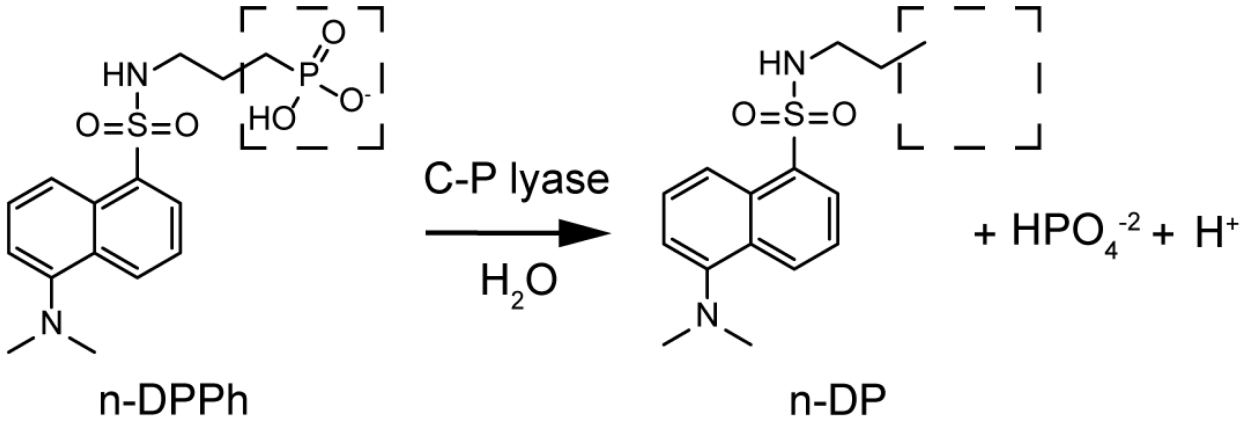

Figure 4.1: Hydrolysis of n-DPPh by C-P lyase. The substrate n-DPPh (left) incorporates a fluorescent dansyl group and phosphonate (black box). After the C-P lyase acts on the substrate, the phosphonate is hydrolyzed to P_i, releasing n-DP, which retains the fluorescent dansyl group.

4.3 MATERIALS AND METHODS

4.3.1 Synthesis of n-DPPh and n-DP

Synthesis of n-DPPh was performed in three steps modified from the procedure of He et al. (2009). A detailed description of the synthesis can be found in the Supplemental Information (S1). In brief, diethyl (2-cyanoethyl)phosphonate was reduced to diethyl 3-aminopropylphosphonate by reaction with sodium borohydride and the transition metal catalyst, cobalt (Co(II)) (Osby et al., 1986). Diethyl 3-aminopropylphosphonate was then reacted with dansyl chloride to produce diethyl 3-(5-(dimethylamino)naphthalene-1-sulfonamido)propylphosphonate. The product was purified by flash chromatography (Blunt et al., 1987) followed by high performance liquid chromatography (HPLC). ^{1}H-NMR and ^{31}P-NMR (Figure S1A,B) were used to confirm formation of the product. Finally, diethyl 3-(5-(dimethylamino)naphthalene-1-sulfonamido)propylphosphonate was reacted with

bromotrimethylsilane, cleaving the protecting ethyl ester groups on the phosphonate, producing n-DPPh. The product was purified using reverse-phase HPLC. The purity of n-DPPh was confirmed by ^{1}H-NMR and ^{31}P-NMR (Figure S1C,D). The final yield of the synthesis was 82 mg (4%).

Synthesis of the expected enzymatic cleavage product, n-DP, was performed following the procedure of Summers et al. (1975) modified by He et al. (2009). Dansyl chloride was reacted with propylamine and the n-DP was separated and purified with flash chromatography. The purity of n-DP was confirmed by ^{1}H-NMR. The final yield was 350 mg (60%).

4.3.2 Microbial Degradation of n-DPPh

Pseudomonas stutzeri (HI00D01) and *Sulfitobacter* sp. (HI0054) which are known to encode the C-P lyase pathway (Repeta et al., 2016; Sosa et al., 2017, p. 201), and a mutant strain of *P. stutzeri* (*phnK*491::Tn5) in which the C-P lyase pathway was disabled by a transposon insertion in the gene encoding the C-P lyase subunit *phnK* (Repeta et al., 2016), were incubated with n-DPPh (100 nM) under P_i replete (sodium phosphate added to the medium to a final concentration of 1 mM P_i) and deplete (<1μM P_i) conditions. *P. stutzeri* cultures were grown in MOPS (morpholinepropanesulfonic acid) minimal medium amended to a final concentration of 4 mM of glucose as a carbon source (Neidhardt et al., 1974). *Sulfitobacter* cultures were grown in a medium prepared with filtered, autoclaved Station ALOHA surface seawater amended to a final concentration of 3.3 mM glycerol as a carbon source. *Pseudoalteramonas shioyasakiensis* (HI0053), which contains genes *phnW* and *phnX* encoding the 2-aminoethylphosphonate:pyruvate aminotransferase (AEP transaminase) and phosphonoacetaldehyde hydrolase (phosphonatase) phosphonate degradation pathways, but not C-P lyase, was also grown under P_i limitation with n-DPPh (Sosa et al., 2017). *P.*

shioyasakiensis cultures were grown in a medium prepared with filtered, autoclaved Station ALOHA surface seawater amended to a final concentration of 4 mM of glucose as a carbon source. All heterotrophic bacterial cultures were grown in the dark.

Some ecotypes of *Prochlorococcus marinus*, an abundant picocyanobacterium in the NPSG, are capable of degrading phosphonate compounds (Sosa, Casey, et al., 2019) through a two-gene pathway (*phnY* and *phnZ*) that encode 2-oxoglutarate dioxygenase and phosphohydrolase, respectively (Gama et al., 2019; Martínez et al., 2010, 2013). The *P. marinus* high-light-adapted strain MIT9301 containing *phnY* and *phnZ* but not C-P lyase was grown under P_i depleted conditions in Pro99 medium (Moore et al., 2007) prepared with autoclaved Station ALOHA seawater following the procedure described in Sosa et al. (2019). Cultures were grown under a 12 h light/dark cycle with an irradiance of 30 μmol photons m^{-2} s^{-1} during the light period.

n-DPPh spikes were prepared at a concentration of 50 μM in high purity water (18.2 MΩ cm [MQ-H_2O]). Companion cultures of all bacteria were grown with n-DP (100 nM) to determine if n-DP could be degraded by these bacteria, and to quantify recoveries. Ammonium was the sole nitrogen source in all treatments and was in excess throughout the incubation. Culture growth was monitored by optical density (λ = 600 nm). After 24 h, 1 mL of culture was collected and centrifuged to separate the medium from the cell pellet for each treatment. Both medium and pellet were frozen for analysis.

Cell pellets were sonic extracted in methanol for 30 min to recover fluorophores that were adsorbed to, or taken up by, the cells. After sonication, the cell material was pelleted by centrifuge and the methanol supernatant analyzed.

4.3.3 Sample Extraction and Analysis

n-DPPh and n-DP were recovered by solid phase extraction (SPE) using 200 mg Agilent Bond Elut ENV columns. Columns were preconditioned with 5 mL methanol and rinsed with 5 mL MQ-H_2O before use. Samples were pumped through the SPE column at a rate of 6 mL min^{-1} after which the columns were rinsed three times with 3 mL of MQ-H_2O to remove salts. n-DPPh and n-DP were eluted with 9 mL of methanol. Sample extracts were dried under vacuum, and the final sample volume brought to 50 µL with 1:1 ACN:MQ-H_2O. n-DPPh and n-DP were separated by HPLC (Agilent 1200 Series, Agilent, Santa Clara, CA) on a C-18 column (2.1 x 100 mm, 3 µm; Supelco Ascentis® C18) eluted with a gradient from 10% ACN in a 20 mM P_i buffer with a pH of 4.2 to 85% ACN in the P_i buffer over 14 min at a flow rate of 0.3 mL min^{-1}. Both compounds were quantified by measuring their respective peak areas using a fluorescence detector set to $\lambda_{(ex)}$ 341 and $\lambda_{(em)}$ 528 nm. n-DPPh and n-DP eluted from the column at 7 and 11 min, respectively. A P_i buffer was used to prevent interactions between the phosphonate fluorophore and the stainless-steel column.

4.3.4 Profiles of C-P Lyase Activity

Two profiles of CLA were collected at Station ALOHA on the HOT 297 cruise (KM1717; November, 2017) between the surface and 1000 m following the standard HOT sampling scheme. Two additional profiles incorporating finer resolution sampling around the deep chlorophyll maximum (DCM) were collected on HOT 307 (KM1821; November, 2018) and HOT 318 (KM2001; January, 2020). In each case, water samples (1 L for HOT 297 and 125 mL for HOT 307 and HOT 318) drawn from polyvinyl chloride (PVC) bottles mounted on a CTD rosette were transferred to clean polycarbonate bottles and spiked with 50 µM n-DPPh dissolved in MQ-H_2O to achieve a final n-DPPh concentration of 5 nM. On HOT 297, samples

collected between 0-300 m were incubated in the dark at ambient temperature (~ 20ºC). Samples collected deeper than 300 m were incubated at 4ºC in the dark. After 24 h, the samples were filtered through a 0.22 µM Durapore membrane filter (EMD Millipore Sterivex™ SVGV010RS) and frozen for post-cruise extraction and analysis. All samples from HOT 307 and HOT 318, were incubated in the dark at ambient temperature (~ 20ºC). After 24 h, the samples were filtered through 0.22 µM Durapore filters and extracted immediately. SPE cartridges were stored at -20ºC until analysis.

Four water column profiles were also collected in the vicinity of Station ALOHA on the SCOPE-Falkor cruise (FK180310-2; March-April, 2018). Samples were collected and treated as described above for HOT 297, but incubated at their respective sampling depths for 24 h on a free-drifting array based on the methods of Böttjer et al. (2017). After incubation, the samples were frozen and sent ashore for filtration, extraction, and analysis in the lab. To determine the concentration of n-DPPh required for enzyme saturation, CLA was measured on samples from HOT 318 amended to final substrate concentrations of between 0.5 and 100 nM. The kinetic experiment samples were incubated for 24 h to ensure sufficient CLA for detection in all treatments. Kinetic parameters were determined utilizing a non-linear least squares regression of the Haldane equation:

$$V(S) = \frac{V_{max}S}{K_m+S+\frac{S^2}{K_i}} \quad (1)$$

where V(S) is the enzyme activity, V_{max} is the maximum hydrolysis rate, S is the substrate concentration, K_m is the minimum substrate concentration at ½ V_{max}, and K_i is the maximum substrate concentration at ½ V_{max} (Haldane, 1930; Koper et al., 2010; Suzumura et al., 2012).

4.4 ASSESSMENT

4.4.1 Assay Sensitivity

Detector response factors were determined by linear regressions of peak areas against mass of n-DPPh and n-DP analyzed. All regressions were linear (r^2 >0.99; Figure 2) over the range of masses we expected to recover from our incubations (10-200 pmoles of n-DPPh and 0.5-5 pmoles of n-DP). At Station ALOHA, the concentration of n-DPPh at the end of 24 h incubations was always greater than the concentration of n-DP. Therefore, the sensitivity of this method is constrained by the limit of quantification (LOQ) for n-DP, which is calculated to be 8.6 fmol by the following equation:

$$LOQ = \frac{10\sigma_{n-DP}}{m} \quad (2)$$

where $\sigma_{n\text{-}DP}$ is the standard deviation of the n-DP standard with the lowest concentration (0.06 pmol; n = 11) and m is the slope of the regression line. Activities are presented here in picomoles of P liberated from n-DPPh by C-P lyase per liter of seawater per day (pmol P L^{-1} d^{-1}) and all reported values are at least two orders of magnitude above the LOQ. As part of our measurement protocol, for each field campaign we incorporated "control samples" consisting of 0.2 μm filtered seawater spiked with n-DPPh, or n-DP alone, and with n-DPPh + n-DP. We could not detect formation of n-DP in any filtered samples spiked with n-DPPh alone (n = 9), suggesting abiotic and extracellular enzymatic hydrolyses of n-DPPh were < 0.01% of the added spike and therefore not important processes at our study site. From filtered seawater samples spiked with n-DPPh or n-DP and incubated for 24 h, we recovered 58 – 107 % of the n-DPPh spike with an average recovery of 86±16.1% (1 SD; n = 10), and 68 – 102% of the n-DP spike with an average recovery of 83±14.8% (1 SD; n = 4). The rates of n-DPPh hydrolysis we report incorporate a

correction factor (1.16 for n-DPPh, 1.20 for n-DP) for the average recovery of n-DPPh and n-DP from seawater. Finally, we also processed unamended filtered seawater samples to monitor potential interference by background fluorescence from dissolved organic matter. No peaks in fluorescence ($\lambda_{(ex)}$ 341 and $\lambda_{(em)}$ 528) were detected, indicating that all signals in our chromatograms can be attributed to n-DPPh or n-DP.

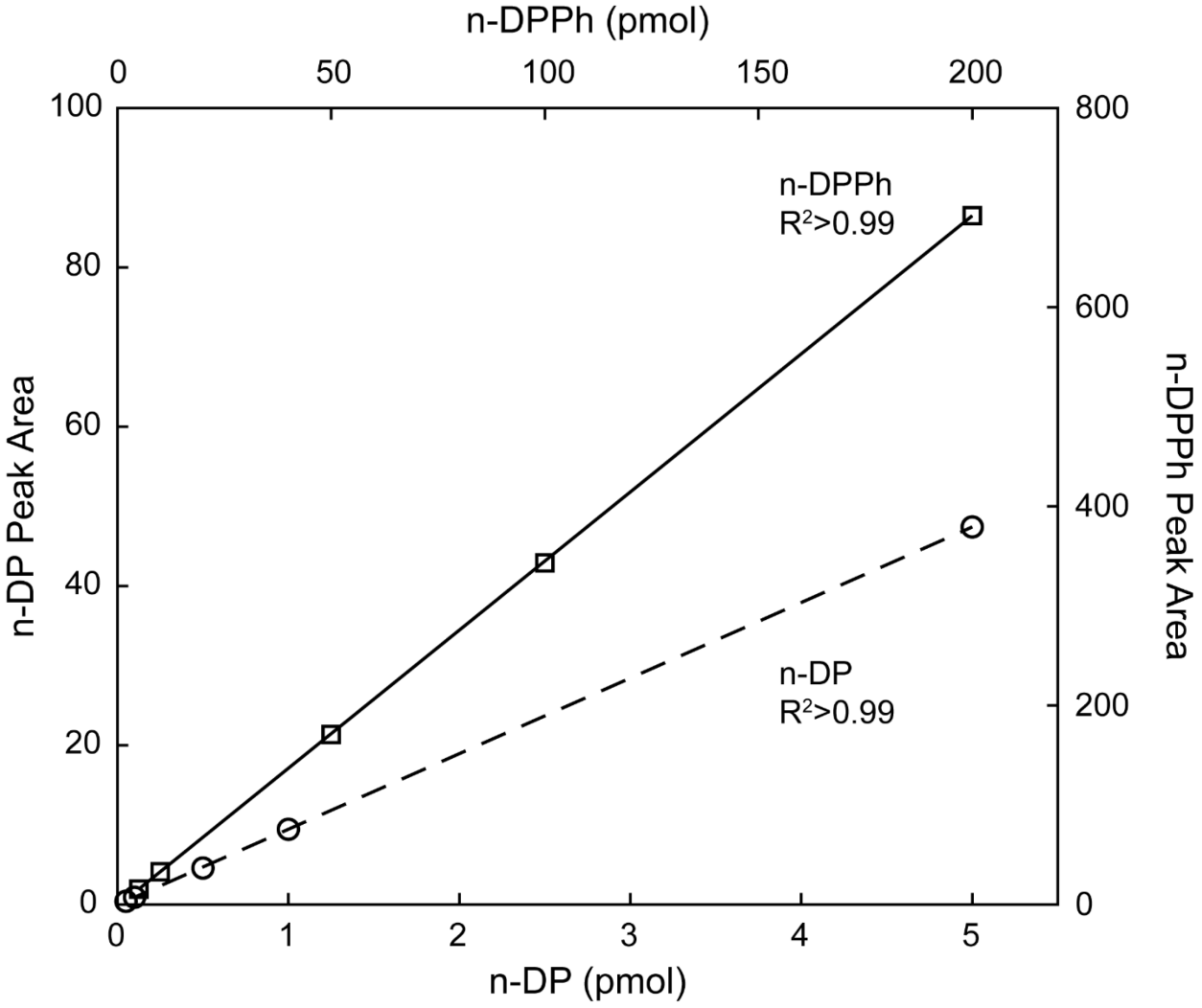

Figure 4.2: HPLC fluorescence ($\lambda_{(ex)}$ 341 and $\lambda_{(em)}$ 528 nm) detector peak area vs. mass for n-DPPh (square, solid) and n-DP (circle, dashed). Both plots are highly linear over two orders of magnitude with r^2 values greater than 0.99.

4.4.2 Hydrolysis of n-DPPh by Microbes

Pure culture experiments were designed to both confirm the degradation of the substrate by C-P lyase and to determine if other phosphonate-degrading enzymes hydrolyze n-DPPh. Prior to this study, the substrate had only been tested on *Escherichia coli* HO1429, which is known to express CLA under P_i limitation (He et al., 2009). In experiments with *P. stutzeri* and *Sulfitobacter* sp. grown in low P_i medium, we easily measured the production of n-DP, indicating that these bacteria, which also express the C-P lyase pathway, are capable of degrading n-DPPh. In the P_i replete (1 mM) experiments, no production of n-DP was detected, indicating low or no CLA under these conditions (Table 1, Figure 3).

Table 4.1: Specificity of the fluorescent assay for the C-P lyase pathway. P_i replete conditions are defined by medium P_i concentration of 1 mM.

Species	Strain	C-P Lyase Pathway Genes Present	P_i Condition	CLA Detected
P. stutzeri	HI00D01	Yes	Replete	No
P. stutzeri	HI00D01	Yes	Limited	Yes
Sulfitobacter sp.	HI0054	Yes	Replete	No
Sulfitobacter sp.	HI0054	Yes	Limited	Yes
*P. stutzeri phnK491::*Tn*5*	HI00D01	Non-Functional†	Replete	No
*P. stutzeri phnK491::*Tn*5*	HI00D01	Non-Functional†	Limited	No
P. shioyasakiensis	HI0053	No	Limited	No
P. marinus	MIT9301	No	Limited	No

†The C-P lyase pathway was disabled by a transposon insertion in the gene encoding the C-P lyase subunit PhnK.

Cultures of the *P. stutzeri* C-P lyase pathway mutant showed no evidence of CLA, confirming that C-P lyase catalyzes the hydrolysis of n-DPPh. Production of n-DP was also not detected in n-DPPh-spiked cultures of *P. shioyasakiensis* or *P. marinus* MIT9301, both of which contain alternative phosphonate degradation pathways (Gama et al., 2019; Sosa, Casey, et al., 2019; Sosa et al., 2017).

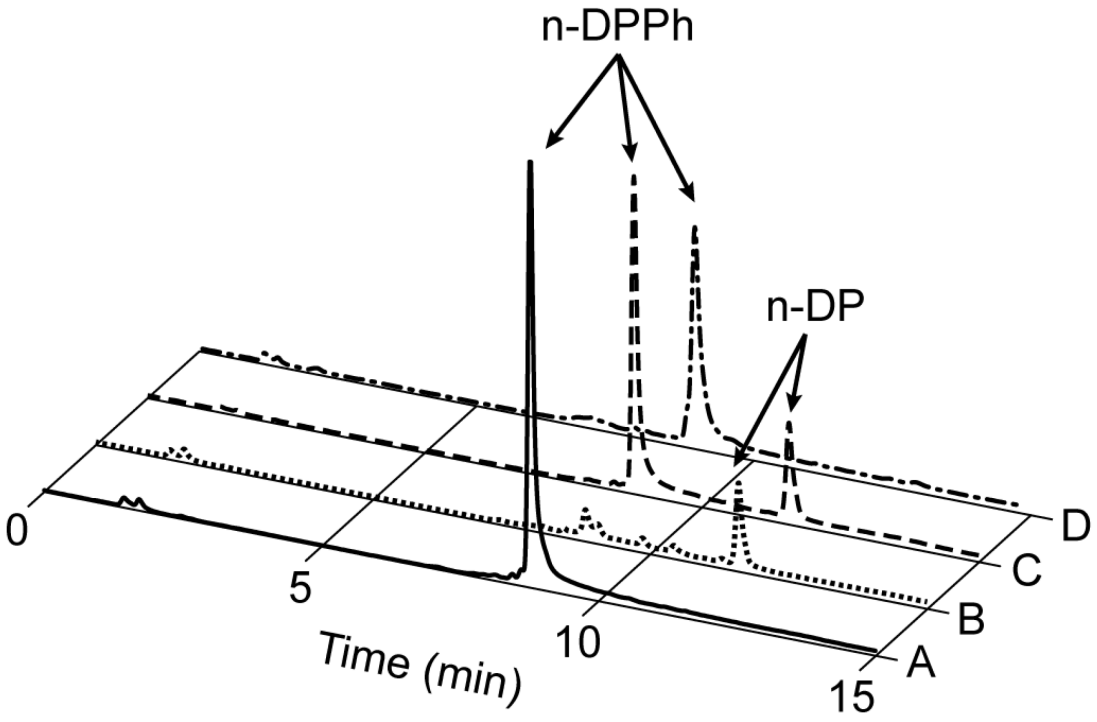

Figure 4.3: Chromatograms from the *P. stutzeri* incubations grown with (**A**) n-DPPh in P_i replete medium, (**B**) n-DP in P_i depleted medium, and (**C**) n-DPPh in P_i depleted medium. The *P. stutzeri* C-P lyase pathway mutant (*phnK491*::Tn*5*) incubation results are also shown (**D**). Peaks associated with n-DPPh (7 min) are only detected in **A**, **C**, and **D**. Peaks associated with n-DP (11 min) are only detected in **B** and **C**.

4.4.3 Profiles of C-P Lyase Activity

A maximum in CLA coincides with the DCM in all profiles (dashed line). CLA was detected in all of the depth profiles collected for this study (n = 8), confirming the assay is sensitive enough for natural water samples (Figure 4). Kinetic analysis (Figure 5) showed that CLA follows a Haldane substrate inhibition model with rates of hydrolysis increasing with substrate concentrations between 0.5-10 nM, and decreasing slightly with n-DPPh concentrations $\geq$ 10 nM (Haldane, 1930).

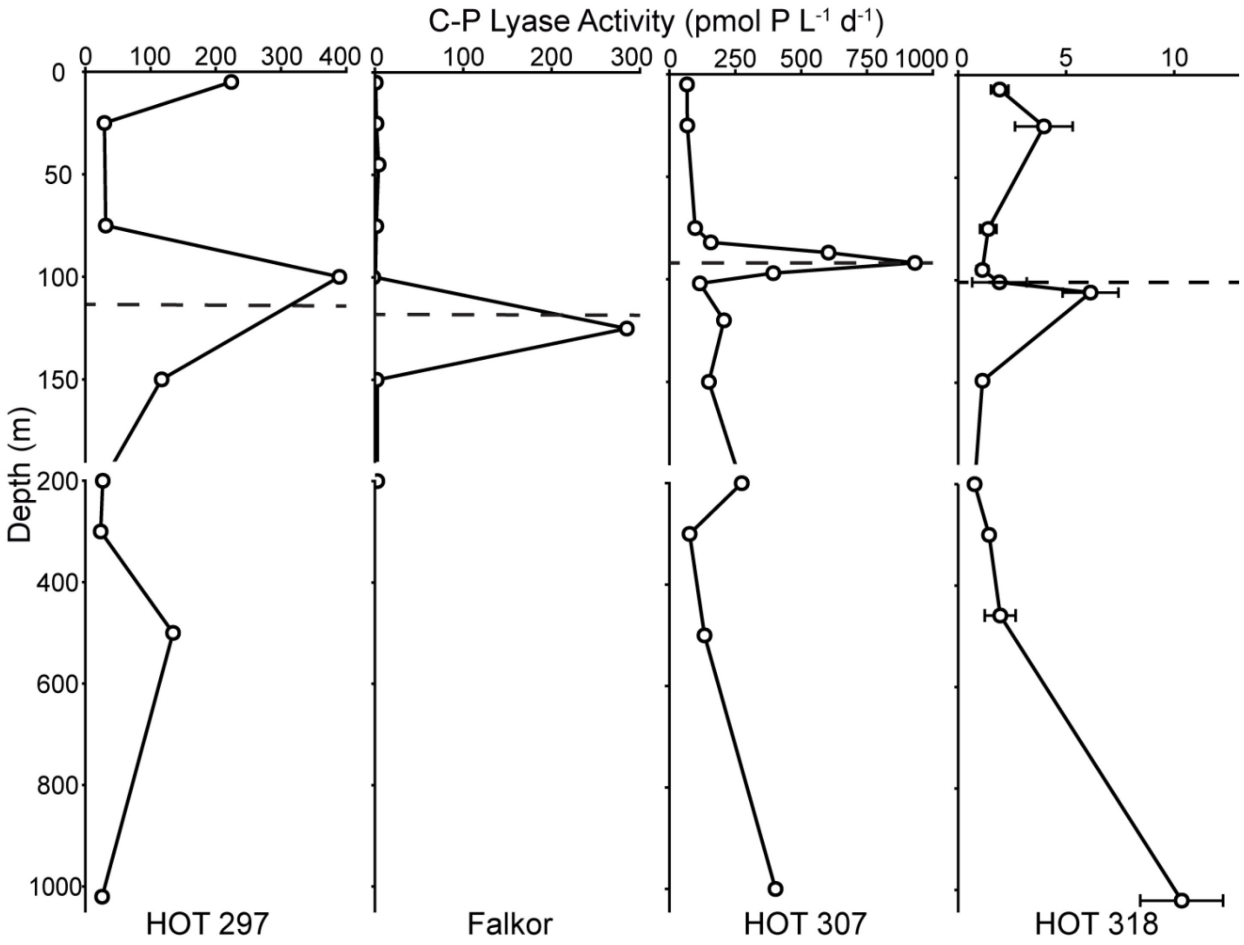

Figure 4.4: Water column profiles of CLA. Samples collected at Station ALOHA to 1000 m on the HOT 297, HOT 307, and HOT 318 were incubated in the dark at room temperature (~ 20°C). Samples collected near Station ALOHA to 200 m during the Scope-Falkor Cruise were incubated under *in situ* light and temperature conditions on drifting arrays. Error bars on the HOT 318 profile represent the standard error of the mean of biological replicate (n = 3) measurements.

Biological replicates (n = 3) collected at all sampled depths on HOT 318 showed good agreement (Figure 4). Rates of n-DPPh hydrolysis were variable in surface waters where P_i concentrations were low but primary production was high. Rates ranged from 1 to 223 pmol P L^{-1} d^{-1}, bracketing the rates of phosphonate degradation (5 – 47 pmol P L^{-1} d^{-1}) estimated by other approaches in Station ALOHA surface waters (Karl et al., 2008; Repeta et al., 2016) indicating the n-DPPh fluorescent assay may provide a good estimate of CLA. Hydrolysis rates were low in

the upper euphotic zone, typically containing a minimum within the first 100 m. In every profile collected, a sharp maximum in CLA was observed around the DCM where the highest chlorophyll concentrations in the subsurface ocean (between 75 and 200 m depth) were found despite lower cellular abundance due to photoadaptation (Campbell & Vaulot, 1993). Below the DCM, n-DPPh hydrolysis rates decreased again to a minimum near 300 m. Hydrolysis rates in the mesopelagic exhibited a high degree of variability (CV = 1.6) with no consistent trend. Enzyme activity was detected to 1000 m, the deepest depth sampled in this study. CLA profile data are available at: https://doi.org/10.5281/zenodo.3862760

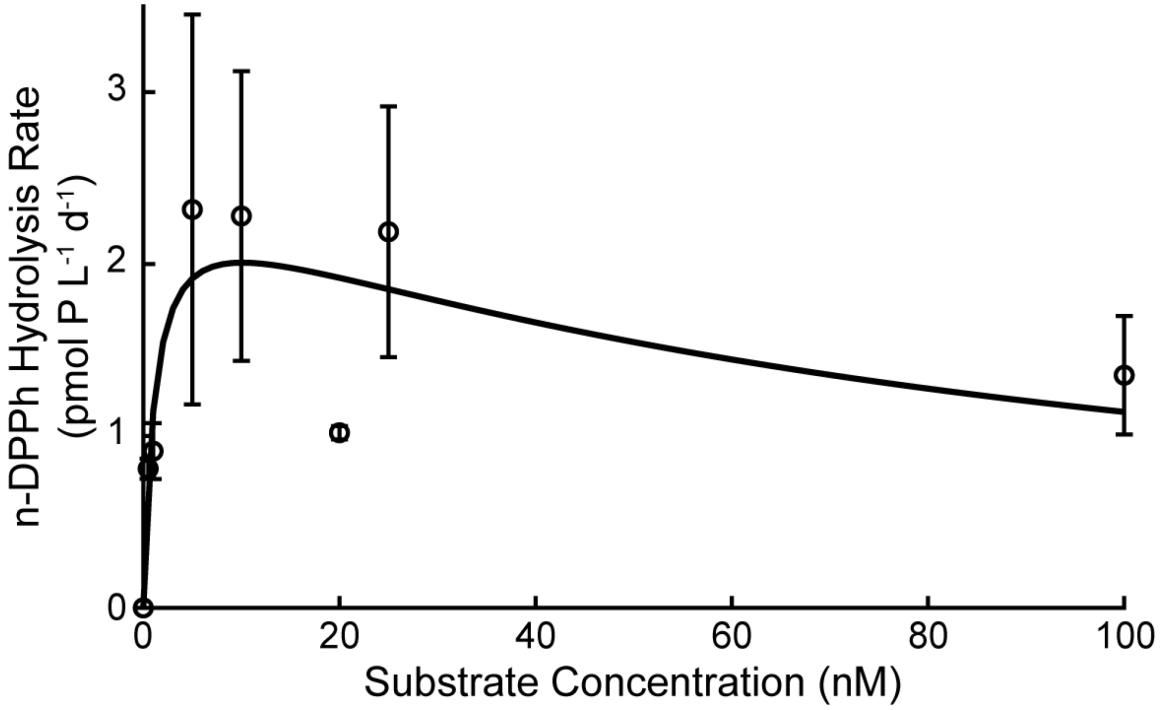

Figure 4.5: Environmental C-P lyase hydrolysis kinetics on n-DPPh as a substrate. Samples were collected in triplicate at Station ALOHA and spiked with n-DPPh to various final concentrations. Error bars represent the standard error of the mean of biological replicate measurements (n = 3). The black line shows the result of the non-linear, least squares fit of the data to the Haldane kinetic model with V_{max} = 2.5 pmol P L^{-1} d^{-1}, K_m = 1.6 nM, and K_i = 87 nM.

4.5 DISCUSSION

In oligotrophic surface waters with low concentrations of P_i, microbes supplement their P needs using AP to hydrolyze organic phosphate esters (Duhamel et al., 2011; Dyhrman & Ruttenberg, 2006; Ivančić et al., 2016). However, the ubiquity of phosphonate degradation pathways in environmental genomes (Stosiek et al., 2019), as well as the high rates of methane production from methylphosphonate in lakes (Li et al., 2020; Wang et al., 2017) and marine surface waters (Repeta et al., 2016; Sosa et al., 2020) suggest that microbes also supplement their P needs through the hydrolysis of phosphonates. A method comparable to the AP fluorescent assay that specifically targets the microbial utilization of phosphonates is not currently available. The purpose of this study was to develop a rapid assay for CLA that can be easily deployed in the field. The assay capitalizes on the hydrolysis of a fluorescently-labeled phosphonate (n-DPPh) by the C-P lyase enzyme complex, followed by chromatographic separation of its hydrolysis product (n-DP). Given that CLA has been previously detected in a freshwater lake and marine waters, we expect the assay will be applicable to a broad range of environmental samples across the aquatic continuum (del Valle & Karl, 2014; Repeta et al., 2016; Wang et al., 2017).

4.5.1 Methodological Considerations

Three classes of phosphonate degradation pathways have been identified in marine microbes. In addition to the C-P lyase pathway, there is a group of substrate–specific phosphonohydrolases and a group of phosphonate oxidative pathways (Gama et al., 2019; Martínez et al., 2013; Quinn et al., 2007; Sosa, Casey, et al., 2019). Our study included bacteria expressing all three degradation pathway classes. Microbes containing C-P lyase (*P. stutzeri* and *Sulfitobacter*) were able to hydrolyze n-DPPh but cultures of *P. shioyasakiensis*, which utilizes a

phosphonohydrolase, and *P. marinus*, which contains a phosphonate oxidative pathway to degrade phosphonates, were not. We conclude that the assay is specific for CLA and does not measure the activity of other phosphonate degradation pathways.

From a suite of measurements made on samples amended with between 0.5 and 100 nM n-DPPh, we determined that a 5 nM n-DPPh amendment, equal to between 2-5% of total DOP concentration at Station ALOHA (Karl et al., 2001) was sufficient to yield maximum rates of hydrolysis. If Station ALOHA is representative of other subtropical gyres, amendments of 5-10 nM n-DPPh should yield consistent results in this type of ecosystem. Other aquatic systems characterized by higher rates of phosphonate degradation may require higher concentrations of n-DPPh than used in our study.

Water column samples collected on HOT 297, HOT 307, and HOT 318 were incubated in the dark and at room temperature. On the SCOPE-Falkor cruise, free-drifting arrays were used to incubate the samples *in situ* under environmental light and temperature conditions. Profiles from all four cruises, under both incubation conditions, exhibit similar trends (Figure 4). Incubation temperature likely affects the absolute rate of CLA as predicted by Macromolecular Rate Theory (Hobbs et al., 2013) and further measurements are needed to determine the temperature dependence on CLA. However, we found that incubations carried out at room temperature yielded activity profiles for the euphotic zone similar to incubations carried out *in situ*. We also observed no variation in trends of CLA between samples incubated in the dark compared to those incubated under natural day-night light cycles.

Filtered water samples frozen for long periods (6 months) showed lower recoveries (56±13%; $n = 5$) of n-DPPh and n-DP than samples extracted immediately after collection, suggesting slow degradation of the fluorophore, even when stored in the dark at low temperature

(-20ºC). These results are consistent with previous reports of dansyl fluorophore decay in aqueous solutions (Summers et al., 1975). Once extracted onto SPE columns however, fluorophore recovery was consistent over 2 months of storage. We recommend that samples be extracted onto SPE columns as soon as possible after collection, and that long-term storage (> 2 months) of samples be avoided whenever possible.

On HOT 318, three discrete samples were collected directly from the PVC bottle for replication. Biological replicates showed good agreement between samples with the highest variability observed at the DCM (CV = 0.7; Figure 4, HOT 318). No CLA was detected in samples that were first filtered through 0.2 μm, indicating that all measurable CLA was associated with suspended particulate matter.

4.5.2 Field Campaign Results

All NPSG profiles displayed a subsurface maximum in CLA near the DCM (Figure 4), suggesting that biogeochemical properties in the subsurface promote microbial degradation of phosphonates. While the cause of this feature has not yet been determined, we present three, non-mutually exclusive, hypotheses. First, the production of phosphonate-containing DOM may be higher at the DCM than in other regions of the water column, promoting a higher activity of phosphonate-degrading pathways such as C-P lyase. For example, Van Mooy et al. (2015) found rates of P_i incorporation into phosphonates increased with depth through the euphotic zone in the Western Tropical Atlantic Ocean. If this same feature occurs in the NPSG, phosphonate production rates could be high near the DCM providing substrate for C-P lyase. Second, it is possible that the unique microbial consortia that inhabit the DCM may have higher expression levels of C-P lyase. Measurements of C-P lyase gene abundance at Station ALOHA found a maximum in the percentage of C-P lyase-containing genomes between 125 and 200 m,

suggesting a higher expression potential for C-P lyase near the DCM (Luo et al., 2011; Sosa et al., 2017). Finally, CLA could be enhanced due to an imbalance of inorganic nutrients delivered to the DCM relative to microbial stoichiometry. Both P_i and nitrate concentrations are low in surface waters of the NPSG and increase rapidly with depth between 100 and 200 m, resulting in a phosphocline and nitracline, respectively (Dore & Karl, 1996; Karl et al., 2001). In regions of persistent P_i limitation, such as the Western Tropical Atlantic Ocean and Mediterranean Sea, the phosphocline is often deeper than the nitracline, potentially leading to a local deficit in P_i supply relative to nitrogen supply at depth (Fernández et al., 2013; Krom et al., 2005). At Station ALOHA, the phosphocline and nitracline oscillate with respect to one another, resulting in periodic pulses of nutrients that could cause local P limitation and drive the community towards phosphonate degradation (Karl et al., 2001). Microbes may employ the C-P lyase pathway to access P stored in DOM to compensate for the P_i deficit, resulting in an activity maximum near the DCM. APA in the NPSG shows a similar, variable subsurface maximum between 70 and 150 m (Duhamel et al., 2011). Both enzymes are utilized for the remineralization of P stored in DOM, and similar controls may govern their activity in the water column.

4.6 COMMENTS AND RECOMMENDATIONS

Our synthesis of n-DPPh and n-DP yielded quantities sufficient for several thousand analyses, and these compounds are available to other laboratories on request. The assay measures C-P lyase hydrolysis of n-DPPh and does not directly measure hydrolysis of other phosphonates, however, like the APA assay, this assay can be used to measure the relative CLA of different samples. A comparison of spatial and temporal variability of C-P lyase gene abundance and enzyme activity, P_i concentration, APA, and rates of methane and ethylene production should yield valuable insights into P cycling by microbes. While amendments of 5 nM or greater of n-

DPPh yielded maximum rates of substrate hydrolysis at Station ALOHA, we recommend that studies of saturation kinetics be made at other sites with different environmental conditions to better understand appropriate levels of amendment. We also suggest that replicate samples be collected from a single, large sample of water that is well mixed before subsampling to reduce heterogeneity between replicates.

We did not find measurable hydrolysis of n-DPPh incubated in filtered seawater. CLA is associated with suspended particulate matter captured by a 0.22 μm filter. We were also unable to detect n-DPPh or n-DP in filter extracts, suggesting that once hydrolyzed, the fluorophore is released into solution and not transported into or absorbed onto cells. n-DPPh and n-DP are stable in filtered, frozen seawater up to two months, and samples can be collected and returned to the laboratory for analyses when necessary. However, we found samples extracted onto SPE columns immediately after incubation followed by HPLC analyses < 2 months after collection yielded the most consistent results.

4.7 REFERENCES

Björkman, K. M., & Karl, D. M. (2003). Bioavailability of dissolved organic phosphorus in the euphotic zone at station ALOHA, North Pacific Subtropical Gyre. *Limnology and Oceanography*, *48*(3), 1049–1057. https://doi.org/10.4319/lo.2003.48.3.1049

Blunt, J. W., Calder, V. L., Fenwick, G. D., Lake, R. J., McCombs, J. D., Munro, M. H. G., & Perry, N. B. (1987). Reverse phase flash chromatography: A method for the rapid partitioning of natural product extracts. *Journal of Natural Products*, *50*(2), 290–292. https://doi.org/10.1021/np50050a039

Böttjer, D., Dore, J. E., Karl, D. M., Letelier, R. M., Mahaffey, C., Wilson, S. T., Zehr, J., & Church, M. J. (2017). Temporal variability of nitrogen fixation and particulate nitrogen export at Station ALOHA. *Limnology and Oceanography*, *62*(1), 200–216. https://doi.org/10.1002/lno.10386

Campbell, L., & Vaulot, D. (1993). Photosynthetic picoplankton community structure in the subtropical North Pacific Ocean near Hawaii (station ALOHA). *Deep-Sea Research Part I: Oceanographic Research Papers*, *40*(10), 2043–2060.

Clark, L. L., Ingall, E. D., & Benner, R. (1999). Marine organic phosphorus cycling: Novel insights from nuclear magnetic resonance. *American Journal of Science*, *299*, 724–737. https://doi.org/10.2475/ajs.299.7-9.724

del Valle, D. A., & Karl, D. M. (2014). Aerobic production of methane from dissolved water-column methylphosphonate and sinking particles in the North Pacific Subtropical Gyre. *Aquatic Microbial Ecology*, *73*(2), 93–105. https://doi.org/10.3354/ame01714

Dore, J. E., & Karl, D. M. (1996). Nitrite distributions and dynamics at Station ALOHA. *Deep-Sea Research Part II: Topical Studies in Oceanography*, *43*(2), 385–402.

Duhamel, S., Björkman, K. M., Van Wambeke, F., Moutin, T., & Karl, D. M. (2011). Characterization of alkaline phosphatase activity in the North and South Pacific Subtropical Gyres: Implications for phosphorus cycling. *Limnology and Oceanography*, *56*(4), 1244–1254. https://doi.org/10.4319/lo.2011.56.4.1244

Dyhrman, S. T., Chappell, P. D., Haley, S. T., Moffett, J. W., Orchard, E. D., Waterbury, J. B., & Webb, E. A. (2006). Phosphonate utilization by the globally important marine diazotroph *Trichodesmium*. *Nature*, *439*(7072), 68–71. https://doi.org/10.1038/nature04203

Dyhrman, S. T., & Ruttenberg, K. C. (2006). Presence and regulation of alkaline phosphatase activity in eukaryotic phytoplankton from the coastal ocean: Implications for dissolved organic phosphorus remineralization. *Limnology and Oceanography*, *51*(3), 1381–1390. https://doi.org/10.4319/lo.2006.51.3.1381

Fernández, A., Graña, R., Mouriño-Carballido, B., Bode, A., Varela, M., Domínguez-Yanes, J. F., Escánez, J., de Armas, D., & Marañón, E. (2013). Community N_2 fixation and *Trichodesmium* spp. Abundance along longitudinal gradients in the eastern subtropical North Atlantic. *Journal of Marine Science*, *70*(1), 223–231. https://doi.org/10.1093/icesjms/fss142

Gama, S. R., Vogt, M., Kalina, T., Hupp, K., Hammerschmidt, F., Pallitsch, K., & Zechel, D. L. (2019). An oxidative pathway for microbial utilization of methylphosphonic acid as a phosphate source. *ACS Chemical Biology*, *14*(4), 735–741. https://doi.org/10.1021/acschembio.9b00024

Haldane, J. B. S. (1930). *Enzymes*. Longmans, Green.

He, S. M., Luo, Y., Hove-Jensen, B., & Zechel, D. L. (2009). A fluorescent substrate for carbon-phosphorus lyase: Towards the pathway for organophosphonate metabolism in bacteria. *Bioorganic and Medicinal Chemistry Letters*, *19*(20), 5954–5957. https://doi.org/10.1016/j.bmcl.2009.08.035

Hobbs, J. K., Jiao, W., Easter, A. D., Parker, E. J., Schipper, L. A., & Arcus, V. L. (2013). Change in heat capacity for enzyme catalysis determines temperature dependence of enzyme catalyzed rates. *ACS Chemical Biology*, *8*(11), 2388–2393. https://doi.org/10.1021/cb4005029

Hoppe, H. G., & Ullrich, S. (1999). Profiles of ectoenzymes in the Indian Ocean: Phenomena of phosphatase activity in the mesopelagic zone. *Aquatic Microbial Ecology*, *19*(2), 139–148. https://doi.org/10.3354/ame019139

Ivančić, I., Pfannkuchen, M., Godrijan, J., Djakovac, T., Marić Pfannkuchen, D., Korlević, M., Gašparović, B., & Najdek, M. (2016). Alkaline phosphatase activity related to phosphorus stress of microphytoplankton in different trophic conditions. *Progress in Oceanography*, *146*, 175–186. https://doi.org/10.1016/j.pocean.2016.07.003

Jochimsen, B., Lolle, S., McSorley, F. R., Nabi, M., Stougaard, J., Zechel, D. L., & Hove-Jensen, B. (2011). Five phosphonate operon gene products as components of a multi-subunit complex of the carbon-phosphorus lyase pathway. *Proceedings of the National Academy of Sciences of the United States of America*, *108*(28), 11393–11398. https://doi.org/10.1073/pnas.1104922108

Johansson, O., & Wedborg, M. (1979). Stability constants of phosphoric acid in seawater of 5-40‰ salinity and temperatures of 5-25°C. *Marine Chemistry*, *8*, 57–69.

Kamat, S. S., & Raushel, F. M. (2013). The enzymatic conversion of phosphonates to phosphate by bacteria. *Current Opinion in Chemical Biology*, *17*(4), 589–596. https://doi.org/10.1016/j.cbpa.2013.06.006

Karl, D. M. (2014). Microbially mediated transformations of phosphorus in the sea: New views of an old cycle. *Annual Review of Marine Science*, *6*(1), 279–337. https://doi.org/10.1146/annurev-marine-010213-135046

Karl, D. M., Beversdorf, L. J., Björkman, K. M., Church, M. J., Martínez, A., & Delong, E. F. (2008). Aerobic production of methane in the sea. *Nature Geoscience*, *1*(7), 473–478. https://doi.org/10.1038/ngeo234

Karl, D. M., Björkman, K. M., Dore, J. E., Fujieki, L., Hebel, D. V., Houlihan, T., Letelier, R. M., & Tupas, L. M. (2001). Ecological nitrogen-to-phosphorus stoichiometry at station ALOHA. *Deep-Sea Research Part II: Topical Studies in Oceanography*, *48*(8–9), 1529–1566. https://doi.org/10.1016/S0967-0645(00)00152-1

Karl, D. M., & Yanagi, K. (1997). Partial characterization of the dissolved organic phosphorus pool in the oligotrophic North Pacific Ocean. *Limnology and Oceanography*, *42*(6), 1398–1405. https://doi.org/10.4319/lo.1997.42.6.1398

Kolowith, L. C., Ingall, E. D., & Benner, R. (2001). Composition and cycling of marine organic phosphorus. *Limnology and Oceanography*, *46*(2), 309–320. https://doi.org/10.4319/lo.2001.46.2.0309

Kononova, S. V., & Nesmeyanova, M. A. (2002). Phosphonates and their degradation by microorganisms. *Biochemistry. Biokhimiia*, *67*(2), 184–195. https://doi.org/10.1023/A:1014409929875

Koper, T. E., Stark, J. M., Habteselassie, M. Y., & Norton, J. M. (2010). Nitrification exhibits Haldane kinetics in an agricultural soil treated with ammonium sulfate or dairy-waste compost. *FEMS Microbiology Ecology*, *74*(2), 316–322. https://doi.org/10.1111/j.1574-6941.2010.00960.x

Krom, M. D., Woodward, E. M. S., Herut, B., Kress, N., Carbo, P., Mantoura, R. F. C., Spyres, G., Thingstad, T. F., Wassmann, P., Wexels-Riser, C., Kitidis, V., Law, C. S., & Zodiatis, G. (2005). Nutrient cycling in the south east Levantine basin of the eastern Mediterranean: Results from a phosphorus starved system. *Deep-Sea Research Part II:*

Topical Studies in Oceanography, *52*(22–23), 2879–2896. https://doi.org/10.1016/j.dsr2.2005.08.009

Li, W., Dore, J. E., Steigmeyer, A. J., Cho, Y.-J., Kim, O. S., Liu, Y., Morgan-Kiss, R. M., Skidmore, M. L., & Priscu, J. C. (2020). Methane production in the oxygenated water column of a perennially ice-covered Antarctic lake. *Limnology and Oceanography*, *65*(1), 143–156. https://doi.org/10.1002/lno.11257

Luo, H., Zhang, H., Long, R. A., & Benner, R. (2011). Depth distributions of alkaline phosphatase and phosphonate utilization genes in the North Pacific Subtropical Gyre. *Aquatic Microbial Ecology*, *62*(1), 61–69. https://doi.org/10.3354/ame01458

Manav, M. C., Sofos, N., Hove-Jensen, B., & Brodersen, D. E. (2018). The Abc of phosphonate breakdown: A mechanism for bacterial survival. *BioEssays*, *40*(11), 1–11. https://doi.org/10.1002/bies.201800091

Martínez, A., Tyson, G. W., & Delong, E. F. (2010). Widespread known and novel phosphonate utilization pathways in marine bacteria revealed by functional screening and metagenomic analyses. *Environmental Microbiology*, *12*(1), 222–238. https://doi.org/10.1111/j.1462-2920.2009.02062.x

Martínez, A., Ventouras, L. A., Wilson, S. T., Karl, D. M., & DeLong, E. F. (2013). Metatranscriptomic and functional metagenomic analysis of methylphosphonate utilization by marine bacteria. *Frontiers in Microbiology*, *4*(NOV), 1–18. https://doi.org/10.3389/fmicb.2013.00340

Metcalf, W. W., & Wanner, B. L. (1993). Evidence for a fourteen-gene, *phnC* to *phnP* locus for phosphonate metabolism in *Escherichia coli*. *Gene*, *129*(1), 27–32. https://doi.org/10.1016/0378-1119(93)90692-V

Monaghan, E. J., & Ruttenberg, K. C. (1999). Dissolved organic phosphorus in the coastal ocean: Reassessment of available methods and seasonal phosphorus profiles from the Eel River Shelf. *Limnology and Oceanography*, *44*(7), 1702–1714. https://doi.org/10.4319/lo.1999.44.7.1702

Moore, L. R., Coe, A., Zinser, E. R., Saito, M. A., Sullivan, M. B., Lindell, D., Frois-Moniz, K., Waterbury, J., & Chisholm, S. W. (2007). Culturing the marine cyanobacterium *Prochlorococcus*. *Limnology and Oceanography: Methods*, *5*(10), 353–362. https://doi.org/10.4319/lom.2007.5.353

Neidhardt, F. C., Bloch, P. L., & Smith, D. F. (1974). Culture medium for enterobacteria. *Journal of Bacteriology*, *119*(3), 736–747.

Osby, J. O., Heinzman, S. W., & Ganem, B. (1986). Studies on the mechanism of transition-metal-assisted sodium borohydride and lithium aluminum hydride reductions. *Journal of Bacteriology*, *108*(1), 67–72.

Quinn, J. P., Kulakova, A. N., Cooley, N. A., & McGrath, J. W. (2007). New ways to break an old bond: The bacterial carbon-phosphorus hydrolases and their role in biogeochemical phosphorus cycling. *Environmental Microbiology*, *9*(10), 2392–2400. https://doi.org/10.1111/j.1462-2920.2007.01397.x

Repeta, D. J., Ferrón, S., Sosa, O. A., Johnson, C. G., Repeta, L. D., Acker, M., Delong, E. F., & Karl, D. M. (2016). Marine methane paradox explained by bacterial degradation of dissolved organic matter. *Nature Geoscience*, *9*(12), 884–887. https://doi.org/10.1038/ngeo2837

Seweryn, P., Van, L. B., Kjeldgaard, M., Russo, C. J., Passmore, L. A., Hove-Jensen, B., Jochimsen, B., & Brodersen, D. E. (2015). Structural insights into the bacterial carbon–phosphorus lyase machinery. *Nature*, *525*(7567), 68–72. https://doi.org/10.1038/nature14683

Sosa, O. A., Burrell, T. J., Wilson, S. T., Foreman, R. K., Karl, D. M., & Repeta, D. J. (2020). Phosphonate cycling supports methane and ethylene supersaturation in the phosphate-depleted western North Atlantic Ocean. *Limnology and Oceanography*, 1–17. https://doi.org/10.1002/lno.11463

Sosa, O. A., Casey, J. R., & Karl, D. M. (2019). Methylphosphonate oxidation in *Prochlorococcus* strain MIT9301 supports phosphate acquisition, formate excretion, and carbon assimilation into purines. *Applied and Environmental Microbiology*, *85*(13), e00289-19. https://doi.org/10.1128/AEM.00289-19

Sosa, O. A., Repeta, D. J., DeLong, E. F., Ashkezari, M. D., & Karl, D. M. (2019). Phosphate-limited ocean regions select for bacterial populations enriched in the carbon–phosphorus lyase pathway for phosphonate degradation. *Environmental Microbiology*, *21*(7), 2402–2414. https://doi.org/10.1111/1462-2920.14628

Sosa, O. A., Repeta, D. J., Ferrón, S., Bryant, J. A., Mende, D. R., Karl, D. M., & DeLong, E. F. (2017). Isolation and characterization of bacteria that degrade phosphonates in marine dissolved organic matter. *Frontiers in Microbiology*, *8*(SEP), 1–16. https://doi.org/10.3389/fmicb.2017.01786

Stosiek, N., Talma, M., & Klimek-Ochab, M. (2019). Carbon-Phosphorus Lyase—The state of the art. *Applied Biochemistry and Biotechnology*. https://doi.org/10.1007/s12010-019-03161-4

Summers, W. A., Lee, J. Y., & Burr, J. G. (1975). Synthesis of Fluorescent Labeled Derivatives of Aminopropylpyrimidines. *Journal of Organic Chemistry*, *40*(11), 1559–1561. https://doi.org/10.1021/jo00899a009

Suzumura, M., Hashihama, F., Yamada, N., & Kinouchi, S. (2012). Dissolved phosphorus pools and alkaline phosphatase activity in the euphotic zone of the western North Pacific Ocean. *Frontiers in Microbiology*, *3*(MAR), 1–13. https://doi.org/10.3389/fmicb.2012.00099

Thomson, B., Wenley, J., Currie, K., Hepburn, C. D., Herndl, G. J., & Baltar, F. (2019). Resolving the paradox: Continuous cell-free alkaline phosphatase activity despite high phosphate concentrations. *Marine Chemistry*, *214*(June), 103671. https://doi.org/10.1016/j.marchem.2019.103671

Van Mooy, B. A. S., Krupke, A., Dyhrman, S. T., Fredricks, H. F., Frischkorn, K. R., Ossolinski, J. E., Repeta, D. J., Rouco, M., Seewald, J. D., & Sylva, S. P. (2015). Major role of planktonic phosphate reduction in the marine phosphorus redox cycle. *Science*, *348*(6236), 783–785. https://doi.org/10.1126/science.aaa8181

Villarreal-Chiu, J. F., Quinn, J. P., & McGrath, J. W. (2012). The genes and enzymes of phosphonate metabolism by bacteria, and their distribution in the marine environment. *Frontiers in Microbiology*, *3*(JAN), 1–13. https://doi.org/10.3389/fmicb.2012.00019

Wackett, L. P., Shames, S. L., Venditti, C. P., & Walsh, C. T. (1987). Bacterial carbon-phosphorus lyase: Products, rates, and regulation of phosphonic and phosphinic acid metabolism. *Journal of Bacteriology*, *169*(2), 710–717.

Wang, Q., Dore, J. E., & McDermott, T. R. (2017). Methylphosphonate metabolism by *Pseudomonas* sp. Populations contributes to the methane oversaturation paradox in an oxic freshwater lake. *Environmental Microbiology*, *19*(6), 2366–2378. https://doi.org/10.1111/1462-2920.13747

White, A. K., & Metcalf, W. W. (2007). Microbial metabolism of reduced phosphorus compounds. *Annual Review of Microbiology*, *61*(1), 379–400. https://doi.org/10.1146/annurev.micro.61.080706.093357

4.8 SUPPLEMENTAL MATERIAL

4.8.1 Detailed Procedure for n-DPPh and n-DP Syntheses

Diethyl (2-cyanoethyl)phosphonate (CEPh; 1 g, Sigma-Aldrich) and cobalt chloride ($CoCl_2$; 0.124 g) were dissolved in 60 mL of a 2:1 (v/v) mixture of tetrahydrofuran (THF; >99.9%,) and MQ-H_2O. THF was passed through an activated alumina column before use to remove peroxides and was stored under nitrogen. The solution was cooled in an ice bath and 0.396 g of sodium borohydride was added with stirring over 8 min, promoting the reduction of CEPh to diethyl 3-aminopropylphosphonate (APPh). After two hours, 28% (w/v) ammonium hydroxide was added to neutralize the solution, after which the mixture was filtered to remove particulate cobalt boride. THF was vacuum evaporated, the residue extracted 4 times, each with 40 mL of methylene chloride (CH_2Cl_2). Residual water was removed from the organic fraction with anhydrous sodium sulfate.

The CH_2Cl_2 solution containing APPh was reduced in volume to ~ 40 mL, and dansyl chloride (≥99%, Sigma; 0.633 g) and triethylamine (0.415 g) were added. The solution was stirred for 32 h at room temperature under nitrogen to yield diethyl 3-(5-

(dimethylamino)naphthalene-1-sulfonamido)propylphosphonate (E-n-DPPh), which was purified by pouring the solution onto a 21 mm ID medium pressure, flash chromatography column dry packed with 16 g of 100 – 200 mesh silica gel. Unreacted dansyl chloride passes through the column and E-n-DPPh is concentrated in a small band at the top of the column. E-n-DPPh was recovered by washing the column with 80 mL of 3% methanol (MeOH) in CH_2Cl_2. The product was further purified by high performance liquid chromatography (HPLC) using a silica column (4.6 x 150 mm, 3 μm; Supelcosil™ LC-Si) with a mobile phase of 5% methanol in CH_2Cl_2 for 7 min at a flow rate of 1 mL min^{-1}. E-n-DPPh eluted at 3.7 min. ^{1}H-NMR and ^{31}P-NMR were used to confirm formation of the product (figure 4.6). ^{1}H NMR ($CDCl_3$, 400 MHz): δ 1.28 (t, 6H, J = 7.1 Hz), 1.71 (m, 4H), 2.90 (s, 6H), 3.00 (q, 2H, J = 6.3 Hz), 4.03 (m, 4H), 7.19 (d, 1H, J = 7.5 Hz), 7.54 (quint, 2H, J = 8.1 Hz), 8.24 (d, 1H, J = 7.3 Hz), 8.33 (d, 1H, J = 8.7 Hz), 8.55 (d, 1H, J = 8.5 Hz). ^{31}P NMR ($CDCl_3$, 162 MHz): δ 31.51 (s, 1P).

The final step of the synthesis removed the protecting ethyl esters from the phosphonate. E-n-DPPh was dried under vacuum and dissolved in 20 mL of acetonitrile (ACN). The solution was cooled in an ice bath, bromotrimethylsilane (≥97%, Sigma-Aldrich; 0.894 g) was added dropwise and allowed to react for 24 h at room temperature under nitrogen (Frost et al. 1987). ACN was removed by vacuum evaporation and the product dissolved in 20 mL of a 90% aqueous MeOH. The solution was stirred for 2 h, and the product purified by HPLC using a C-18 column (2.1 x 100 mm, 3 μm; Supelco Ascentis® C18) with a gradient from 45% ACN in a 20 mM P_i buffer with a pH of 6.2 to 85% ACN in the P_i buffer over 7 min at a flow rate of 0.3 mL min^{-1}. n-DPPh eluted at 1.5 min while unreacted E-n-DPPh eluted at 3 min. The final yield of the synthesis was 82 mg (4%). The purity of n-DPPh was confirmed by ^{1}H-NMR and ^{31}P-NMR (Figure S1C,D). ^{1}H NMR (D_2O, 400 MHz): δ 1.33 (m, 2H), 1.52 (m, 2H), 2.79 (s, 6H), 2.83 (t,

2H, J = 6.7 Hz), 7.33 (d, 1H, J = 7.5 Hz), 7.61 (q, 2H, J = 8.1 Hz), 8.16 (d, 1H, J = 7.3 Hz), 8.21 (d, 1H, J = 8.9 Hz) 8.40 (d, 1H, J = 8.5 Hz). ^{31}P NMR (D_2O, 162 MHz): δ 24.74.

Synthesis of the expected cleavage product, n-DP, was performed following the procedure of Summers et al. (1975) modified by He et al. (2009). Dansyl chloride (0.054 g) was dissolved in 20 mL of dry ACN, to which 0.144 g of propylamine was added. The solution was stirred for one hour at room temperature after which the solvent was removed under vacuum. The residue was extracted 3 times, each with 20 mL of chloroform and the organic fraction was poured through a 21 mm ID chromatography column dry packed with 10 g of silica gel (200 – 400 mesh) to remove unreacted dansyl chloride. n-DP was recovered by washing the column further with 60 mL of chloroform. The product in chloroform was dehydrated over anhydrous sodium sulfate, filtered, then dried under vacuum to yield 35 mg of product (60%) (^{1}H-NMR (MeOD, 400 MHz): δ 0.77 (t, 3H, J = 7.4 Hz), 1.39 (m, 2H), 2.90 (s, 6H), 3.32 (t, 2H, J = 6.8 Hz), 7.29 (d, 1H, J = 7.4 Hz), 7.59 (quint, 2H, J = 4.9 Hz), 8.20 (d, 1H, J = 7.5 Hz), 8.38 (d, 1H, J = 8.7 Hz), 8.57 (d, 1H, J = 8.6 Hz); ^{31}P-NMR (MeOD, 162 MHz): δ 24.79 (s, 1P)).

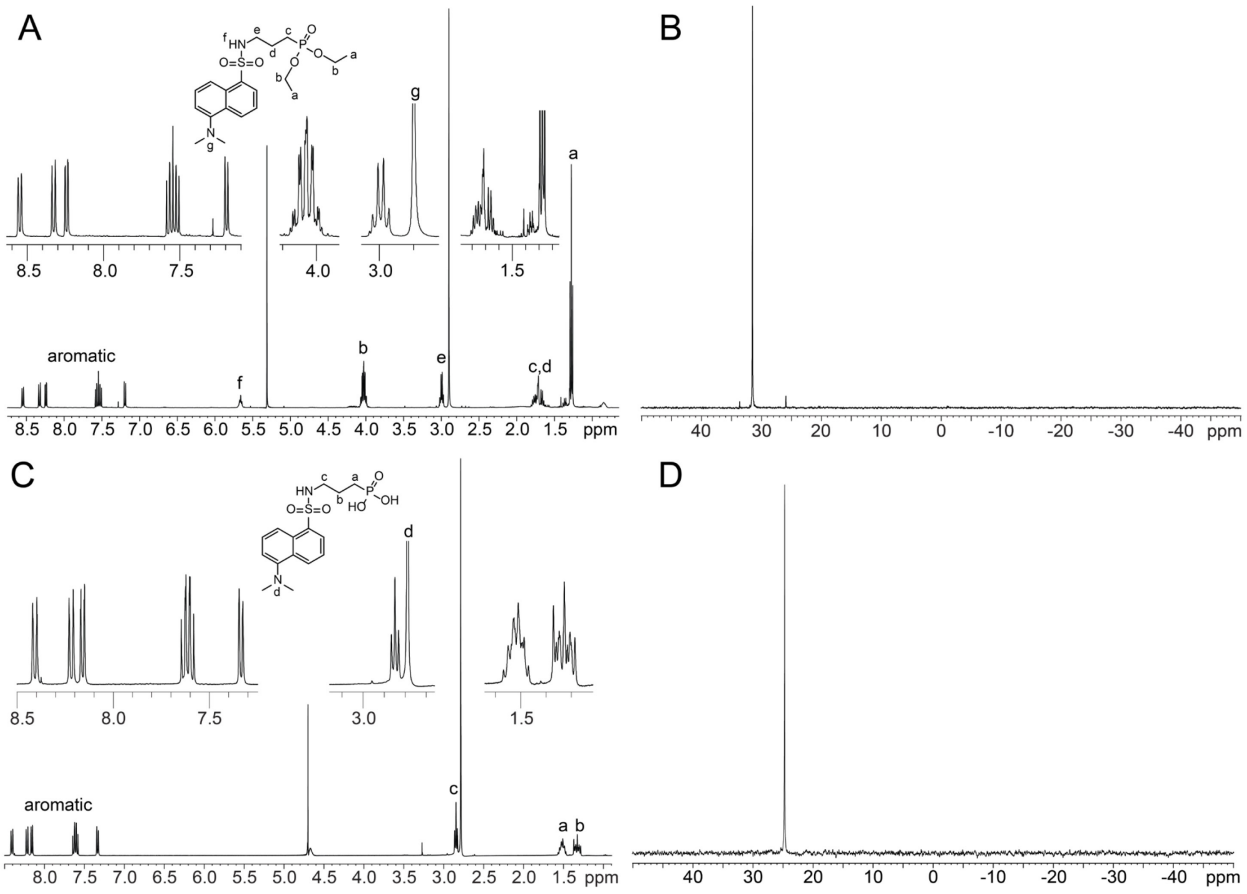

Figure 4.6: ^{1}H-NMR and ^{31}P-NMR spectra of **(A)** ^{1}H-NMR and **(B)** ^{31}P-NMR of E-n-DPPh in $CDCl_3$. **(C)** ^{1}H-NMR and **(D)** ^{31}P-NMR of n-DPPh in MeOD. Peaks in ^{1}H spectra are labeled with a corresponding proton. The inset spectra show the peak splitting.

CHAPTER 5. DYNAMICS OF ORGANIC PHOSPHORUS UTILIZATION IN THE NORTH PACIFIC SUBTROPICAL GYRE

5.1 ABSTRACT

In oligotrophic regions of the ocean, dissolved organic phosphorus (DOP) serves as an important P source for microbes. DOP is composed of several forms of P including phosphate esters and phosphonate esters. The C-P lyase enzyme hydrolyzes phosphonates and is a key enzyme in the remineralization of phosphonates. In Chapter 4, profiles of C-P lyase activity (CLA) showed a strong maximum in activity coincident with the deep-chlorophyl maximum (DCM). In this chapter, two hypotheses which explain the subsurface CLA maximum were tested. High-resolution profiles of inorganic nitrate and phosphate were collected in the region around the DCM, along with CLA and alkaline phosphatase activity measurements to determine if the diapycnal nutrient flux from the mesopelagic was resulting in a region of localized P limitation. The nutrient flux ratios had a low N/P ratio and no maximum in CLA was observed. This result served as a negative test of the hypothesis. To determine if the CLA maximum is the result of high concentrations of phosphonates near the DCM, rates of phosphonate production were measured. Phosphonate production rates were constant through the top 200 m of the water column, and were lower than phosphonate production rates measured in the Sargasso Sea, suggesting that phosphonate production is not elevated in the lower euphotic zone. Particulate organic matter (POC) was also collected through the euphotic zone to examine intracellular phosphonates. Phosphonates were not detected via ^{31}P-NMR of suspended particulate matter, however phosphonates were detected in net trap particles collected at 150 m. This result suggests that large particles, potentially of eukaryotic origin, may be an important source of phosphonates to the environment.

5.2 INTRODUCTION

Dissolved organic phosphorus (DOP) is a critical source of phosphorus for marine microorganisms in oligotrophic regions of the ocean where inorganic phosphorus (P_i) concentrations are low (< 100 nmol L^{-1}) and life relies on alternative P sources for growth (Karl & Björkman, 2002). DOP is a complex mixture of compounds containing phosphate mono- and diesters, as well as phosphonates (Björkman & Karl, 2003; Dyhrman & Ruttenberg, 2006; Karl & Yanagi, 1997; Kolowith et al., 2001; Monaghan & Ruttenberg, 1999). To access the P in DOP, marine microbes employ catabolic enzymes to hydrolyze P from organic matter and release P_i, which can then be repurposed and incorporated into microbial biomass. While many enzymes are used to remineralize DOP, two enzymes which have been identified as being critical for P nutrition are alkaline phosphatase (AP), which hydrolyzes phosphomonoesters, and C-P lyase, which hydrolyzes phosphonates (Coleman, 1992; Duhamel et al., 2010; Kamat & Raushel, 2013, 2014; Seweryn et al., 2015; Vidal et al., 2003).

While alkaline phosphonate activity (APA) has been studied extensively in the ocean, few measurements of C-P lyase activity (CLA) have been made as its role in DOP remineralization was only recently recognized (Karl et al., 2008; Repeta et al., 2016; Sosa et al., 2017, 2020). Chapter 4 describes the development of a fluorescent assay to measure CLA in the ocean. Profiles collected in the North Pacific Subtropical Gyre (NPSG) on three field expeditions found that CLA displayed a sharp maximum concurrent with the deep chlorophyll maximum (DCM) (Granzow et al., 2021). This result was unexpected as P_i concentrations are lower in the surface than near the DCM, and it was expected that phosphate limitation would drive phosphonate remineralization in the same way that APA is promoted under low P conditions (Duhamel et al., 2010). To explain this enigmatic CLA maximum in the subsurface, several

hypotheses were proposed. CLA may be promoted by an imbalance between the diapycnal nitrate and P_i fluxes from depth. In the NPSG, the base of the nitracline and phosphocline typically occur near the DCM, with the phosphocline starting ~0–10 m above the nitracline (Karl et al., 2001). The sharp increase in nutrient flux and the vertical separation of the nitracline and phosphocline may create a localized pocket of P_i limitation that promotes DOP remineralization. This hypothesis is supported by measurements of high APA in the subsurface as well, suggesting that bulk DOP degradation is enhanced, not just phosphonate degradation (Duhamel et al., 2011; Karl, 2014; Thomson et al., 2019).

The subsurface CLA maximum may also be the result of enhanced phosphonate production near the DCM, which would provide more substrate for C-P lyase. Additional phosphonates could potentially result in an increase in C-P lyase gene expression and an increase in CLA. Metagenomic analysis of CLA-containing genomes suggests a slight increase in CLA genes between 100 and 150 m in the NPSG, concurrent with the observed CLA maximum (Luo et al., 2011; Sosa et al., 2017). Additionally, increased phosphonate production in the subsurface has been detected previously in the Sargasso Sea (Van Mooy et al., 2015).

To test these two hypotheses, a holistic study of the inorganic and organic nutrient dynamics around the DCM must be undertaken. High resolution nutrient flux measurements are needed to determine if localized phosphorus stress is present in the subsurface. Additionally, measurements of cellular P concentrations and production rates are needed to determine if CLA is enhanced due to greater substrate availability. This investigation will lead to a better understanding of the controls on DOP remineralization and the microbial response to shifting nutrient regimes.

5.3 MATERIALS AND METHODS

5.3.1 Description of the Study Site

Sample collection was conducted aboard the R/V Kilo Moana during the PARAGON I (KM2112) and PARAGON II (KM2209) expeditions in the NPSG. The aim of PARAGON I was to study particle and nutrient flux in the mesopelagic region of the oligotrophic Pacific. The two-week expedition took place in July and August, 2021 and was centered in an anticyclonic eddy (21.5–22.5ºN, 155.3–156.5ºW) ~300 km east of Station ALOHA and ~300 km northeast of Honolulu, HI. The eddy contained a surface bloom of large diatoms, primarily *Hemiaulus* and *Rhizosolenia*, which faded toward the latter half of the cruise. PARAGON I also coincided with a full moon that induced a radiolarian spine detachment event.

PARAGON II was a 5-day expedition centered in a large bloom feature (23.4ºN, 154.6ºW) ~350 km east-northeast of Station ALOHA. This study site was chosen as it provided an opportunity to examine the dynamics of microbial-mediated particulate formation and the role of nitrogen fixation on bloom formation in the NPSG. The bloom consisted primarily of *Hemiaulus* and large colonial radiolarians were collected via net tows throughout the voyage, suggesting the microbial community was similarly structed during both years of the PARAGON program. In addition to those collected within the bloom, one set of water column samples was collected outside the bloom under conditions thought to be more representative of the NPSG near Station ALOHA. This profile will be referred to as the “blue water” profile for the rest of this chapter.

5.3.2 Inorganic Nutrient Flux Assessment

Inorganic nutrients were measured throughout the top 500 m of the water column using the standard Hawaii Ocean Time-series (HOT) protocols. Description of the nutrient analysis methods can be found on the HOT website (https://hahana.soest.hawaii.edu/hot/protocols/protocols.html). High resolution measurements of inorganic nutrients were taken in the water column centered on the DCM. Nitrate and nitrite (N+N) and soluble reactive phosphorus (SRP) were measured in 5 m increments in the 50 m above and below the DCM. The areal flux of nutrients (J_{diff}; nmol m^{-2} d^{-1}) was calculated around the DCM using these high-resolution measurements, which provides an estimate of the diapycnal nutrient flux into the DCM layer. The areal flux was calculated by equation 1:

$$J_{diff} = \frac{\partial C}{\partial z} \times k_z \quad (1)$$

Where $\frac{\partial C}{\partial z}$ is the vertical nutrient gradient below the DCM, and k_z is the vertical eddy diffusivity measured at DCM. Eddy diffusivity was measured using a vertical microstructure profiler (Micropod; Rockland Scientific) attached to an underwater glider, which made repeat measurements of vertical shear through the top 400 m of the water column near the ship at the same time as water was collected for the biogeochemical measurements. The vertical eddy diffusivity measured on PARAGON was 5×10^{-6} m^2 s^{-1}, an order of magnitude lower than typical diffusivities measured in the lower euphotic zone in the NPSG (Hamme & Emerson, 2006)

5.3.3 Phosphorus Uptake and Phosphonate Production

P_i uptake and phosphonate production were measured throughout the top 300 m of the water column on PARAGON I using ^{33}P labeled phosphate (Pasek et al., 2014; Pech et al., 2011; Van Mooy et al., 2015). 500 mL whole seawater samples were drawn from polyvinyl chloride

(PVC) bottles mounted to a CTD rosette into acid-washed polycarbonate (PC) bottles. These samples were divided into six 60 mL subsamples. Each subsample was spiked with 20 μCi of a ^{33}P labeled phosphoric acid solution. The total P addition was less than 4 pmol and should not have impacted the P biochemistry of the system, as the ambient P_i concentration in the surface was 43 nM. Three of the subsamples were also poisoned with a 10% paraformaldehyde solution to act as killed controls. Each sample was incubated for 9 hours in deck-board incubators. Samples collected above 100 m were incubated at surface seawater temperatures (~26ºC) with 50% PAR irradiance light levels. Samples collected between 100 m and 250 m were incubated at 18ºC with a 1% irradiance light level. Samples between 250 m and 1000 m were incubated in the dark at 15ºC.

After incubation, 10 mL of each sample were vacuum filtered onto nucleopore filters (0.2 um pore size, 25 mm) for measurement of total P_i uptake rates. These filters were placed in liquid scintillation vials with 5 mL of counting solution (Ultima Gold, Perkin Elmer). The samples were then counted on a liquid scintillation counter (LSC; Perkin Elmer). Subtraction of sample blanks was used to remove background activity, and the raw activity was corrected for radioactive decay of the spike during the cruise. Turnover time of the ^{33}P-phosphoric acid was calculated by dividing the corrected daily uptake by the total activity of the spike. P_i uptake was then calculated by dividing the ambient seawater P_i concentration by the measured turnover time. The remaining 50 mL of sample were vacuum filtered onto a second nucleopore filter. The filters were placed in cryovials and frozen for further analysis.

In the lab, 1 mL of high purity water (18.2 MΩ cm [MQ-H2O]) was added to each frozen filter and the samples were immersed in boiling water for 10 min. The samples were then frozen in liquid nitrogen for 1 minute. This freeze-thaw cycle was repeated three times to lyse the cells

and liberate the P-containing compounds. After mixing, 800 µL of each sample was collected and dried under vacuum. The samples were resuspended in 250 µL of MQ-H_2O. Methylphosphonic acid, sodium phosphate, and sodium phosphite were added as internal standards. To separate phosphate and phosphonate esters, the samples were injected into an ion chromatograph (IC; Thermo Scientific Dionex ISC-2100) equipped with an IonPac AS18 column (Thermo Scientific Dionex) and a fraction collector. The samples were eluted at 1 mL/min using an aqueous KOH solution mobile phase. A KOH concentration of 23 mM (pH = 12.4) was maintained for 15 min. followed by a linear gradient to 90 mM KOH (pH = 13.0) over 15 min. Eluent was collected between 5 and 10 minutes and between 20 and 25 minutes, corresponding to the expected elution times of phosphonate esters and phosphate esters, respectively, based on the internal standard signals. To these fractions, 15 mL of counting solution was added and the ^{33}P activity was counted via LSC. Background activity and sample decay were accounted for in the same manner as described previously for the P uptake measurements. The relative amount of phosphonate production was calculated by comparing the activity of the phosphonate samples isolated by IC with the total activity of the filtered sample.

5.3.4 C-P Lyase Activity

CLA was measured using the fluorescent phosphonate substrate n-dansyl-propylphosphonate (n-DPPh). 1 L whole seawater samples for CLA were drawn from CTD rosette mounted PVC bottles into acid-washed PC bottles. From the 1 L sample, triplicate 125 mL samples were collected in PC bottles and spiked with 1.25 nmol n-DPPh of to a final concentration of 10 nM. Control samples were collected at 25 m following the same procedure and spikes with 0.125 nmols of the synthetic C-P lyase cleavage product n-dansyl-propane (n-DP) for a final concentration of 1 nM. All samples were placed in deck-board incubators and

incubated for 24 hours under the same conditions described for the ^{33}P uptake and phosphonate production samples above.

After incubation, the samples were filtered through 0.2 um Durapore membrane filters (EMD Millipore Sterivex™ SVGV010RS) and the fluorescent tracer was recovered via solid phase extraction (SPE) onto 200 mg Agilent Bond Elut ENV columns at a flow rate of 5 mL min^{-1}. SPE columns were stored at 4ºC until analysis. In the lab, the samples were rinsed with 9 mL of MQ-H_2O eluted with 6 mL of methanol, dried under vacuum, and resuspended in 50% aqueous acetonitrile. Samples were analyzed via HPLC with fluorescence detection ($\lambda_{(ex)}$ 341 nm, $\lambda_{(em)}$ 528 nm) using a C-18 column. Samples were eluted with a gradient from 10% acetonitrile to 85% acetonitrile in 20mM phosphate buffer (pH = 4.2) at a flow rate of 0.3 mL min^{-1}. n-DPPh and n-DP eluted at 7 and 11 min, respectively. See Granzow et al. (2021) for a complete description of the CLA analysis.

5.3.5 Alkaline Phosphatase Activity

Particulate alkaline phosphatase activity (APA) was measured through the water column to 500 m on PARAGON II. 1 L seawater samples were split into three 300 mL replicates and filtered onto 0.2 µm Nuclepore PC filters. The filters were placed in PC Petri dishes and frozen (-20ºC) for onshore analysis.

In the Dyhrman lab at Lamont-Doherty Earth Observatory, APA was measured fluorometrically (Dyhrman & Ruttenberg, 2006). The filters were incubated at room temperature in 2 mL of phosphate-free artificial seawater. The fluorogenic phosphatase substrate 6,8-difluoro-4-methylumbelliferyl phosphate (DiFMUP) was added to a final concentration of 10 µM. Hydrolysis of the DiFMUP was monitored via fluorescence measurements (λ_{ex} = 360 nm, λ_{em} = 460 nm) using at CytoFluor multiwell plate reader at 25ºC. Subsamples were collected

from the plate at the start of the analysis and at intervals such that a linear activity curve was measured. A standard curve was used to convert the fluorescence measurement to the amount of P liberated by AP.

5.3.6 Large Volume Suspended Particulate Organic Matter

Suspended particulate matter (SPM) was collected from five depths on PARAGON I (5, 50, 100, 130, 200 m) in the euphotic zone. A ¾-inch high density polyethylene hose (McMaster-Carr) was lowered to depth and 1200 L of seawater were pumped into polytetrafluoroethylene-lined barrels using a pneumatic double diaphragm pump. The pumping flowrate decreased with increased sample depth and varied from 12 L/min at the surface to 5 L/min at 200 m. The hose was flushed with sample water for 10 minutes before collection.

A custom tangential flow filtration (TFF) system was built to concentrate SPM. The system consisted of seven hollow fiber filters (M-C-100-B; Mar Cor) with a pore size of 0.1 μm plumbed in parallel. Seawater was pumped from each barrel through the TFF system using a 2 horsepower 3 phase 240 V pump running at a flow rate of 20 L/min. Permeate water was discarded while the retentate containing the SPM was recycled and concentrated in one barrel to a final volume of 18 L. This concentrate was transferred to a smaller TFF system comprised of a single hollow fiber filter. On this smaller system, the volume was reduced further to 2.5 L and the concentrate was collected in an acid-washed PC bottle and frozen at -20^{o}C for further processing on shore.

To test the recovery efficiency of the TFF filters, *Synechococcus 7803* was grown in culture to a cell density of 5.8×10^{7} cells mL^{-1}. 1 L aliquots of culture were diluted in ultrafiltered surface seawater collected from the Sargasso Sea to a final volume of 20 L. The cells were then

concentrated using a TFF cartridge to a final volume of 1 L and the cell density was measured. Cell recovery was greater than 95% (n = 3).

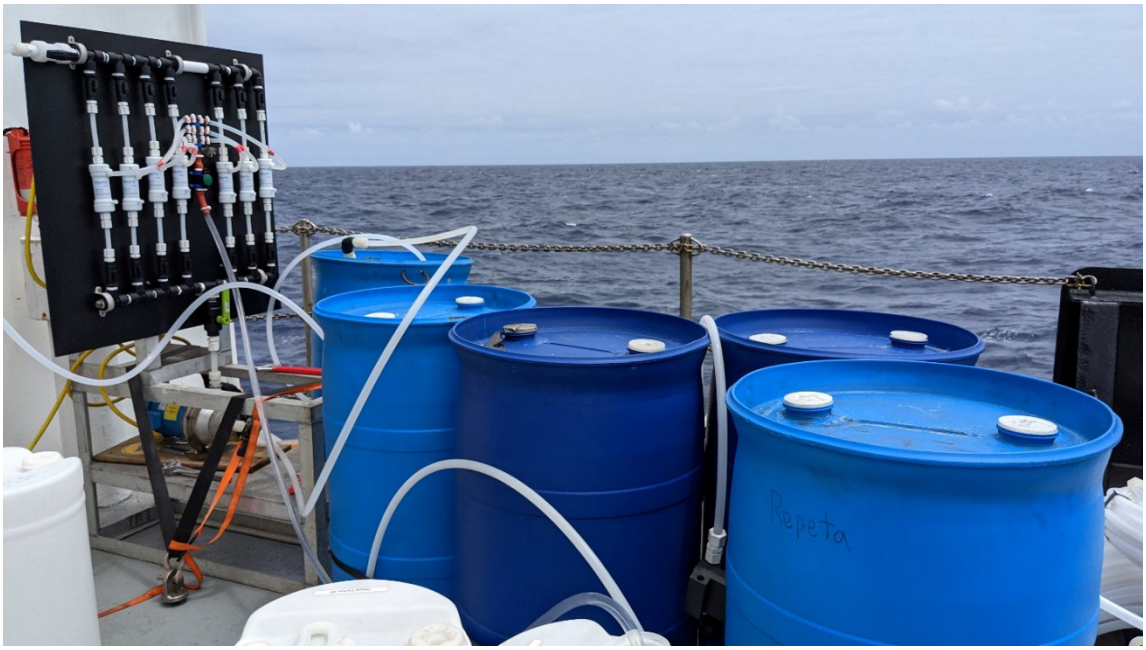

Figure 5.1: Custom large volume POM concentrator used on PARAGON I to collected SPM samples. The seven hollow fiber filters (white) retain particles larger than 0.1 µm.

In the lab, each sample was thawed. Triplicate 10 mL samples were collected for POC analysis, and the remaining concentrate was transferred to 250 mL conical centrifuge flasks and centrifuged at 4641 rcf for 24 hr to pellet the SPM. The pellet was transferred to successively smaller vials to concentrate and separate the SPM. The pelleted SPM samples were washed with MQ-H_2O three times to remove salts then lyophilized.

In addition to the SPM samples, a POM sample was also collected from 150 m using a 1.25 m diameter net trap (Peterson et al., 2005). The net trap particles (NTP) were filtered through a 350 µm screen and concentrated by centrifuge in the same manner as described above. In this study, POM will refer to all particulate matter, regardless of settling state, while SPM will

refer only to suspended matter isolated by TFF, and NTP will refer to sinking material caught in the net trap.

5.3.7 Nuclear Magnetic Resonance Spectroscopy

POM samples were packed into 20 µL Kel-F rotor inserts, which were placed in 4 mm Zr magic angle spinning rotors. ^{13}C and ^{31}P solids-NMR experiments were performed on a Bruker Avance Neo NMR (400 MHz ^{1}H frequency) equipped with a 4 mm double-resonance solids probe for high resolution magic angle spinning NMR spectroscopy (MAS). Samples were spun at a speed of 12 kHz. ^{13}C compositional information was obtained using a cross polarization (CP-MAS) experiment with a CP time of 2 ms, a ^{1}H 90^{o} pulse length of 4.8 µs, and a recycle delay of 1 s. 65k scans were collected for each sample. ^{31}P spectra were also collected using a CP-MAS experiment with a CP time of 2 ms, a ^{1}H 90^{o} pulse length of 4.8 µs, and a recycle delay of 2 s. 64k scans were collected during acquisition for each sample.

Following MAS, the NTP was treated with strong base (2N KOH) for 36 hours at 60^{o}C to hydrolyze phosphate and phosphonate esters, allowing for a liquid extraction of the organic phosphorus species. After hydrolysis, the extract was filtered to remove all remaining solids and neutralized by stirring it with 5 mg of a cation exchange resin (AG 50W-X2, H^{+} form; Bio-Rad) for approximately 10 min. The resin was removed by filtration and the dissolved material was lyophilized and redissolved in D_2O for ^{31}P-NMR analysis. Samples were analyzed using 1D ^{31}P (ZGPG30; Bruker) and 2D HMQC (HMQCGPQF; Bruker) experiments to study the composition of P compounds. The HMQC included decoupling of the proton dimension during acquisition.

5.4 RESULTS AND DISCUSSION

5.4.1 Nutrient Dynamics and Organic Phosphorus Cycling on PARAGON

5.4.1.1 Depression of the Nutriclines

High resolution measurements of inorganic nutrients collected on casts 10 and 43 of PARAGON I show a sharp nitracline and phosphocline (Figure 5.2). On cast 10, which was collected at the start of the cruise under strong bloom conditions, the nitrate and phosphate nutriclines were depressed 15 m below the DCM, with the inflection points of both nutrients occurring around 155 m. These conditions are abnormal for the NPSG, where the nitracline typically occurs at a similar depth to the DCM and the phosphocline is elevated 0-10 m above the nitracline (Karl et al., 2001). Cast 43 occurred at the end of the cruise, after the demise of the diatom bloom, a weakening of the anticyclonic eddy and as the system was returning to conditions more typically observed the NPSG. The nitracline inflection depth on cast 43 rose to 150 m and the phosphocline rose 10 m above the nitracline to 140 m, just 2 m below the DCM. The shoaling of the nutriclines likely occurred due to the weakening of the eddy feature. In addition, the DCM became more pronounced as pigment concentrations increased.

5.4.1.2 Organic Phosphorus Remineralization

CLA did not show the characteristic peak in activity concurrent with the DCM on any of the profiles collected on PARAGON I (Figure 5.2). CLA was slightly elevated in the surface (114.0 ± 0.9 pmol P L^{-1} d^{-1}) and decreased to a broad minimum in the subsurface around 100 meters (105.5 ± 0.6 pmol P L^{-1} d^{-1}). These rates are low, but consistent with previously measured rates of CLA in the NPSG (6.1–931.0 pmol P L^{-1} d^{-1}; Granzow et al., 2021). The high-resolution sampling around the DMC conducted on the PARAGON I expedition showed that CLA was highly variable in that region. Replicate measurements were consistent, providing evidence that

this feature is real and suggesting highly localized variability in nutrients, light, and community composition drive CLA.

CLA rates measured in the bloom on PARAGON II were an order of magnitude lower than those measured on PARAGON I, but showed a similar trend of highly localized variability. This high-resolution sampling effort targeted a region 80 m below the broad chlorophyll maximum, which may have resulted in the low CLA detected. The blue water profile displayed a different pattern to the bloom samples. Two sharp peaks in CLA are present at 50 m and 80 m. These peaks correspond to two maxima in the chloropigment profile, suggesting a return to the patterns previously observed in CLA. Variability on these measurements was high, with just one of the three replicates showing high activity in the 50 m, 70 m, and 80 m samples. It is possible that C-P lyase responsible for these signals was associated with suspended particles, and was heterogeneously dispersed in the seawater sample, leading to the poor replication.

In Chapter 4, several hypotheses were proposed to explain the CLA maximum concurrent with the DCM. One hypothesis proposed that this feature is caused by an elevated nitrate flux due to increased diapycnal mixing from depth at the base of the nitracline. The additional nitrate would promote the uptake and metabolism of alternative P sources and would facilitate the production of enzymatic systems for phosphonate metabolism.

The results of the high-resolution nutrient sampling lend support to the nutrient flux hypothesis. Unlike in previous studies, the nitracline in both PARAGON sample sets was depressed well below the DCM, and so a high nitrate flux into the DCM region was not present. Consequently, a peak in CLA was not detected near the DCM, consistent with the hypothesis. Analysis of all CLA data with companion nutrient measurements in the NPSG revealed a potential relationship. When the ratio of N-flux to P-flux at the DCM was well above 16, the

canonical Redfield Ratio (Redfield, 1934), a strong maximum in CLA was detected. However, when the flux ratio dropped well below 16, CLA at the DCM was suppressed (Table 5.1). While a significant relationship between the magnitude of the flux ratio and CLA was not found, this threshold around the Redfield Ratio is intriguing and merits further study.

The APA profile collected at the blue water station displayed the same trends as CLA, indicating that organic phosphorus remineralization as a whole was promoted near the DCM at that station (Figure 5.3). A similar coherence between APA and CLA was observed previously at Station ALOHA on HOT318 (Figure 5.7). APA rates were several orders of magnitude greater than CLA, although hydrolysis rates based on fluorescent tracer assays cannot be directly compared to total hydrolysis rates of DOP as the fluorescent substrate efficiency is not well constrained. Additionally, the APA assay specifically measures phosphate ester hydrolysis by particle-associated AP, while the CLA assay measures C-P lyase-associated hydrolysis in whole water samples. No CLA is detected in cell lysate, or in filtered seawater samples, however, suggesting that most or all C-P lyase is cell or particle associated, allowing for a more rigorous comparison of the two enzyme assays (Granzow et al., 2021; Metcalf & Wanner, 1993)

It is important to recognize that macronutrient balance may not be the only control on DOP remineralization. Several studies have found CLA to be somewhat independent of P_i concentration and have suggested that C-P lyase may be utilized as a mechanism for extracting labile C and N from organic matter (Benitez-Nelson et al., 2004; Chin et al., 2018). These conclusions are supported by the high CLA rates observed in seawater collected from the mesopelagic, although it is unclear what effects pressure and temperature modulation during incubation have on those results (Granzow et al., 2021). Recently, a phosphate insensitive cosmopolitan phosphomonoesterase produced by *Bacteroidetes* was found to be associated with

phytoplankton and POM and was hypothesized to be used in C acquisition from phosphorylated compounds (Lidbury et al., 2022). While the evidence presented here supports nutrient availability as a primary driver of phosphonate remineralization near the DCM, it is clear that several factors could drive the rate of DOP diagenesis.

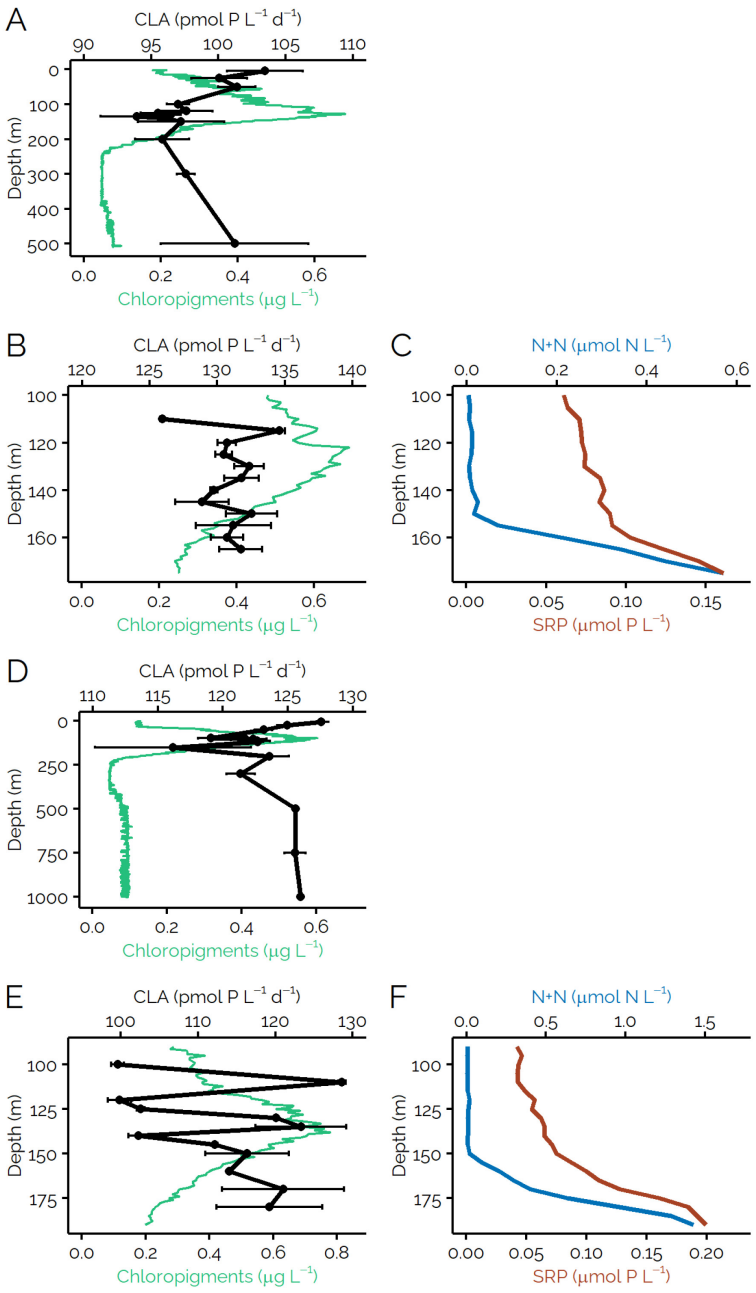

Figure 5.2: CLA and nutrient profiles collected on PARAGON I. Cast 6 (**A**) and cast 22 (**D**) were CLA surveys of the upper water column while cast 10 (**B&C**) and cast 43 (**E&F**) employed a high-resolution sampling scheme around the DCM. Error bars associated with each value represent the standard error of the mean (n = 3).

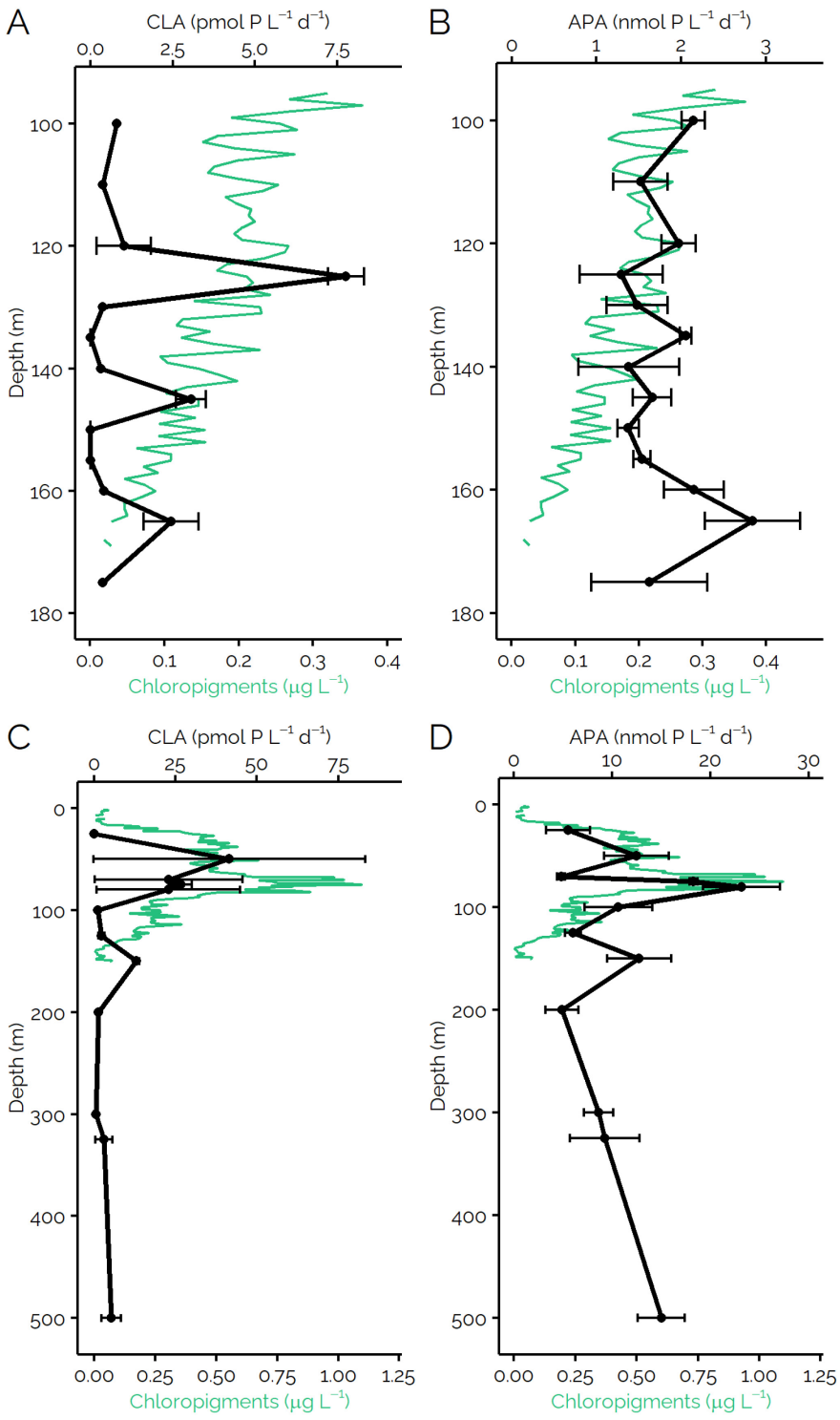

Figure 5.3: CLA and APA profiles collected on PARAGON II. High-resolution sampling was performed around the nitrite maximum at 140 m in the bloom profile (**A&B**) while a full depth profile was collected at the Blue Water Station (**C&D**). Error bars on each measurement represent the standard error of the mean (n = 3).

Table 5.1: Summary of CLA maxima and nutrient fluxes in the NPSG. DCM depth was determined by the depth of the fluorescence maximum detected by the CTD.

Research Cruise	Location	Depth of DCM (m)	N+N Flux (nmol m^{-2} d^{-1})	SRP Flux (nmol m^{-2} d^{-1})	N:P Flux Ratio	CLA Prominence† (nmol P L^{-1} d^{-1})
HOT 297 (KM1717)	Station ALOHA	110	5.86	0.22	26.9	362.3
SCOPE-Falkor (FK180310)	Cyclonic Eddy- NPSG	121	5.74	0.10	55.6	282.9
HOT 307 (KM1821)	Station ALOHA	92	4.04	0.11	35.6	800.0
HOT 318 (KM2001)	Station ALOHA	101	0.48	0.10	5.1	4.4
PARAGON I (KM2112)	Anticyclonic Eddy- NPSG	122	0.12	0.04	3.2	4.1
PARAGON II (KM2209)	Diatom Bloom- NPSG	59	—	—	—	7.8

†CLA prominence is the CLA maximum value with the CLA baseline subtracted.

5.4.1.3 Phosphate Uptake and Phosphonate Production

To study the formation of phosphonates, rates of P_i uptake and phosphonate production were measured through the euphotic zone. P_i uptake rates were highest in the surface—where inorganic phosphate concentrations were low—and decreased with depth. Rates ranged from 0.34 ± 0.04 to 4.45 ± 0.19 nM P d^{-1}, which are consistent with previously reported values of P_i uptake (3–8 nM P d^{-1} in the surface) in the NPSG near Station ALOHA (Björkman et al., 2000; Popendorf et al., 2020). The lowest rates of uptake were observed in the lower euphotic zone around the DCM, on both cast 10 and 43, although two samples on cast 43 (130 m and 140 m) had the highest measured rates of P_i uptake. Cast 43 sampled the water column as it was returning to average conditions, and as the phosphocline was shoaling, relative to the nitracline. The highest measured uptake rate occurred at 140 m, concurrent with the base of the phosphocline. The infusion of P_i could explain the high P_i uptake rates observed on that cast.

The amount of P incorporated into phosphonates was uniform throughout the water column, with no significant difference in the relative phosphonate production detected between the mixed layer ($\bar{x} = 0.6\%$, $\sigma = 0.2\%$, $n = 9$) and DCM ($\bar{x} = 1.2\%$, $\sigma = 0.6\%$, $n = 24$); Student's T-Test; $t(31) = 0.60$, $p > 0.05$. This suggests that the formation of phosphonates was not enhanced in the DCM. This may be due to the deepening of the nutriclines and the weakening of the DCM due to the eddy feature, however, no increase in phosphonate production was detected on Cast 43, despite the enhanced P_i uptake rates. While additional measurements of P_i uptake and the formation of phosphonates should be made in the NPSG under more standard conditions, these results do not lend support to the hypothesis that phosphonate production is enhanced in the region around the DCM or at the top of nitracline.

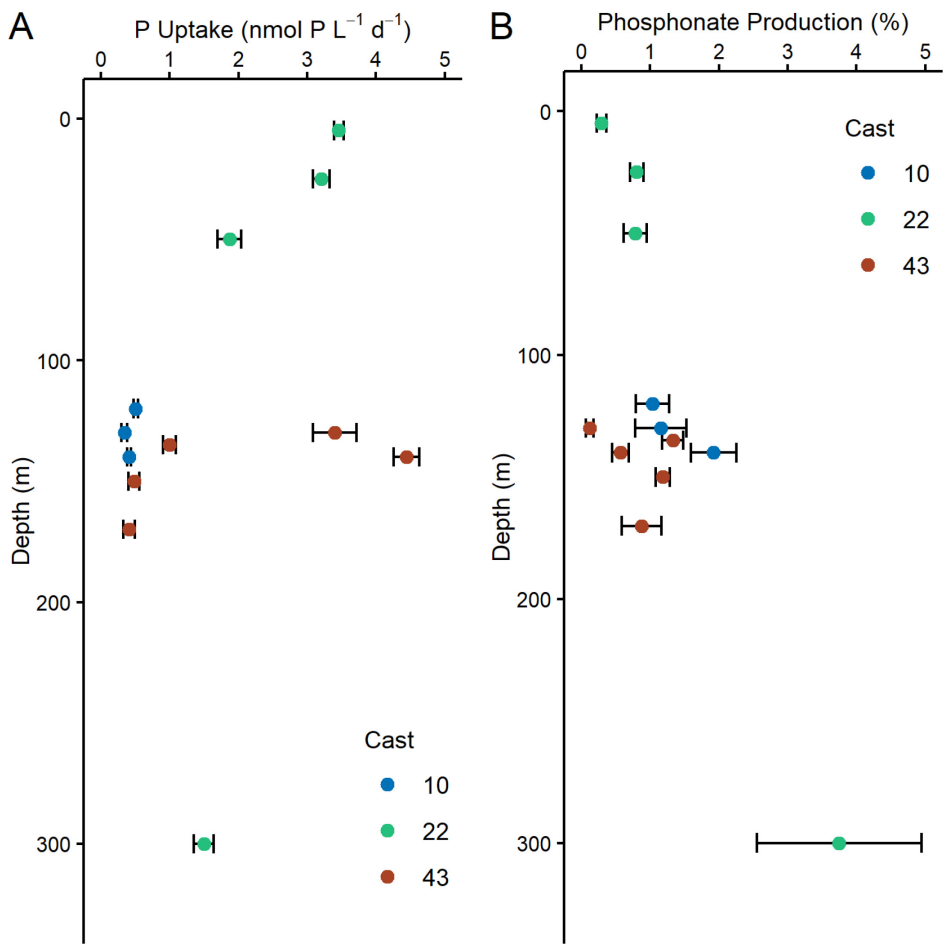

Figure 5.4: (**A**) Inorganic phosphate uptake rates and (**B**) phosphonate production as a percentage of radiolabel uptake measured on three casts during PARAGON I using ^{33}P labeled phosphoric acid. Cast 10 and cast 43 focused on high-resolution sampling around the DCM. Error bars indicate the standard error of the mean (n = 3).

5.4.2 POM Structural Observations

^{13}C-MAS spectra of POM contain resonances from expected biomolecules including proteins, unsaturated and saturated lipids, and polysaccharides (Figure 5.8) A complete annotation and comparison of features in the ^{13}C was not performed as part of this work, but a more in-depth analysis of the broad biomolecular groups detected is described in the Supplemental Material of this chapter.

5.4.2.1 Suspended Particulate Matter

SPM collected using the custom POM concentrator is expected to reflect the major suspended particles in the water column. Prokaryotic amplicon analysis of seawater samples collected through the top 200 m of the water column indicates that the major bacterial taxa present during PARAGON I were Alphaproteobacteria including SAR 11 and SAR 86, as well as *Prochlorococcus*, a dominant oligotrophic cyanobacteria. *Prochlorococcus* amplicon abundance was highest in the mixed layer with a maximum abundance at 75 m, and decreasing abundance through the lower euphotic zone.

^{31}P-NMR spectra of SPM collected through the top 200 m of the water column are shown in Figure 5.5. Each spectrum has one broad peak centered around -2.9 ppm with significant resonances between 4.6 and -12.5 ppm. The width of the peak and the ratio of width-to-intensity did not change with depth, suggesting that P composition of SPM remained consistent through the euphotic zone. The signal is attributable to P_i, phosphate monoesters, and phosphate diesters, which are the most common forms of P found in cells (Quin & Williams, 2004).

No signal was detected around the 24 ppm region, which is characteristic of phosphonates. These results suggest that phosphonates do not comprise a detectable amount of P (10 μmol) in SPM. If the CLA maxima around the DCM were a result of enhanced phosphonate biosynthesis and a greater stock of dissolved organic phosphonates, elevated intracellular phosphonate concentrations would likely have been detected. As was discussed in a prior section, the nutrient and chlorophyll distributions were perturbated by the eddy feature away from typical NPSG conditions. These results may reflect a dampening of phosphonate cycling due to the low nitrate flux near the DCM, and may not be representative of typical phosphonate

production and remineralization present under more typical conditions. A replication of this study should be performed under standard nutrient conditions to determine if these results were anomalous, or representative of the phosphonate cycling in the NPSG.

5.4.2.2 Net Trap Material

Prokaryotic amplicon analysis of the NTP indicated that sinking particles collected by the net trap contained material produced by Gammaproteobacteria taxa, including *Pseudoalteromonas, Vibrionaceae*, and *Bermanella*. Additionally, eukaryotic transcriptomic analysis identified material from dinoflagellates and *Rhizeria*, as well as a significant amount of material from unidentified eukaryotes. NTP was composed of material from a different source than SPM, indicating that the two particle collection methods are sampling complementary pools of POM.

NTP collected by the 150 m net trap was analyzed for phosphorus composition in the same manner as SPM (Figure 5.5). In addition to the broad peak centered at -2.9 ppm (Peak A), which was observed in the SPM samples, a second broad peak centered at 18.2 ppm was observed (Peak B). Peak B had area that was 63% of the area of Peak A, suggesting the organophosphorus compounds responsible for this signal comprise a large fraction (~40%) of the P in the NTP. Peak B was composed of signals between 28. 7 and 7.8 ppm, suggesting a contribution from phosphonates and phosphate esters (Quin & Williams, 2004). While further structural elucidation is not possible, due to the broadness of the peaks, these results provide evidence that a large portion of NTP-P contains phosphonates.

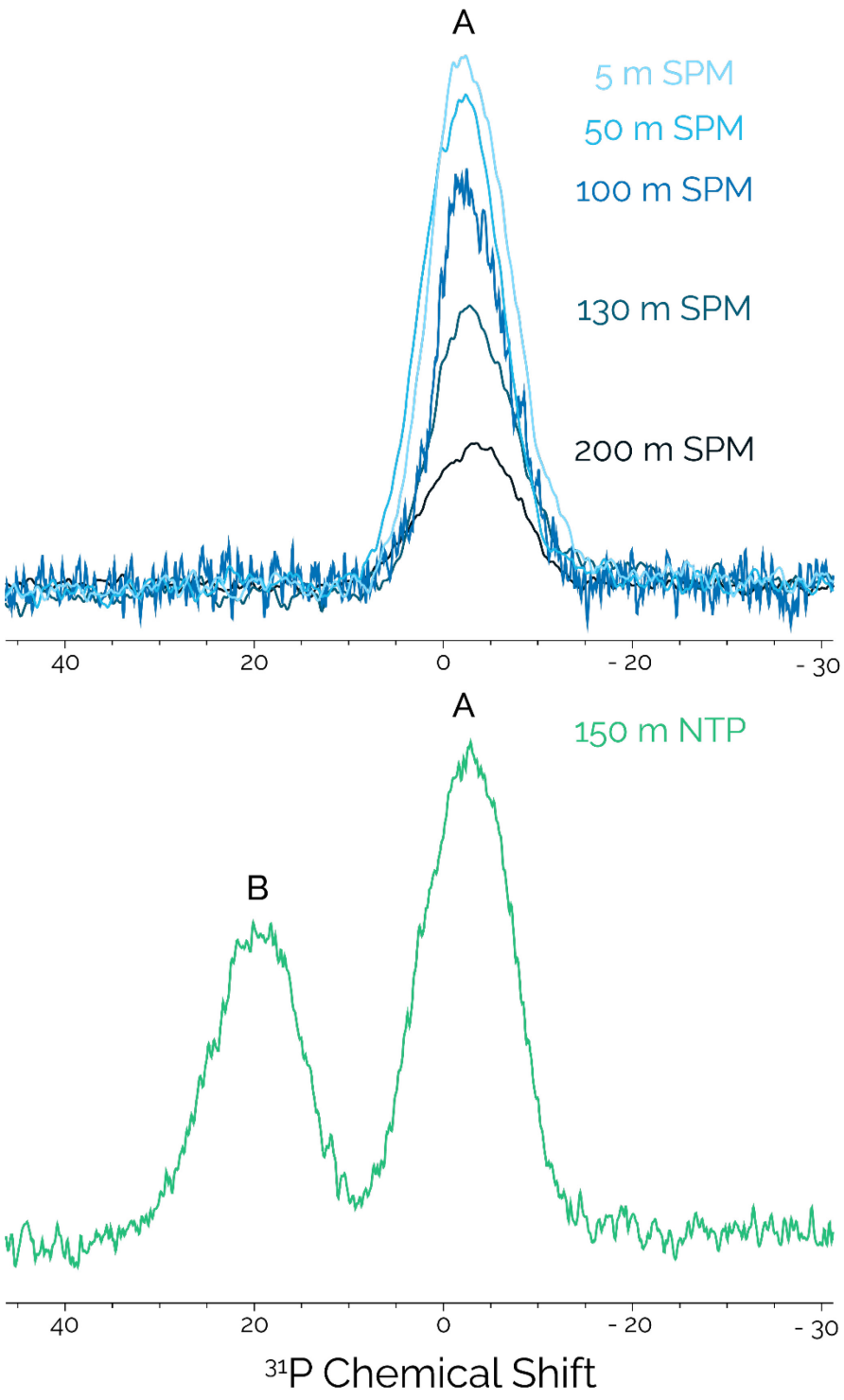

Figure 5.5: ^{31}P CP-MAS NMR spectra of SPM from five different depths in the euphotic zone and (top) and NTP (bottom) collected at 150 m. Peak **A** corresponds to P_i and phosphate esters, and peak **B** corresponds to phosphate esters and phosphonates.

5.4.2.3 Unique Phosphorus-Containing Compounds in Net Trap Material

To determine which phosphonate compounds were present in NTP, the sample was hydrolyzed by strong base to depolymerize the organic matter, simplifying the material, and enabling analysis in the dissolved phase. Solution state ^{31}P-NMR of the aqueous hydrolysis product shows 5 well-resolved peaks (Figure 5.6). A 2D HMQC experiment was employed to ascertain information about the proton chemical shifts associated with each P resonance. All peaks had splitting consistent with ^{1}H-^{31}P coupling (~17 Hz). Peak P1 has no associated ^{1}H resonances and is likely P_i. P2 and P3 have proton cross peaks at δ 4.1 ppm, δ 3.9 ppm, and δ 3.8 ppm, suggesting they come from phosphoglycans or nucleotides, common P containing biomolecules.

Peak P5 has strong proton cross peaks at δ 1.7 ppm and weaker cross peaks at δ 3.8 ppm and δ 3.1 ppm. ^{31}P-coupled ^{1}H-NMR signals at δ 1.8 ppm and δ 3.1 ppm are characteristic of aminoethylphosphonate (APE; Cioni et al., 2014; Urai et al., 2009; Vinogradov et al., 2001). A diverse array of aminophosphonates have been detected previously in sediment trap material, although their contribution to the total particulate phosphorus pool was not quantified (Acker, 2021). Based on peak area analysis, AEP could comprise ~5% of P in the hydrolysis product of the NTP sample. P recovery was not measured, and so it is not clear what portion of total P was extracted from the NTP, although strong base hydrolysis of organic matter has been shown to quantitatively extract phosphorus (Anderson, 1960). Therefore, the contribution of AEP to the total particulate P pool captured by the net trap was likely close to ~5%. Few examples of marine AEP production are known; AEP-containing glycoproteins were found in the mucin of a coastal jellyfish species and in benthic mollusk (Eckmair et al., 2016; Lucas, 2001; Urai et al., 2009). The jellyfish mucin is a good match for the P5 compound, as the mucin AEP moiety is attached

to an n-acetylgalactosamine molecule, which gives rise to a ^{1}H resonance at 3.8 ppm. Detection of AEP in NTP from the NPSG suggests that phosphonate production may be more cosmopolitan than has been previously recognized and that eukaryotic biomass may supply a significant amount of phosphonate containing compounds to the open ocean.

Peak P4 has three sets of proton cross peaks that are shifted downfield into the region denoting alkenes (δ 6.1 ppm, δ 5.7 ppm, and δ 5.5 ppm). The proton peaks suggest that the phosphate is attached to a terpenoid. The synthesis pathway of terpenoids involves several phosphorylation steps, and the presence of phosphorylated terpenoids in cellular material is not surprising (Ashour et al., 2010). Based on the chemical shifts of the ^{31}P-^{1}H cross peaks, a putative chemical structure is shown in Figure 5.6. This motif has been described previously as part of labdane-type diterpenoids in terrestrial plants, however no such structure has been annotated in marine organisms (Shen et al., 2019). Similar terpenoids are synthesized by marine mollusks and fungi lending support to the hypothesis that phosphorylated labdane terpenoids were detected in NTP (Avila, 2020). These data provide new insight in the P composition of sinking POM and suggest that a diverse array of enzymatic machinery is required to remineralize and utilize particle-associated organic P.

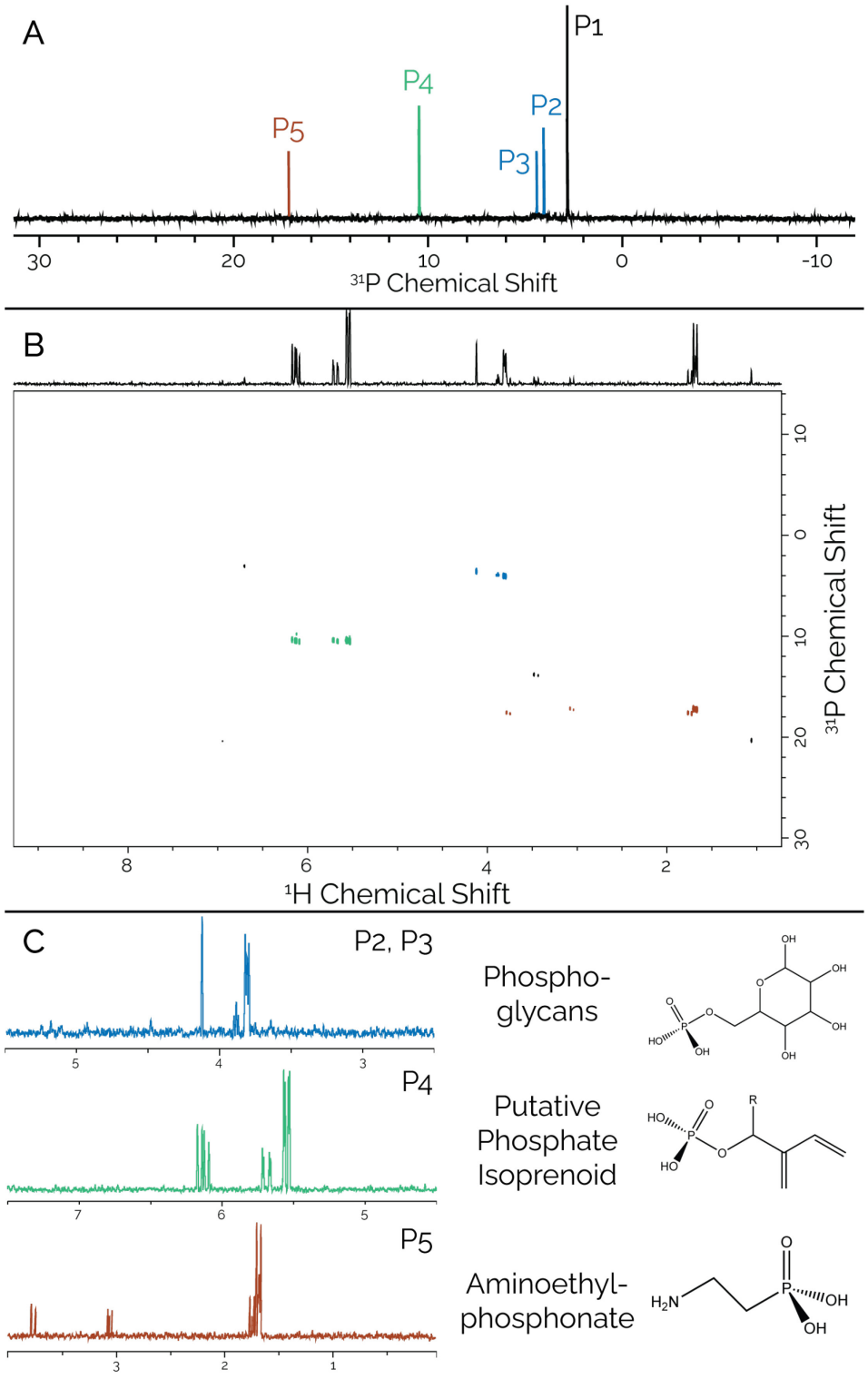

Figure 5.6: NMR analysis of the products of NTP hydrolysis. **A)** 1D ^{31}P-NMR and **B)** 2D HMQC of the hydrolyzed material showing 5 peaks indicating unique phosphorus compounds, each with corresponding proton cross peaks. **C)** Extracted ^{1}H-NMR spectra for the phosphorus peaks along with putative annotations of each compound class.

5.5 CONCLUSIONS

The subsurface CLA maximum detected on previous expeditions appears to occur only under specific environmental conditions. It can be depressed by bloom-driven shifts in water column nutrients, and by fluctuations in the nutrient fluxes from the mesopelagic. Although a strong CLA maximum was not detected on either PARAGON expedition, the nutrient analysis results suggest that localized P_i limitation did not occur, resulting in a negative test to the nutrient flux hypothesis. Future studies of the effect of inorganic nutrient flux on DOP remineralization are needed to continue to explore this theory.

Enhanced phosphonate production was not detected near the DCM, a result in contrast to phosphonate production in the North Atlantic. No phosphonates were detected in the SPM, suggesting that suspended microbes may not be the primary source of phosphonates to the DOP pool. A significant phosphonate signal was detected in the NTP, emphasizing the need to consider large eukaryotic organisms when studying P cycling and dynamics. This study builds upon the established body of work suggesting that organic P production and remineralization is a complex and dynamic cycle with important implications for the marine carbon cycle and for microbial growth in the oligotrophic ocean.

5.6 REFERENCES

Acker, M. (2021). *Phosphonate biogeochemical cycling in the marine environment: From an ocean scale to a molecular scale* [Doctor of Philosophy]. Massachusetts Institute of Technology.

Anderson, G. (1960). Factors affecting the estimation of phosphate esters in soil. *Journal of the Science of Food and Agriculture*, *11*(9), 497–503. https://doi.org/10.1002/jsfa.2740110902

Ashour, M., Wink, M., & Gershenzon, J. (2010). Biochemistry of terpenoids: Monoterpenes, sesquiterpenes and diterpenes. In *Biochemistry of Plant Secondary Metabolism: Second Edition* (Vol. 40, pp. 258–303). https://doi.org/10.1002/9781444320503.ch5

Avila, C. (2020). Terpenoids in marine heterobranch molluscs. *Marine Drugs*, *18*(3). https://doi.org/10.3390/md18030162

Benitez-Nelson, C. R., O'Neill, L., Kolowith, L. C., Pellechia, P., & Thunell, R. (2004). Phosphonates and particulate organic phosphorus cycling in an anoxic marine basin. *Limnology and Oceanography*, *49*(5), 1593–1604. https://doi.org/10.4319/lo.2004.49.5.1593

Björkman, K. M., & Karl, D. M. (2003). Bioavailability of dissolved organic phosphorus in the euphotic zone at station ALOHA, North Pacific Subtropical Gyre. *Limnology and Oceanography*, *48*(3), 1049–1057. https://doi.org/10.4319/lo.2003.48.3.1049

Björkman, K. M., Thomson-Bulldis, A. L., & Karl, D. M. (2000). Phosphorus dynamics in the North Pacific subtropical gyre. *Aquatic Microbial Ecology*, *22*(2), 185–198. https://doi.org/10.3354/ame022185

Cao, X., Aiken, G. R., Butler, K. D., Huntington, T. G., Balch, W. M., Mao, J., & Schmidt-Rohr, K. (2018). Evidence for major input of riverine organic matter into the ocean. *Organic Geochemistry*, *116*, 62–76. https://doi.org/10.1016/j.orggeochem.2017.11.001

Chin, J. P., Quinn, J. P., & McGrath, J. W. (2018). Phosphate insensitive aminophosphonate mineralisation within oceanic nutrient cycles. *ISME Journal*, 1–8. https://doi.org/10.1038/s41396-017-0031-7

Cioni, J. P., Doroghazi, J. R., Ju, K.-S., Yu, X., Evans, B. S., Lee, J., & Metcalf, W. W. (2014). Cyanohydrin Phosphonate Natural Product from *Streptomyces regensis*. *Journal of Natural Products*, *77*(2), 243–249. https://doi.org/10.1021/np400722m

Coleman, J. E. (1992). Structure and mechanism of alkaline phosphatase. *Annual Review of Biophysics and Biomolecular Structure*, *21*, 441–483. https://doi.org/10.1146/annurev.bb.21.060192.002301

Duhamel, S., Björkman, K. M., Van Wambeke, F., Moutin, T., & Karl, D. M. (2011). Characterization of alkaline phosphatase activity in the North and South Pacific Subtropical Gyres: Implications for phosphorus cycling. *Limnology and Oceanography*, *56*(4), 1244–1254. https://doi.org/10.4319/lo.2011.56.4.1244

Duhamel, S., Dyhrman, S. T., & Karl, D. M. (2010). Alkaline phosphatase activity and regulation in the North Pacific Subtropical Gyre. *Limnology and Oceanography*, *55*(3), 1414–1425. https://doi.org/10.4319/lo.2010.55.3.1414

Dyhrman, S. T., & Ruttenberg, K. C. (2006). Presence and regulation of alkaline phosphatase activity in eukaryotic phytoplankton from the coastal ocean: Implications for dissolved organic phosphorus remineralization. *Limnology and Oceanography*, *51*(3), 1381–1390. https://doi.org/10.4319/lo.2006.51.3.1381

Eckmair, B., Jin, C., Abed-Navandi, D., & Paschinger, K. (2016). Multistep Fractionation and Mass Spectrometry Reveal Zwitterionic and Anionic Modifications of the N- and O-

glycans of a Marine Snail. *Molecular & Cellular Proteomics*, *15*(2), 573–597. https://doi.org/10.1074/mcp.M115.051573

Granzow, B. N., Sosa, O. A., Gonnelli, M., Santinelli, C., Karl, D. M., & Repeta, D. J. (2021). A sensitive fluorescent assay for measuring carbon-phosphorus lyase activity in aquatic systems. *Limnology and Oceanography: Methods*, *19*(4), 235–244. https://doi.org/10.1002/lom3.10418

Hamme, R. C., & Emerson, S. R. (2006). Constraining bubble dynamics and mixing with dissolved gases: Implications for productivity measurements by oxygen mass balance. *Journal of Marine Research*, *64*(1), 73–95. https://doi.org/10.1357/002224006776412322

Hertkorn, N., Benner, R., Frommberger, M., Schmitt-Kopplin, P., Witt, M., Kaiser, K., Kettrup, A., & Hedges, J. I. (2006). Characterization of a major refractory component of marine dissolved organic matter. *Geochimica et Cosmochimica Acta*, *70*(12), 2990–3010. https://doi.org/10.1016/j.gca.2006.03.021

Kamat, S. S., & Raushel, F. M. (2013). The enzymatic conversion of phosphonates to phosphate by bacteria. *Current Opinion in Chemical Biology*, *17*(4), 589–596. https://doi.org/10.1016/j.cbpa.2013.06.006

Kamat, S. S., & Raushel, F. M. (2014). PhnJ – A novel radical SAM enzyme from the C–P lyase complex. *Perspectives in Science*, *4*, 32–37. https://doi.org/10.1016/j.pisc.2014.12.006

Karl, D. M. (2014). Microbially mediated transformations of phosphorus in the sea: New views of an old cycle. *Annual Review of Marine Science*, *6*(1), 279–337. https://doi.org/10.1146/annurev-marine-010213-135046

Karl, D. M., Beversdorf, L. J., Björkman, K. M., Church, M. J., Martínez, A., & Delong, E. F. (2008). Aerobic production of methane in the sea. *Nature Geoscience*, *1*(7), 473–478. https://doi.org/10.1038/ngeo234

Karl, D. M., & Björkman, K. M. (2002). Dynamics of DOP. In *Biogeochemistry of Marine Dissolved Organic Matter* (pp. 249–366). Elsevier. https://doi.org/10.1016/B978-012323841-2/50008-7

Karl, D. M., Björkman, K. M., Dore, J. E., Fujieki, L., Hebel, D. V., Houlihan, T., Letelier, R. M., & Tupas, L. M. (2001). Ecological nitrogen-to-phosphorus stoichiometry at station ALOHA. *Deep-Sea Research Part II: Topical Studies in Oceanography*, *48*(8–9), 1529–1566. https://doi.org/10.1016/S0967-0645(00)00152-1

Karl, D. M., & Yanagi, K. (1997). Partial characterization of the dissolved organic phosphorus pool in the oligotrophic North Pacific Ocean. *Limnology and Oceanography*, *42*(6), 1398–1405. https://doi.org/10.4319/lo.1997.42.6.1398

Kolowith, L. C., Ingall, E. D., & Benner, R. (2001). Composition and cycling of marine organic phosphorus. *Limnology and Oceanography*, *46*(2), 309–320. https://doi.org/10.4319/lo.2001.46.2.0309

Lidbury, I. D. E. A., Scanlan, D. J., Murphy, A. R. J., Christie-Oleza, J. A., Aguilo-Ferretjans, M. M., Hitchcock, A., & Daniell, T. J. (2022). A widely distributed phosphate-insensitive phosphatase presents a route for rapid organophosphorus remineralization in the

biosphere. *Proceedings of the National Academy of Sciences*, *119*(5), e2118122119. https://doi.org/10.1073/pnas.2118122119

Lucas, C. H. (2001). Reproduction and life history strategies of the common jellyfish, *Aurelia aurita*, in relation to its ambient environment. *Jellyfish Blooms: Ecological and Societal Importance*, 229–246. https://doi.org/10.1007/978-94-010-0722-1_19

Luo, H., Zhang, H., Long, R. A., & Benner, R. (2011). Depth distributions of alkaline phosphatase and phosphonate utilization genes in the North Pacific Subtropical Gyre. *Aquatic Microbial Ecology*, *62*(1), 61–69. https://doi.org/10.3354/ame01458

Mao, J., Cao, X., Olk, D. C., Chu, W., & Schmidt-Rohr, K. (2017). Advanced solid-state NMR spectroscopy of natural organic matter. *Progress in Nuclear Magnetic Resonance Spectroscopy*, *100*, 17–51. https://doi.org/10.1016/j.pnmrs.2016.11.003

Metcalf, W. W., & Wanner, B. L. (1993). Evidence for a fourteen-gene, *phnC* to *phnP* locus for phosphonate metabolism in *Escherichia coli*. *Gene*, *129*(1), 27–32. https://doi.org/10.1016/0378-1119(93)90692-V

Monaghan, E. J., & Ruttenberg, K. C. (1999). Dissolved organic phosphorus in the coastal ocean: Reassessment of available methods and seasonal phosphorus profiles from the Eel River Shelf. *Limnology and Oceanography*, *44*(7), 1702–1714. https://doi.org/10.4319/lo.1999.44.7.1702

Pasek, M. A., Sampson, J. M., & Atlas, Z. (2014). Redox chemistry in the phosphorus biogeochemical cycle. *Proceedings of the National Academy of Sciences of the United States of America*, *111*(43), 15468–15473. https://doi.org/10.1073/PNAS.1408134111

Pech, H., Vazquez, M. G., Van Buren, J., Foster, K. L., Shi, L., Salmassi, T. M., Ivey, M. M., & Pasek, M. A. (2011). Elucidating the redox cycle of environmental phosphorus using ion chromatography. *Journal of Chromatographic Science*, *49*(8), 573–581. https://doi.org/10.1093/chrsci/49.8.573

Peterson, M. L., Wakeham, S. G., Lee, C., Askea, M. A., & Miquel, J. C. (2005). Novel techniques for collection of sinking particles in the ocean and determining their settling rates. *Limnology and Oceanography: Methods*, *3*(12), 520–532. https://doi.org/10.4319/lom.2005.3.520

Popendorf, K. J., Koblížek, M., & Van Mooy, B. A. S. (2020). Phospholipid turnover rates suggest that bacterial community growth rates in the open ocean are systematically underestimated. *Limnology and Oceanography*, 1–15. https://doi.org/10.1002/lno.11424

Quin, L. D., & Williams, A. J. (2004). Practical interpretation of P-31 NMR spectra and computer assisted structure verification. In *Angewandte Chemie International Edition* (Issue 45). Advanced Chemistry Development. https://onlinelibrary.wiley.com/doi/10.1002/anie.200485333

Redfield, A. C. (1934). On the proportions of organic derivatives in sea water and their relation to the composition of plankton. *James Johnstone Memorial Volume, University Press of Liverpool*, 176–192.

Repeta, D. J., Ferrón, S., Sosa, O. A., Johnson, C. G., Repeta, L. D., Acker, M., Delong, E. F., & Karl, D. M. (2016). Marine methane paradox explained by bacterial degradation of dissolved organic matter. *Nature Geoscience*, *9*(12), 884–887. https://doi.org/10.1038/ngeo2837

Seweryn, P., Van, L. B., Kjeldgaard, M., Russo, C. J., Passmore, L. A., Hove-Jensen, B., Jochimsen, B., & Brodersen, D. E. (2015). Structural insights into the bacterial carbon–phosphorus lyase machinery. *Nature*, *525*(7567), 68–72. https://doi.org/10.1038/nature14683

Shen, C. C., Wei, W. C., & Lin, L. C. (2019). Diterpenoids and bisnorditerpenoids from *Blumea aromatica*. *Journal of Natural Products*, *82*(11), 3181–3185. https://doi.org/10.1021/acs.jnatprod.9b00674

Sosa, O. A., Burrell, T. J., Wilson, S. T., Foreman, R. K., Karl, D. M., & Repeta, D. J. (2020). Phosphonate cycling supports methane and ethylene supersaturation in the phosphate-depleted western North Atlantic Ocean. *Limnology and Oceanography*, 1–17. https://doi.org/10.1002/lno.11463

Sosa, O. A., Repeta, D. J., Ferrón, S., Bryant, J. A., Mende, D. R., Karl, D. M., & DeLong, E. F. (2017). Isolation and characterization of bacteria that degrade phosphonates in marine dissolved organic matter. *Frontiers in Microbiology*, *8*(SEP), 1–16. https://doi.org/10.3389/fmicb.2017.01786

Thomson, B., Wenley, J., Currie, K., Hepburn, C. D., Herndl, G. J., & Baltar, F. (2019). Resolving the paradox: Continuous cell-free alkaline phosphatase activity despite high phosphate concentrations. *Marine Chemistry*, *214*(June), 103671. https://doi.org/10.1016/j.marchem.2019.103671

Urai, M., Nakamura, T., Uzawa, J., Baba, T., Taniguchi, K., Seki, H., & Ushida, K. (2009). Structural analysis of O-glycans of mucin from jellyfish (*Aurelia aurita*) containing 2-aminoethylphosphonate. *Carbohydrate Research*, *344*(16), 2182–2187. https://doi.org/10.1016/j.carres.2009.08.001

Van Mooy, B. A. S., Krupke, A., Dyhrman, S. T., Fredricks, H. F., Frischkorn, K. R., Ossolinski, J. E., Repeta, D. J., Rouco, M., Seewald, J. D., & Sylva, S. P. (2015). Major role of planktonic phosphate reduction in the marine phosphorus redox cycle. *Science*, *348*(6236), 783–785. https://doi.org/10.1126/science.aaa8181

Vidal, M., Duarte, C. M., Agustí, S., Gasol, J. M., & Vaqué, D. (2003). Alkaline phosphatase activities in the central Atlantic Ocean indicate large areas with phosphorus deficiency. *Marine Ecology Progress Series*, *262*, 43–53. https://doi.org/10.3354/meps262043

Vinogradov, E., Egbosimba, E. E., Perry, M. B., Lam, J. S., & Forsberg, C. W. (2001). Structural analysis of the carbohydrate components of the outer membrane of the lipopolysaccharide-lacking cellulolytic ruminal bacterium *Fibrobacter succinogenes* S85. *European Journal of Biochemistry*, *268*(12), 3566–3576. https://doi.org/10.1046/j.1432-1327.2001.02264.x

Wakeham, S. G., Hedges, J. I., Lee, C., Peterson, M. L., & Hernes, P. J. (1997). Compositions and transport of lipid biomarkers through the water column and surficial sediments of the

equatorial Pacific Ocean. *Deep Sea Research Part II: Topical Studies in Oceanography*, *44*(9–10), 2131–2162. https://doi.org/10.1016/S0967-0645(97)00035-0

Wakeham, S. G., Lee, C., Hedges, J. I., Hernes, P. J., & Peterson, M. L. (1997). Molecular indicators of diagenetic status in marine organic matter. *Geochimica et Cosmochimica Acta*, *61*(24), 5363–5369. https://doi.org/10.1016/S0016-7037(97)00312-8

5.7 SUPPLEMENTAL MATERIAL

5.7.1 CLA and APA on HOT318

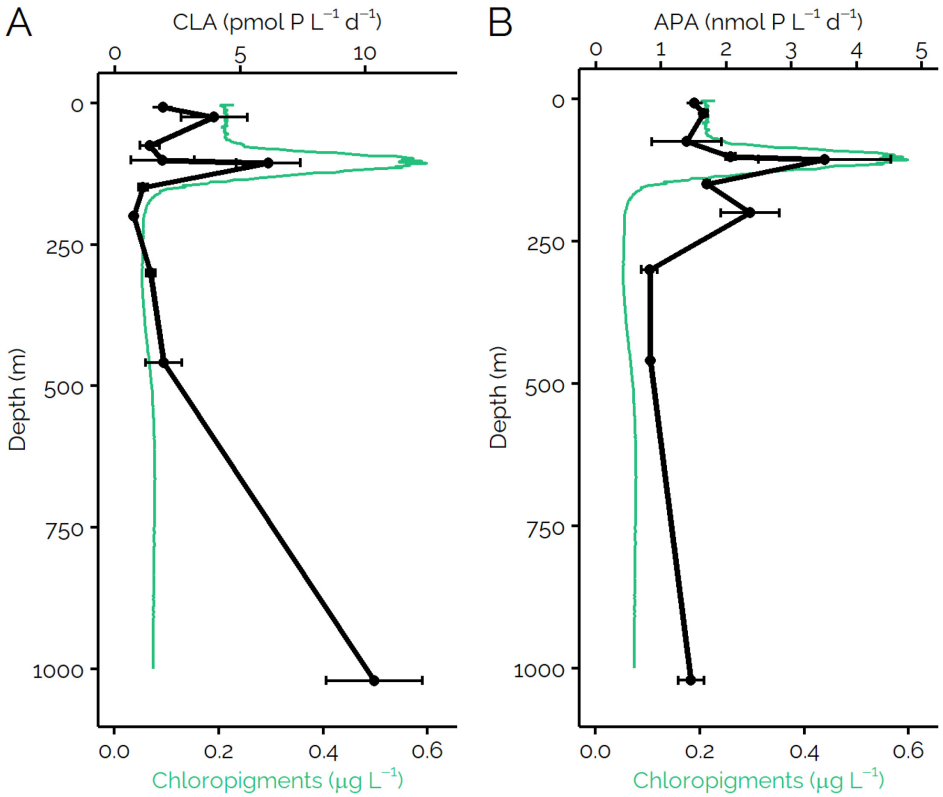

Figure 5.7: A) CLA and **B)** APA profiles collected on HOT318 in January, 2020. Error bars denote the standard error of the mean of biological replicate (n = 3) measurements. Profiles show strong coherence with local maxima concurrent with the DCM.

5.7.2 Major Compositional Changes of POM Through the Water Column

Common biomolecule signals are present in all POM ^{13}C CP-MAS spectra (Figure 5.8).

A suit of ^{13}C-MAS experiments is needed to fully characterize each spectrum, but based on these

initial results, some broad patterns can be identified (Mao et al., 2017). All spectra were normalized at 36 ppm, which is the chemical shift associated with C on a sterol ring. This value was chosen for normalization as sterols are likely to be more stable in POM than other biomolecules, allowing for the detection of diagenetic signatures, although future analyses of these samples should involve the addition of an internal standard, such as tetramethylsilane (TMS) for normalization (Cao et al., 2018; Hertkorn et al., 2006). Peak E (173 ppm), which results from the carboxylic acid resonances found primarily in amino acids and nucleic acids, decreases with sampling depth, suggesting that the relative abundance of these compounds decrease below the surface. This could be the result of a remineralization processes or could indicate that the proportion of non-living biomass increases with depth (Wakeham, Lee, et al., 1997) . The relative magnitude of the broad peaks C and D, associated with carbohydrate carbon (72 and 54 ppm), also decrease with depth. Carbohydrate removal processes include remineralization, hydrolysis and dissolution, and flocculation and settling, and it is expected that all these processes would remove these compounds from the SPM pool. Lastly, there was a noticeable shift in the ratio of peak B (32.8 ppm) to peak A (30.7 ppm) which may provide a measure of the unsaturated:saturated fatty acid (FA) ratio. The surface sample has a much greater proportion of unsaturated FA as compared to the rest of the samples, a result that agrees with previous observations of unsaturated FA export (Wakeham, Hedges, et al., 1997). This result needs further verification via additional MAS experiments as peak B and A can be partially attributed to other biomolecules such as leucine, isoleucine, and valine. Taken together this evidence provides preliminary evidence for enhanced diagenesis, and removal of labile biomolecules in SPM.

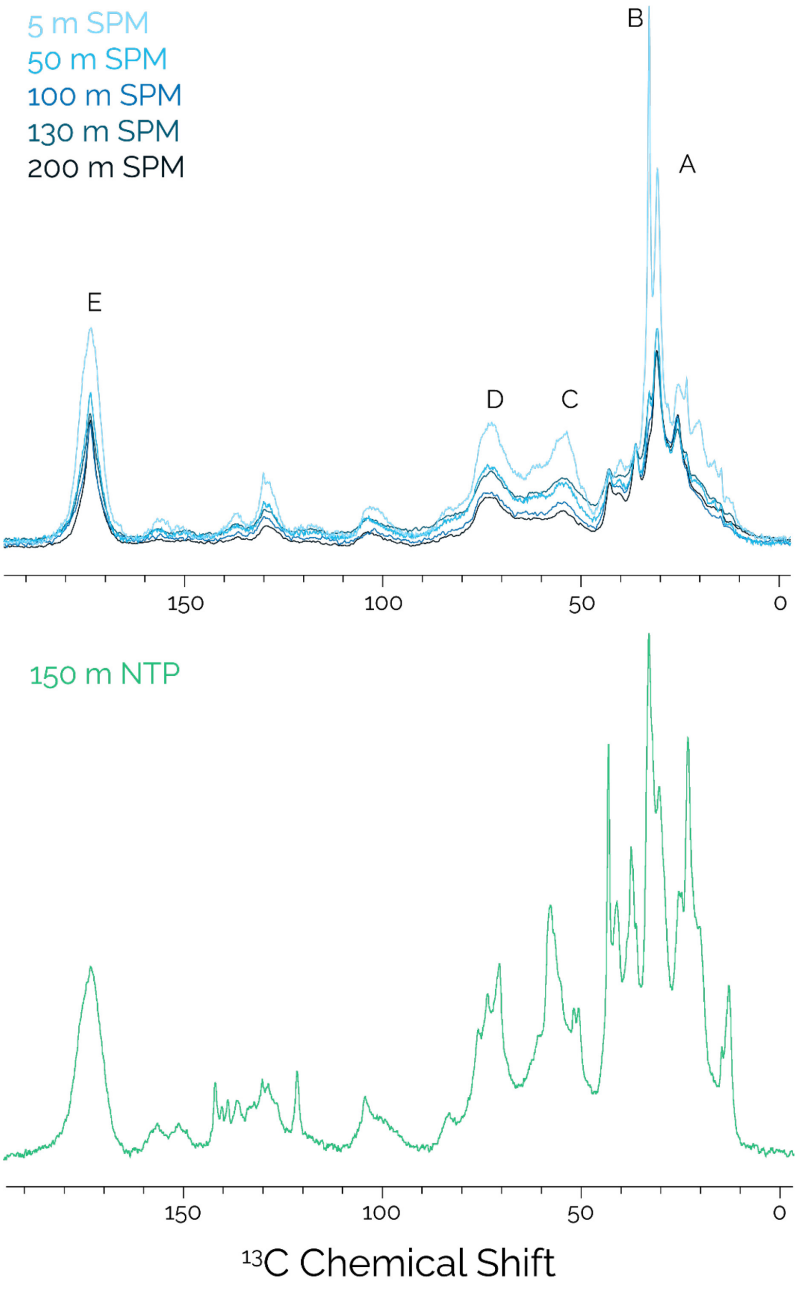

Figure 5.8: ^{13}C CP-MAS spectra of the SPM and NTP samples collected on PARAGON I. SPM samples were normalized to a sterol ring C peak (36 ppm) to allow for comparison of the relative concentration of biomolecules.

CHAPTER 6. CONCLUSIONS AND FUTURE DIRECTIONS

6.1 SUMMARY OF PROJECT 1: AN EXAMINATION OF THE SIZE DISTRIBUTION AND DIAGENETIC FATE OF HIGH MOLECULAR WEIGHT DISSOLVED ORGANIC MATTER

High molecular weight dissolved organic matter (HMWDOM) is a major fraction of marine semi-labile DOM ($_{sl}$DOM) that is operationally defined based on retention by an ultrafiltration membrane. While studies of HMWDOM composition have gleaned insight into its compositional makeup and potential origins, important questions about the diverse diagenetic fate of HMWDOM have remained unanswered. While studies of the evolution in radiocarbon content over the course of ultrafiltration have demonstrated the heterogeneity of HMWDOM $\Delta^{14}C$, analysis of HMWDOM has treated the material as homogenous with respect to turnover time, and larger theories regarding the reactivity of DOM are based on these assumptions.

In chapter 2, I demonstrated that the two major components of HMWDOM, acylpolysaccharides (APS) and humic substances (HS) fall into a narrow envelope of MWs between 1 and 10 kDa. By examining changes in the size distribution of these components with depth, I developed a conceptual model that describes the diagenetic fate of each fraction. APS is produced autochthonously and remineralized quickly, likely through a continuous hydrolysis of monosaccharides. HS in the surface is comprised of two fractions, a larger, young fraction of newly produced photosynthate, and an old, advected fraction of refractory OM ($_{r}$DOM). As the concentration of HS is constant between the surface and deep samples, despite a decrease in HS MW, either the newly produced HS is decomposed into smaller compounds but resist degradation, or the remineralized material is replaced by HS in the deep ocean with a smaller MW.

In chapter 3, I used radiocarbon analysis of size fractions of HMWDOM to constrain the radiocarbon ages of APS and HS. Through linear modeling, I demonstrated that the $\Delta^{14}C$ of HMWDOM is correlated with HS content. Extrapolation of this model yielded $\Delta^{14}C$ values for the two endmember components. APS in all HMWDOM samples displayed a radiocarbon age similar to $\Delta^{14}C$-DIC suggesting autochthonous production and a rapid turnover time of approximately 1.5 yrs. While the HS endmember had a greater degree of uncertainty due to extrapolation, the predicted $\Delta^{14}C$ values at both depths were similar and fell between modern material and TDOM. Additionally, the stable carbon isotope signature of HS decreased from typical marine values to a highly depleted signature, suggesting a shift in composition. The results of the mixing analysis match the predictions from the model proposed in Chapter 2. APS is autochthonously produced and rapidly remineralized. HS in the surface is a mixture of new and refractory material. The new material is likely remineralzied but an additional source of HS supplies ^{13}C isotopically light material to the deep ocean, balancing the loss of carbon from remineralization. HMWDOM does not represent an intermediate in the decomposition of POC, as the SRC proposes. Instead, HMWDOM should be thought of as a size-fraction of DOM that contains both fresh photosynthate and complex, degraded material with unique cycling mechanisms.

6.2 FUTURE STUDIES OF DISSOLVED ORGANIC MATTER SIZE DISTRIBUTION

This work emphasizes that the compound diversity of an operationally defined pool of DOM provides necessary context for interpreting bulk properties such as elemental stoichiometry and isotopic composition. Compounds isolated by ultrafiltration have a diverse diagenetic fate and models of DOM dynamics that rely on HMWDOM, such as the size–

reactivity continuum hypothesis, need to take this into account when ascribing reactivity to a pool of DOM. There are still several questions left to be answered regarding the composition and cycling of the components of HMWDOM.

6.2.1 What happens to APS smaller than 3 kDa in the surface ocean?

I found that the MW of APS in the surface ocean plateaus around 3.5 kDa and no signal of smaller APS in HMWDOM was detected. There are several possible explanations for this observation. Most of the APS produced in the surface may be greater than 3.5 kDa, and diagenetic processes may not result in the production of APS of an intermediate size. This discovery would be surprising as APS with a MW lower than 3.5 was measured in the 900 m sample. If the MW of APS is controlled by microbial synthesis, the difference is size between the surface and 900 m samples would suggest that APS is produced through different mechanisms or by different organisms in the mesopelagic.

It is also possible that APS below 3.5 kDa is rapidly remineralized, such that no standing stock of material persists in the surface. Microbes employ a diverse suite of strategies for metabolizing large exopolysaccharides, and it has been shown that the direct uptake of polysaccharides is size-limited. It is possible, that a microbial strategy for APS remineralization in the surface has an upper MW threshold of 3.5 kDa, allowing for the persistence of large material and the rapid removal of APS once its MW drops below that critical threshold.

To test these hypotheses and to confirm that APS smaller than 3.5 kDa is not present in the surface, multi-dimensional HPLC can be used to further fractionate HMWDOM by size, while specifically targeting strong APS separation. As DOSY analysis yields the average diffusivity for a given NMR resonance, a higher-resolution separation is needed to confirm that

APS smaller than 3.5 kDa is absent in surface HMWDOM. A separate experiment could use soft acid hydrolysis to artificially produced APS of a lower MW, which could be used as substrate in heterotrophic incubation experiments to study the effect of size on uptake. Fluorescently labeled APS could also be used, in conjunction with fluorescence *in situ* hybridization to study the potential uptake mechanism that is preferentially removing APS smaller than 3.5 kDa.

6.2.2 Is a significant fraction of APS produced by chemoautotrophs in mesopelagic?

One of the surprising discoveries described in chapter 3 is that the APS radiocarbon endmember calculated for the 900 m sample resembled Δ^{14}C-DIC from 900 m, instead of a modern radiocarbon value. I suggested two explanations for this observation. While APS in the surface ocean has a rapid turnover time of 1.5 yrs, advected material may survive for a much longer period of time due to slower metabolism in the subsurface, as evidenced by the low rates of respiration. Thus, APS that is advected before remineralization would have a radiocarbon signature equivalent to local DIC. Alternatively, the radiocarbon-depleted APS could be produced *in situ* in the mesopelagic through chemoautotrophy. While canonically, chemoautotrophy was thought to account for only a small fraction of DOC production, new evidence suggests that archaeal carbon reduction can produced a significant amount of DOC. Future global studies of HMWDOM can look for hot spots of chemoautotrophy to determine if a significant portion of APS is produced in the mesopelagic.

6.2.3 Does HS undergo polymerization in the surface ocean?

The conceptual model proposed in chapter 2 attributes surface HS with a MW greater than 3 kDa to new production, and posits almost all of the young HS is remineralized quickly. A potential additional source of large HS is the photopolymerization of advected refractory HS

($_r$HS). If the polymerization of $_r$HS creates weak intramolecular bonds, the dissociation of these structures could contribute to the decrease in MW observed in the 900 m sample. While further observations are needed to determine if polymerization of $_r$HS occurs, radiocarbon analysis of size fractions of HS could provide insights in to the carbon source of HMW HS. Using ramped pyrolysis, the distribution of $\Delta^{14}C$ values can be measured for each HMWDOM MMC fraction. If large HS is produced through photopolymerization of $_r$HS, radiocarbon depleted HS would be detected in the early eluting MMC fractions. This analysis could also provide insight into structural differences between $_r$HS and modern HS, based on pyrolysis temperature. What is the primary mechanism of humification in the ocean?

The dominant mechanisms of HS formation in the ocean remains a central open question in marine organic geochemistry. Several possible mechanisms include the abiotic condensation of small molecules, the polymerization of refractory biomolecules, and the supramolecular aggregation of refractory DOM. Each of these mechanisms has a potential relationship between size and age associated with it. In the future, I would like to use the methods employed in this thesis to study the size and age distribution of low molecular weight SPE extracted DOM (LMWSPEDOM). If a relationship between age and size is found, it could suggest a primary mechanism of LMWSPEDOM formation in the ocean.

6.3 SUMMARY OF PROJECT 2: REGULATION OF PHOSPHONATE CYCLING IN THE LOWER EUPHOTIC ZONE OF THE NORTH PACIFIC SUBTROPICAL GYRE

In chapter 4, I described the development and validation of an assay to measured C-P lyase activity (CLA) in natural waters. The assay relies on the hydrolysis of a fluorescently

tagged phosphonate molecule, which can be isolated and quantified on via HPLC. The assay allows for high sample throughput, and the use of fluorescence detection provides the sensitivity needed to detect CLA at ambient conditions, mitigating the need for cell concentration. In validating the assay in the North Pacific Subtropical Gyre (NPSG), I observed a frequent CLA maximum concurrent with the DCM at the base of the euphotic zone.

Several hypotheses were developed to explain the subsurface CLA maximum. One hypothesis suggests that the elevated flux of nitrate from the mesopelagic creates zones of localized phosphate limitation near the DCM, which in turn promotes DOP uptake and remineralization. To test this hypothesis, I participated in two field campaigns (PARAGON I & II) to quantify the N and P fluxes into the lower euphotic zone and to determine if DOP degradation as a whole was enhanced, or if only phosphonates were being remineralized. The elevated N:P flux ratios observed on previous expeditions were not present during the PARAGON expeditions, and no CLA maximum was detected. These results still support the hypothesis but acted as a negative test, limiting the conclusions that could be drawn. In one station where CLA was elevated near the DCM, alkaline phosphatase activity (APA) was also enhanced, suggesting that DOP remineralization as a whole was promoted in this region.

The second hypothesis that I tested on the PARAGON expeditions suggested that the high CLA rates can be the result of increased phosphonate production in the subsurface. Using radiolabeled phosphate, I measured P uptake phosphonate production rates through the top 300 m of the water column. Additionally, I collected large volume POM samples to determine if the concentration of cellular phosphonates was enhanced at depth. In both of these experiments, I found no evidence of higher phosphonate production rates near the DCM, suggesting that high

substrate concentrations are not responsible for the CLA maxima. While studying the POM, I did find evidence of phosphonates in sinking particulate matter collected via net traps. This suggests that large particles, potentially derived from eukaryotic organisms, may be a significant source of phosphonate-DOP to the ocean.

6.4 FUTURE STUDIES OF PHOSPHONATE UTILIZATION IN THE OCEAN

6.4.1 How Does CLA Vary with Depth in a P Limited Environment Such as the Sargasso Sea?

In the future, I would like to deploy the CLA assay in phosphate-limited regions of the ocean to study DOP utilization under continuous phosphate limitation. The surface NPSG is typically nitrate limited, resulting in low rates of DOP remineralization. Organic phosphorus cycling in the subtropical Atlantic is much more rapid as DOP is a major source of phosphorus in the surface ocean. I expect that CLA rates to be highest in the surface in the Sargasso Sea, but I would like to know if the subsurface CLA peak near the DCM is also present in other ocean basins. Studying this phenomenon under different nutrient conditions would provide additional insight into the nutrient controls on CLA.

6.4.2 Is C-P Lyase Employed as a Carbon Acquisition Strategy

Canonically, C-P lyase and alkaline phosphatase are considered phosphorus acquisition mechanisms and are regulated by inorganic phosphate concentrations. However, several recent studies have observed CLA under high phosphate conditions, and a phosphate-insensitive phosphomonoesters was described in soil and marine *Bacteroidetes*. These results suggest that DOP degrading enzymes may be employed as part of carbon acquisition, in addition to phosphorus remineralization. I observed elevated CLA were measured in the mesopelagic, below

500 m where inorganic phosphate concentrations are high. This signal may result from CLA as part of carbon metabolism. In the future, studies of CLA under extreme carbon starvation could lead to a new model of phosphonate cycling and utilization.